



UNIVERSIDADE ESTADUAL DE CAMPINAS
Instituto de Física “Gleb Wataghin”

BIANCA MARIA SILVEIRA DE OLIVEIRA

Exploratory Study of the Nonperturbative Four-point Green’s Function
in the Background Field Method

Estudo Exploratório da Função de Green Não Perturbativa do Vértice
de Quatro Pontos no Formalismo de Background Field

Campinas

2021

BIANCA MARIA SILVEIRA DE OLIVEIRA

Exploratory Study of the Nonperturbative Four-point Green's Function
in the Background Field Method

Estudo Exploratório da Função de Green Não Perturbativa do Vértice
de Quatro Pontos no Formalismo de Background Field

*Dissertation presented to the Institute of Physics
“Gleb Wataghin” of the University of Campinas in
partial fulfillment of the requirements for the degree
of Master of Physics, in the area of Physics.*

*Dissertação apresentada ao Instituto de Física
“Gleb Wataghin” da Universidade Estadual de
Campinas como parte dos requisitos exigidos para
a obtenção do título de Mestra em Física, na área
de Física.*

ORIENTADOR: ARLENE CRISTINA AGUILAR

ESTE EXEMPLAR CORRESPONDE À
VERSÃO FINAL DA DISSERTAÇÃO
DEFENDIDA PELA ALUNA BIANCA
MARIA SILVEIRA DE OLIVEIRA, E
ORIENTADA PELA PROFA. DRA.
ARLENE CRISTINA AGUILAR

CAMPINAS

2021

Ficha catalográfica
Universidade Estadual de Campinas
Biblioteca do Instituto de Física Gleb Wataghin
Lucimeire de Oliveira Silva da Rocha - CRB 8/9174

OL4e Oliveira, Bianca Maria Silveira de, 1997-
Exploratory study of the nonperturbative four-point Green's function in the background field method / Bianca Maria Silveira de Oliveira. – Campinas, SP : [s.n.], 2021.

Orientador: Arlene Cristina Aguilar.
Dissertação (mestrado) – Universidade Estadual de Campinas, Instituto de Física Gleb Wataghin.

1. Cromodinâmica quântica. 2. Método de campo de fundo. 3. Equações de Schwinger-Dyson. 4. Métodos não perturbativos. 5. Funções de Green. I. Aguilar, Arlene Cristina, 1977-. II. Universidade Estadual de Campinas. Instituto de Física Gleb Wataghin. III. Título.

Informações para Biblioteca Digital

Título em outro idioma: Estudo exploratório da função de Green não perturbativa do vértice de quatro pontos no formalismo de background field

Palavras-chave em inglês:

Quantum chromodynamics
Background field method
Schwinger-Dyson equations
Nonperturbative methods
Green's functions

Área de concentração: Física

Titulação: Mestra em Física

Banca examinadora:

Arlene Cristina Aguilar [Orientador]
João Paulo Pitelli Manoel
Emerson Gustavo de Souza Luna

Data de defesa: 29-09-2021

Programa de Pós-Graduação: Física

Identificação e informações acadêmicas do(a) aluno(a)

- ORCID do autor: <https://orcid.org/0000-0001-9320-996X>

- Currículo Lattes do autor: <http://lattes.cnpq.br/2087551078809499>

MEMBROS DA COMISSÃO JULGADORA DA DISSERTAÇÃO DE MESTRADO DA BIANCA MARIA SILVEIRA DE OLIVEIRA - RA 164895 APRESENTADA E APROVADA AO INSTITUTO DE FÍSICA “GLEB WATAGHIN”, DA UNIVERSIDADE ESTADUAL DE CAMPINAS, EM 29/09/2021.

COMISSÃO JULGADORA:

- Profa. Dra. Arlene Cristina Aguilár - Orientadora (IFGW / UNICAMP)
- Prof. Dr. João Paulo Pitelli Manoel (IMECC / UNICAMP)
- Dr. Emerson Gustavo de Souza Luna (Universidade Federal do Rio Grande do Sul)

OBS.: Ata da defesa com as respectivas assinaturas dos membros encontra-se no SIGA/Sistema de Fluxo de Dissertação/Tese e na Secretaria do Programa da Unidade.

CAMPINAS

2021

Agradecimentos

Primeiramente gostaria de agradecer minha orientadora Profa. Dra. Arlene Cristina Aguilar pela atenção, cuidado e direção impecável ao longo da minha vida profissional. É um prazer enorme me aprimorar inspirada nessa mulher incrível. Também gostaria de agradecer ao nosso colaborador Prof. Dr. Joannis Papavassiliou, da Universidade de Valência, que mesmo a distância contribuiu com conselhos e comentários ímpares não só para esse trabalho mas também para a minha formação como cientista.

Além disso, esse projeto não seria possível sem ajuda dos meus amigos Dr. Mauricio N. Ferreira, que guia o grupo todo com muita paciência e gentileza, Me. Cleiton de Oliveira Ambrósio, que além de me ensinar e me guiar me trouxe muitos sorrisos, Jhon Mario Córdoba, por sempre estar ao meu lado tirando todas as dúvidas e deixando meus dias mais alegres, e Leonardo Rodrigues dos Santos, que mesmo a distância contribuiu para o meu trabalho e tornou-se um grande amigo.

Gostaria de agradecer aos Professores do Instituto de Física “Gleb Wataghin” (IFGW) que fizeram parte da banca examinadora do meu exame de qualificação do mestrado e de pré-requisito, Prof. Dr. Orlando Luis Goulart Peres, Prof. Dr. Jun Takahashi, Prof. Dr. João Paulo Pitelli Manoel e Prof. Dr. Emerson Gustavo de Souza Luna.

Agradeço ao apoio financeiro, uma vez que o presente trabalho foi realizado com apoio da Coordenação de Aperfeiçoamento de Pessoal de Nível Superior - Brasil (CAPES) - Código de Financiamento 001. Agradeço ainda ao IFGW pela estrutura impecável e pela Universidade de Campinas e seus funcionários pelo suporte que nos é fornecido.

Um agradecimento muito especial para meus pais, Maria José Menezes da

Silveira e Antonio Carlos de Oliveira, pelo apoio desde sempre, pelas conversas e conselhos, e por serem os melhores e me tornarem cada dia melhor. Obrigada aos meus irmãos, Rafael Fonseca da Silveira Neto, Rodrigo Silveira Garcia e Vanessa Silveira Garcia, por me ensinarem a cada dia, de forma leve e alegre.

Ao meu João Guilherme Prado Barbon, por me completar e me fazer a mais feliz. Aos meus amigos da escola, em especial a Juliana Penna Folhadella, Yasmin Navarro Hurtado e Juliana Rodriguez Camacho, por sempre estarem perto. Aos meus amigos de graduação, pós graduação e tecido acrobático, sou profundamente grata pela companhia e pelos sorrisos que vocês me proporcionam.

Por fim gostaria de lembrar e agradecer meu primeiro professor de física, Prof. Claudécir Ricardo Biazoli. Sem ele nada disso teria sido possível, e para sempre serei grata.

Acknowledgements

Firstly I would like to thank my supervisor Profa. Dra. Arlene Cristina Aguilar for the attention, care and impeccable guidance towards my professional life. It is a great pleasure to improve myself inspired in this incredible woman. I would also like to thank our collaborator Prof. Dr. Joannis Papavassiliou, from the University of Valencia, whom even in a distance contributed with indispensable advises and comments not only to this work but also to my formation as a scientist.

In addition, this project would not be possible without the help of my friends Dr. Mauricio N. Ferreira, who guides the group with all the patience and kindness, Me. Cleiton de Oliveira Ambrósio, who apart from teaching and guiding me always brought me many smiles, Jhon Mario Córdoba for always being by my side solving my doubts and letting my days happier, and Leonardo Rodrigues dos Santos, that even miles apart contributed to my work and became a great friend.

I would like to thank my professors in the Institute of Physics “Gleb Wataghin” (IFGW) in the evaluation committees for my qualify examination and dissertation prerequisite examination, Prof. Dr. Orlando Luis Goulart Peres, Prof. Dr. Jun Takahashi, Prof. Dr. João Paulo Pitelli Manoel, and Prof. Dr. Emerson Gustavo de Souza Luna.

I thank my financial support, since this study was financed in part by the Coordenação de Aperfeiçoamento de Pessoal de Nível Superior - Brasil (CAPES) - Finance Code 001. I also thank the IFGW to the impeccable structure and the University of Campinas and its staff for the support.

A very special acknowledgement goes to my parents, Maria José Menezes da Silveira and Antonio Carlos de Oliveira, for the support since the beginning, for the conversations and guidance, and for being the bests, and making me better everyday.

Thanks to my brothers Rafael Fonseca da Silveira Neto, Rodrigo Silveira Garcia and Vanessa Silveira Garcia, for teaching me everyday, in a light and happy way.

To my João Guilherme Prado Barbon, for completing me and making me the most happy woman. To my friends from school, specially Juliana Penna Folhadella, Yasmin Navarro Hurtado and Juliana Rodriguez Camacho, for always being around. To my friends in the graduation, post-graduation, and acrobatic silk, I am profoundly thanked by the companionship and for the smiles you provide me.

Lastly but not least I would like to remember and thank my first physics professor, Prof. Claudécir Ricardo Biazoli. Without him nothing would be possible, and I will always be grateful.

Resumo

Ao utilizarmos o formalismo de Background Field Method para descrever a QCD aparecem novos vértices de interação envolvendo campos de gauge no background. A propriedade mais marcante destas novas funções de Green é que elas satisfazem identidades de Ward-Takahashi do tipo Abelianas, em vez das complexas identidades de Slavnov-Taylor obedecidas pelas funções da QCD convencional. Uma destas novas funções de Green é o vértice de interação de quatro pontos formado por dois glúons no background, um campo de ghost e outro de antighost. O objetivo deste trabalho é fazer um estudo exploratório do comportamento deste vértice na região não perturbativa da QCD. Para isso, vamos derivar a Equação de Schwinger-Dyson que este vértice satisfaz através do formalismo funcional. Dada o alto grau de complexidade envolvido na resolução desta equação em configurações de momentos gerais, vamos nos concentrar neste primeiro estudo no limite cinemático “all-soft”, onde os momentos que entram nas quatro pernas do vértice são zero. Derivamos utilizando a identidade de Ward-Takahashi uma relação exata, válida em todas ordens em teoria de perturbação, onde mostramos que das 10 estruturas tensoriais na qual este vértice pode ser decomposto, somente a estrutura proporcional a métrica sobrevive no limite all-soft. Mais importante, o fator de forma que acompanha essa estrutura se reduz ao valor da função de vestimento do propagador do ghost na origem, valor bem conhecido na literatura através de estudos feitos por Equações de Schwinger-Dyson e simulações da QCD na rede. A derivação desta relação exata para o fator de forma do vértice no limite all-soft é o resultado central deste trabalho e é inédito na literatura. Por fim exploramos alguns cenários de como essa relação exata pode guiar a construção de um esquema de truncamento a ser empregado em um futuro estudo da Equação de Schwinger-Dyson deste vértice de quatro pontos em cinemáticas gerais.

Abstract

Using the Background Field Method formalism to describe QCD leads to new interaction vertices involving background gauge fields. The most important property of this new Green's functions is that they satisfy Abelian Ward-Takahashi identities instead of the complicated Slavnov-Taylor identities, obeyed by the conventional QCD functions. One of these Green's functions from the Background Field Method is the four-point interacting vertex composed of two background gluons, a ghost, and an antighost field. The main purpose of this work is to make an exploratory study of the behavior of this vertex in the nonperturbative region of QCD. For that, we will derive the Schwinger-Dyson equation which this vertex satisfies through the functional formalism. Given the intricate nature of this equation in a general kinematic configuration, in this exploratory study, we focus on the "all-soft" limit, where the momenta of the four legs are zero. Using the Ward-Takahashi identity that this vertex satisfies, we derive an exact relation valid to all orders in perturbation theory. From the ten general tensorial structures that this vertex can be decomposed, we show that only the one proportional to the metric survives in the all-soft limit. More specifically, the form factor accompanying the metric reduces to the ghost dressing function at the origin, whose value is well known from previous Schwinger-Dyson and lattice studies. The derivation of this exact relation for the form factor of the four-point vertex in the all-soft limit is the main result of this work and represents a novel contribution. Finally, we explore some scenarios of how this exact relation may be used as a guideline for developing a future truncation scheme for this vertex in general kinematics.

Lista de Abreviações

1PI One-particle irreducible

BFM Background Field Method

IR Infrared

QCD Quantum Chromodynamics

QED Quantum Electrodynamics

QFT Quantum field theory

RHS Right hand side

SD (SDE) Schwinger-Dyson (Schwinger-Dyson equation)

STI Slavnov-Taylor identity

UV Ultraviolet

WTI Ward-Takahashi identity

VEV Vacuum expectation value

Contents

Introduction	14
1 Brief introduction to QCD	19
1.1 QCD Lagrangian and Feynman rules	19
1.2 Asymptotic freedom	23
2 The Background Field Method	26
2.1 Functional formalism	27
2.2 Background Field Method	30
2.3 BFM Green's functions	34
2.4 SDE for the gluon propagator	37
2.5 Ward-Takahashi identities	39
2.6 Background gluon propagator	40
3 Schwinger-Dyson Equations	44
3.1 The Schwinger-Dyson master equation	44
3.2 The SDE for the ghost propagator	46
3.3 The SDE for the $BB\bar{c}c$ vertex	49
4 All-soft limit for the $BB\bar{c}c$ vertex	54
4.1 The general tensorial structure	55
4.2 Definitions of the full Green's functions	57
4.2.1 Three-point sector	57
4.2.2 Four-point sector	59
4.2.3 Two-point sector	60

4.2.4	Renormalization	61
4.3	Evaluation of the all-soft limit	63
4.4	All-soft limit from the WTI of the $BB\bar{c}c$ vertex	69
4.5	Numerical Analysis: Beyond the all-soft configuration	70
4.5.1	Nonperturbative inputs	70
4.5.2	Exploring truncations schemes for the $BB\bar{c}c$ SDE	73
5	Conclusions	77
	References	81
	Appendices	88
A	SU(N) group theoretical identities	88
B	Nonperturbative structure of the $BB\bar{c}c$ vertex	89
B.1	Color basis construction	89
B.2	Bose symmetry of the background gluon legs	90
C	Transformation rules from Minkowski to Euclidean space	92
D	Numerical method for solving integral equations	94

Introduction

The description of the strong interaction between quarks and gluons is given by the Quantum Chromodynamics (QCD) [1]. Understanding all QCD subtleties consists of one of the main scientific challenges within the Standard Model of elementary particles. QCD is a renormalizable non-Abelian gauge theory [2], based on the color symmetry group $SU(3)$, with quarks being the fermions and gluons the gauge bosons mediators of the strong force [1].

The non-Abelian property of QCD is generated by the self-interacting gauge bosons, which makes it far more complex than Quantum Electrodynamics (QED). Furthermore, QCD is asymptotically free in the ultraviolet (UV) region [3, 4], meaning that the coupling constant becomes smaller as the energy (or equivalently momenta) scale increases.

On the other hand, in the infrared (IR) regime, the coupling is not small enough to apply perturbation theory safely. This fact challenges us to deal with nonperturbative approaches in order to describe this rich region, which accommodates intriguing phenomena, such as confinement [5, 6], dynamical mass generation of quarks and gluons [7–15], and the formation of bound states [8–10, 16–19].

Recently our understanding of the IR region of QCD increased considerably due to nonperturbative formalisms that aim to compute the Green's functions, *i.e.*, the propagators and vertices, which encode all the dynamical information of the theory. The QCD Green's functions are the building blocks of the fundamental degrees of freedom, *i.e.*, quarks, gluons, and ghost fields. Although it is well known that Green's functions are gauge and renormalization scheme dependent quantities, they may be combined in a very precise way to give rise to physical observables, such as cross-sections, decay rates,

and hadron masses.

One of these approaches is the lattice QCD, which discretizes the Euclidean space, transforming the continuum space-time in a four-dimensional grid [20, 21]. In lattice QCD, quark fields are defined at the sites of the lattice, while the gluons are the links connecting neighboring sites, resulting in a discretized version of the QCD Lagrangian. Moreover, lattice QCD employs Monte Carlo simulations [20], in analogy with statistical physics.

Despite the significant progress that lattice simulations brought [22], this formalism has also its own limitations. For example, when we perform the discretization, one may lose some symmetries, which may be recovered in the continuum limit, *i.e.*, when the lattice spacing $a \rightarrow 0$ and the volume of the entire lattice $V \rightarrow \infty$. Therefore, this framework is restricted to the computational power available, since the continuum limit requires more and more computational effort. Moreover, lattice QCD faces additional difficulties in treating fermionic fields and dealing with significant disparities in physical scales present in QCD, such as the contrasting quark mass scales [23–25].

In light of this, it is essential to explore other continuum approaches to deepen our knowledge about the IR region of QCD. Among the functional methods available in the literature [10, 26–36], the present work is focused mainly on the Schwinger-Dyson Equations (SDE) [8–10, 37]. The SDEs are the equations of motion for the Green’s functions of a given Quantum Field Theory (QFT), in analogy to the Euler-Lagrange equation in classical mechanics. The SDEs form an infinite set of coupled integral equations, one for each n -point Green’s function.

Evidently, an infinite system of coupled equations cannot be solved exactly. Therefore, the need for a truncation scheme is mandatory to convert the problem into a finite coupled system of integral equations [8, 16, 37–40]. Implementing such truncation schemes, and at the same time preserving the fundamental symmetries of the theory, is by no means an easy task [9, 11, 13, 38, 39, 41–48]. Nevertheless, if this challenging task is accomplished, there is no formal way of estimating the contribution of the omitted terms since there is no obvious expansion parameter in these equations.

Significant advances were obtained in this way in the last decades due to the implementation of a truncation scheme based on the synthesis between the Pinch Technique (PT) formalism [7, 12, 49–52] with the Background Field Method (BFM) [53–55],

known in the literature as PT-BFM scheme. This truncation scheme was designed to deal with the SDE for the gluon propagator. In this context, the PT-BFM scheme furnishes considerable advantages because it facilitates a systematic truncation that respects manifestly the transversality of the gluon self-energy at every step [11, 38, 39, 46].

The basic idea of the BFM is to split the conventional gluon field, A_μ^a , into a quantum field, Q_μ^a , and a classical background field, B_μ^a [55]. This separation gives rise to a vast set of new Feynman rules, leading to an increase in the possible types of Green's functions that must be considered [12, 55]. In particular, three types of gluon propagators arise: (i) the conventional gluon propagator (defined by two incoming quantum gluons, QQ); (ii) the propagator of the background gluon (two background gluons, BB); and (iii) the mixed background-quantum gluon propagator (one background gluon and one incoming quantum gluon, QB). Moreover, in this formalism, new vertices containing background gluon also appear: e.g., BQQ, BQQQ, $B\bar{c}c$, and $BB\bar{c}c$ ¹. A crucial property of the BFM is that the vertices mentioned above satisfy WTIs when contracted with the momentum of the background gluon B_μ^a , similar to those that appear in an Abelian theory, rather than the complicated STIs, satisfied by the conventional QCD Green's functions [12, 46, 55].

In this work, we will focus on the nonperturbative structure of the $BB\bar{c}c$ vertex, to be denoted by $\widehat{\Gamma}_{\mu\nu}^{abmn}(q, r, p, t)$. This vertex is the simplest four-point Green's functions, with gluon fields, which emerge in the BFM formalism, serving as a good starting point for an exploratory study of the four-point Green's functions.

Although the $BB\bar{c}c$ is one of the most basic four-point structures we have, one should not underestimate the degree of difficulty involved in describing its complete nonperturbative structure. The most general decomposition of this vertex is expressed in terms of 35 form factors, which are functions of six variables, *i.e.*, the three independent momenta and the three angles between them.

Given the intricate nature of this vertex in general kinematic configuration, in this work, we explore the so-called “all-soft” limit, where we set to zero the momenta in the four legs of the vertex.

To do that, we first employ the functional formalism to derive the SDE that this vertex satisfies. As far as we know, this is the first time that the SDE for the $BB\bar{c}c$ vertex appears in the literature. With this equation at hand, we take the all-soft limit, analyzing

¹Here c and \bar{c} denote the ghost and antighost fields, respectively.

the contribution of each one of the $3 + (8 \times 2)$ diagrams (here, the number 2 refers to the possibility of diagrams that have the same topology, but with external gluons legs crossed) entering in the SDE [see Fig. 3.3].

From the $3 + (8 \times 2)$ contributions, we check that in this limit, only 2×2 survives [see Fig. 4.7]. The final expression for those 2×2 diagrams depends only on (i) the gluon, and (ii) the ghost propagators, and (iii) the $BQ\bar{c}c$ vertex in a particular kinematic limit, *i.e.*, $\tilde{\Gamma}_{\mu\nu}^{abmn}(0, -t, 0, t)$. Using the WTI satisfied by the $BQ\bar{c}c$ vertex, it is possible to express $\tilde{\Gamma}_{\mu\nu}^{abmn}(0, -t, 0, t)$ in terms of the well-known ghost-gluon form factor B_1 . Combining the above results, it turns out, the $BB\bar{c}c$ vertex may be expressed in terms of a unique form factor, which accompanies the metric tensor, in the all-soft limit. More specifically, we establish that the form factor is nothing else than the ghost dressing function at the origin, $F(0)$.

It should be emphasized that the above derivation is an exact relation, valid to all orders in perturbation theory, and it consists in the main result of this work and represents a novel contribution in the literature. An alternative way to derive the same relation is using the WTI that the $BB\bar{c}c$ vertex satisfies.

From the point of view of the SDE derivation, it is important to point out that the derivation of exact results is rare in the literature, even considering special limits. With this in mind, we envisage how the exact relation obtained may be used as a guideline for developing a future truncation scheme for this vertex in general kinematics. To do that, we propose three different truncation scenarios for the $BB\bar{c}c$ SDE, in the all-soft limit, and then we check by how much they deviate from the exact value.

This thesis is organized in the following way. Chapter 1 presents a brief introduction to QCD. We start with the QCD Lagrangian, revealing its Feynman rules and discussing the property of asymptotic freedom. Then, in Chapter 2, we begin with the general functional formalism of QFTs, and introduce the BFM and its new Green's functions and Feynman rules. In addition, we show the corresponding WTIs some of these Green's functions satisfy. We also present some remarkable features of the BFM. In Chapter 3, we use the functional formalism to derive the so-called master SDE and then specify to QCD. We begin with the derivation of the SDE for the ghost propagator as a warm-up, and next, we derive the SDE for the $BB\bar{c}c$ vertex, which will be carefully scrutinized throughout this work. In Chapter 4, we present our main results. More specifically, we

perform the all-soft limit in the diagrams contributing to the $BB\bar{c}c$ SDE. Then, combining the previous step with the WTI that $BQ\bar{c}c$ satisfies, we arrive at an exact result, valid to all orders, for the $BB\bar{c}c$ in all-soft limit. We close this Chapter by considering three different truncation schemes for the $BB\bar{c}c$ SDE in the all-soft limit, and we check which one has more potential to produce results which are in better agreement with the exact result. Finally, in Chapter 5, we conclude with a brief discussion about the results of this work.

In addition, we include four appendices. Appendix A collects all helpful relations that the $SU(3)$ totally anti-symmetric structure constant satisfies. Appendix B contains details about the most general basis for rank-2 Minkowski and rank-4 color tensors. In Appendix C, we summarize the transformations rules from Minkowski to Euclidean space. In addition, we define the Euclidean measure in 4D spherical coordinates and the corresponding scalar products. Finally, in Appendix D, we present the numerical integration methods performed in this thesis.

Brief introduction to QCD

In this Chapter we present a brief introduction to QCD, which is the quantum theory that describes the strong interaction between quarks and gluons. In Section 1.1 we introduce the fields and the QCD Lagrangian. Then, we proceed revealing the Feynman rules and mentioning some important properties of this theory. Section 1.2 is dedicated to review the concept of asymptotic freedom.

1.1 QCD Lagrangian and Feynman rules

QCD is a non-Abelian QFT that describes the strong force interaction, acting in elementary particles with *color charge*, the quarks and gluons, composing the hadrons. Hadrons can be baryons, compound by three quarks, or mesons, formed by a quark and an antiquark.

Quarks are the fermions of the theory, they have spin $\frac{1}{2}$ and fractional charge. According to the *standard model of elementary particles*, quarks can have six flavours: up (u), down (d), strange (s), charm (c), bottom (b), and top (t). They can carry three color charges: red, green, and blue (RGB). In nature, quarks (antiquarks) combine to form the hadrons, which are colorless particles.

Gluons have spin 1 and are the gauge bosons, *i.e.*, the interaction mediators, of the theory. They are color charged and therefore interact with each other, giving rise to one of the most peculiar characteristic of QCD, which is the self-interaction between its gauge fields.

QCD is a renormalizable, non-Abelian gauge theory, invariant under the sym-

metry gauge group SU(3) and has the following Lagrangian [56]

$$\mathcal{L}_{\text{QCD}} = \mathcal{L}_{\text{Dirac}} + \mathcal{L}_{\text{YM}} + \mathcal{L}_{\text{GF}} + \mathcal{L}_{\text{Ghost}}, \quad (1.1)$$

with

$$\mathcal{L}_{\text{Dirac}} = \bar{\psi}(i\gamma^\mu D_\mu - m)\psi, \quad (1.2)$$

$$\mathcal{L}_{\text{YM}} = -\frac{1}{4}G_{\mu\nu}^a G_a^{\mu\nu}, \quad (1.3)$$

$$\mathcal{L}_{\text{GF}} = -\frac{1}{2\xi}(\partial^\mu A_\mu^a)^2, \quad (1.4)$$

$$\mathcal{L}_{\text{Ghost}} = \bar{c}^a(-\partial^\mu D_\mu^{ac})c^c, \quad (1.5)$$

where $\mathcal{L}_{\text{Dirac}}$ is the Dirac Lagrangian, \mathcal{L}_{YM} is the Yang-Mills Lagrangian, \mathcal{L}_{GF} is the gauge fixing Lagrangian, and $\mathcal{L}_{\text{Ghost}}$ is the ghost Lagrangian.

The Dirac Lagrangian describes the quarks and antiquarks, represented by the spinors ψ and $\bar{\psi}$, respectively, and generates the *Feynman rules* of the *quark propagator*, $S_F^{(0)ab}(q)$, shown in Fig. 1.1, as well as the interaction between quarks and gluons represented by the *quark-gluon vertex*, $\Gamma_{q,\mu}^{(0)}(q, r, p)$, shown in Fig. 1.2.

The term γ^μ in Eq. (1.2) is the Dirac matrix, while D_μ is the covariant derivative in the fundamental representation given by

$$D_\mu = \partial_\mu - igA_\mu^a \frac{\lambda^a}{2}, \quad (1.6)$$

where g is the coupling constant, A_μ^a is the gauge field representing the gluon, and λ^a is the Gell-Mann matrix, that respects the commutation relation

$$\left[\frac{\lambda^a}{2}, \frac{\lambda^b}{2} \right] = if^{abc} \frac{\lambda^c}{2}, \quad (1.7)$$

with f^{abc} the totally antisymmetric structure constant characterizing the group algebra¹.

The Yang-Mills Lagrangian encodes the non-Abelian property of the theory

¹Some of the properties of the totally antisymmetric structure constant will be presented in Appendix A.

once the tensor $G_{\mu\nu}^a$, that is given by

$$G_{\mu\nu}^a = \partial_\mu A_\nu^a - \partial_\nu A_\mu^a + gf^{abc}A_\mu^b A_\nu^c, \quad (1.8)$$

generates the conventional *three and four-point gluon self-interaction vertices*, $\Gamma_{\alpha\mu\nu}^{(0)abc}(q, r, p)$ and $\Gamma_{\alpha\beta\mu\nu}^{(0)abcd}(q, r, p, t)$, respectively, shown in Fig. 1.2.

The gauge fixing term is introduced during the quantization process of the theory. Together with the Yang-Mills term will generate the gluon propagator, $\Delta_{\mu\nu}^{(0)ab}(q)$, shown in Fig. 1.1. The ξ appearing in Eq. (1.4) is the gauge fixing parameter.

The gauge fixing process leads to the introduction of auxiliary fields, the ghosts and antighosts represented by the scalar fields c and \bar{c} , respectively [57]. In QCD, the ghosts couple to the gauge fields, and their presence are crucial to preserve the unitarity of the theory.

The ghost Lagrangian generates the *ghost propagator*, $D^{(0)mn}(q)$, shown in Fig. 1.1, and also the interaction between ghosts and gluons represented by the *ghost-gluon vertex*, $\Gamma_\mu^{(0)mna}(r, p, q)$, shown in Fig. 1.2. The covariant derivative in Eq. (1.5) is in the adjoint representation and it is given by

$$D_\mu^{ab} = \delta^{ab}\partial_\mu - gf^{abc}A_\mu^c, \quad (1.9)$$

where δ^{ab} is the Kronecker delta.

Ghosts are scalar fields, *i.e.*, they have spin 0, but obey the Fermi-Dirac statistics, violating the *Spin-Statistics theorem*. For that reason the ghosts are strictly virtual particles and cannot appear as asymptotic states.

The Feynman rules quoted above can only be applied in the weak coupling limit of the theory, where the perturbative treatment is valid. However, as we will see in the next Section, the QCD non-Abelian behaviour will induce a weak coupling at high energies, and a strong coupling at low energies.

It is important to stress here that the QCD Lagrangian, \mathcal{L}_{QCD} , given in Eq. (1.1), consisting of the classical term plus the gauge-fixing and the Faddeev–Popov ghost terms is no longer gauge invariant, but rather BRST invariant. As a consequence, off-shell Green’s functions satisfy complicated STIs reflecting BRST invariance [12].

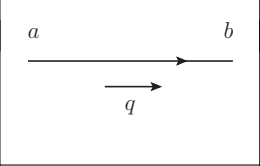
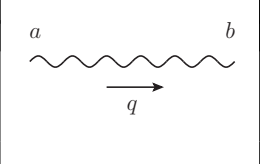
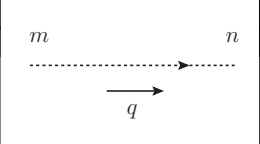
	$S_F^{(0)ab}(q) = i\delta^{ab}S_F^{(0)}(q)$	$S_F^{(0)}(q) = \frac{(\gamma^\mu q_\mu + m)}{q^2 - m^2 + i\epsilon}$
	$\Delta_{\mu\nu}^{(0)ab}(q) = -i\delta^{ab}\Delta_{\mu\nu}^{(0)}(q)$	$\Delta_{\mu\nu}^{(0)}(p) = \frac{1}{q^2 + i\epsilon} \left[g_{\mu\nu} - (1 - \xi) \frac{q_\mu q_\nu}{q^2} \right]$
	$D^{(0)mn}(q) = i\delta^{mn}D^{(0)}(q)$	$D^{(0)}(q) = \frac{1}{q^2 + i\epsilon}$

Figure 1.1: Diagrammatic representations for the quark, gluon, and ghost propagators together with their respective Feynman rules at tree-level.

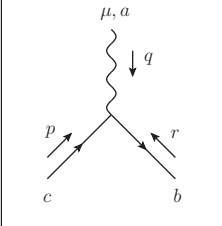
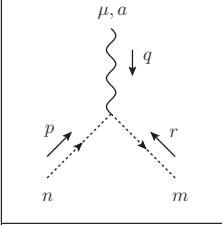
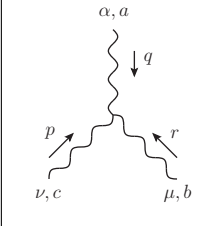
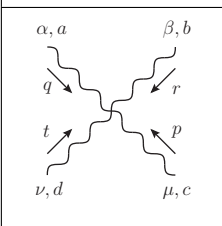
	$\Gamma_{q,\mu}^{(0)}(q, r, p) = ig \frac{\lambda^a}{2} \Gamma_{q,\mu}^{(0)}$ (Qq̄q)	$\Gamma_{q,\mu}^{(0)}(q, r, p) = \gamma^\mu$
	$\Gamma_\mu^{(0)}(r, p, q) = -gf^{mna}\Gamma_\mu^{(0)}$ (Qc̄c)	$\Gamma_\mu^{(0)}(r, p, q) = r_\mu$
	$\Gamma_{\alpha\mu\nu}^{(0)abc}(q, r, p) = gf^{abc}\Gamma_{\alpha\mu\nu}^{(0)}$ (QQQ)	$\Gamma_{\alpha\mu\nu}^{(0)}(q, r, p) = g_{\mu\nu}(r - p)_\alpha$ $+ g_{\alpha\nu}(p - q)_\mu$ $+ g_{\alpha\mu}(q - r)_\nu$
	$\Gamma_{\alpha\beta\mu\nu}^{(0)abcd}(q, r, p, t) = -ig^2\Gamma_{\alpha\beta\mu\nu}^{(0)abcd}$ (QQQQ)	$\Gamma_{\alpha\beta\mu\nu}^{(0)abcd} = f^{adx}f^{xcb}(g_{\alpha\mu}g_{\beta\nu} - g_{\alpha\beta}g_{\mu\nu})$ $+ f^{abx}f^{xdc}(g_{\alpha\nu}g_{\beta\mu} - g_{\alpha\mu}g_{\beta\nu})$ $+ f^{acx}f^{xdb}(g_{\alpha\nu}g_{\beta\mu} - g_{\alpha\beta}g_{\mu\nu})$

Figure 1.2: The diagrammatic representations of the QCD conventional vertices and their respective Feynman rules at tree-level.

1.2 Asymptotic freedom

To understand the *asymptotic freedom* we need to look at the behavior of the QCD coupling constant, $\alpha_s(Q^2) = g^2/4\pi$, which sets the strength of the strong interaction as a function of the transferred momentum, Q^2 . In a renormalizable field theory, the coupling constant and the masses acquire a scale dependent correction. Then, in order to eliminate the UV-cutoff dependence, those corrections are renormalized to known values at a given scale, μ .

The existence of asymptotic freedom in QCD can be verified by studying the β function of the theory, defined through the *Callan-Symanzik* equation [58]. The β function expresses the rate at which the renormalized coupling constant, $\alpha_s(\mu^2)$, changes as the renormalization scale, μ , increases. The calculation of the β function of QCD was first done simultaneously by Gross and Wilczek [3] and Politzer [4].

Then, the renormalization group equation for the QCD β function is given by

$$\beta(\alpha_s) = \mu \frac{d\alpha_s(\mu^2)}{d\mu}. \quad (1.10)$$

Expanding the β function perturbatively, one arrives that

$$\beta(\alpha_s) = \mu \frac{d\alpha_s(\mu^2)}{d\mu} = - \left[\frac{\alpha_s^2}{\pi} \beta_0 + \frac{\alpha_s^3}{\pi^2} \beta_1 + \dots \right], \quad (1.11)$$

with

$$\beta_0 = \left[\frac{11}{6} C_A - \frac{1}{3} n_f \right], \quad \beta_1 = \left[\frac{17}{12} C_A^2 - \frac{1}{24} n_f (10 C_A + 6 C_F) \right], \quad (1.12)$$

where $C_A = N$ ($C_F = \frac{N^2-1}{2N}$) is the eigenvalue of the quadratic Casimir operator from the symmetry group SU(N) in the adjoint (fundamental) representation, and n_f is the number of fermions.

Keeping only the first term of the β function expansion (one-loop approximation) one can solve the above differential equation and determine that the coupling constant is given by

$$\alpha_s(Q^2) = \frac{2\pi}{\beta_0 \ln(Q^2/\Lambda_{\text{QCD}}^2)}, \quad (1.13)$$

where the renormalization scale was removed in favor of the QCD scale, Λ_{QCD} , defined as

$$\Lambda_{\text{QCD}} = \mu \exp \left[\frac{\pi}{\alpha_s(\mu^2)\beta_0} \right]. \quad (1.14)$$

First notice from Eq. (1.13) that as $Q^2 \rightarrow \Lambda_{\text{QCD}}^2$, the denominator has a pole and the coupling diverges. This pole, known as the *Landau pole*, determines the momentum scale in whose neighborhood the perturbative treatment is not anymore applicable. Typically, the value of Λ_{QCD} lies in the range of 300 – 400 MeV, or approximately 1 fm in distance terms (confining region).

Furthermore, one can see that the sign of β_0 defines in which direction the Landau pole is to be found, and hence in which regime the perturbative approach is suitable or not. Therefore, it is crucial to analyze what happens with Eq. (1.13) when the sign of β_0 in Eq. (1.12) flips. If β_0 is negative, the QCD displays a weak coupling in the IR, and this coupling increases towards the UV. Conversely, a positive β_0 assures a weakly-coupled theory in the UV that becomes strongly coupled in the IR. This behavior is called asymptotic freedom [3, 4].

Applying Eq. (1.12) for the color group SU(3), *i.e.*, with $C_A = 3$, one can conclude that, for the known number of quark flavors (or more generally up until $n_f \leq 16$), we have asymptotic freedom, *i.e.*, the coupling decreases when the momentum increases. Such a feature results in the quarks behaving almost as free particles at short distances (high energy limit), as experimentally checked in the deep inelastic scattering. In addition, asymptotic freedom allows us to apply perturbative methods and treat the coupling constant as a good expansion parameter in the UV limit.

In Fig. 1.3, we present the behavior of $\alpha_s(Q^2)$ as a function of the momentum scale Q in GeV, extracted from the Particle Data Group latest review [59]. It is important to point out here that the QCD coupling, $\alpha_s(Q^2)$, is not a physical observable itself, and therefore it cannot be measured directly in an experiment. However, its extraction can be made indirectly, combining theoretical and experimental results. It is precisely this type of procedure that was applied in Fig. 1.3.

Finally, notice that around the region of 1 GeV, we reach the QCD nonperturbative regime. This regime accommodates the most peculiar features of the theory and its challenges, such as color confinement, dynamical mass generation, and bound state formation, which requires techniques beyond perturbation theory. One of these tools are

the SDEs, which will be the main formalism employed in this work. Chapter 3 of this thesis will be entirely dedicated to introducing them.

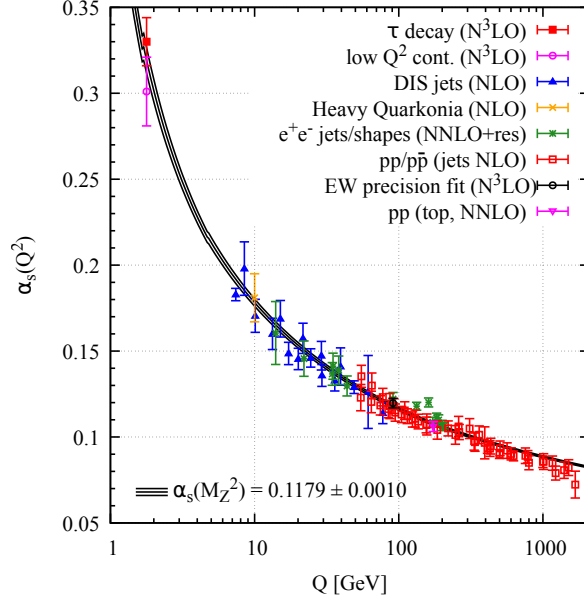


Figure 1.3: Summary of measurements of $\alpha_s(Q^2)$ as a function of the momentum scale Q [GeV] obtained from [59]. The corresponding degree of perturbation theory used in the extraction of $\alpha_s(Q^2)$ is indicated in brackets (NLO: next-to-leading order; NNLO: next-to-next-to-leading order; NNLO+res: NNLO matched to a resummed calculation; N³LO: next-to-NNLO).

The Background Field Method

In the previous Chapter, we have mentioned that in the conventional formulation of QCD, the \mathcal{L}_{QCD} , expressed by Eq. (1.1), is not gauge invariant but rather BRST invariant. In this Chapter, we will introduce the BFM, which allows the evaluation of the effective action by exploiting the background gauge invariance [55]. In this formalism, the QCD effective action is computed by expanding the gauge field, A_μ^a , around a classical “background” field, B_μ^a . After performing this expansion, a new set of Green’s functions emerge in this formalism that automatically satisfies naive, QED-like WTIs [12, 55]. This property is a noticeable technical advantage compared to those Green’s functions that respect the complicated STIs.

One of the consequences of the latter property is that the BFM enormously simplifies the perturbative calculation of the β function, since we do not need to determine the renormalization constants related to the vertices [55].

In addition, the BFM has also been successfully applied to the study of non-perturbative QCD [11, 12, 15]. In the particular case of the SDE for the gluon propagator, it was possible to build a systematic truncation scheme that respects manifestly the transversality of the gluon self-energy at every step.

Here, the main focus of our project is to analyze the nonperturbative structure of the $BB\bar{c}c$ vertex. To do that, we first have to derive the SDE governing its dynamics within the framework of the BFM. Then, in order to compute the behavior of this vertex in the all-soft limit, we will judiciously use the special properties this BFM Green’s function obeys, in conjunction with the ones satisfied by the other BFM n-point functions nested in its SDE. For this reason, the central motivation of this Chapter is to introduce the

main ideas of the BFM and the special properties that this new set of Green's functions are endowed.

This Chapter is organized as follows. In Section 2.1, we briefly review the functional formalism for a scalar theory. Then, in Section 2.2, we discuss the basic ideas of the BFM, revealing the Feynman rules to the new set of Green's functions in Section 2.3. In Section 2.4, we present the difficulty in finding a suitable truncation scheme for the conventional gluon SDE in which the transversality of the self-energy is preserved. In Section 2.5, we collect the WTIs which some of the special BFM Green's functions satisfy. We conclude by presenting, in Section 2.6, the SDE for the gluon propagator in the BFM formalism, which allows for symmetry preserving truncation.

2.1 Functional formalism

The aim of this Section is to introduce the *functional formalism* within the concept of *Feynman path integrals*. The path integral formalism is originated from the theoretical formulation of the *two slits experiment* [60]. The path integrals are the continuum limit of all the possible paths a system can evolve from an initial state to a final one [40]. It is a completely different formalism from the canonical approach based on creation and destruction operators used in the beginnings of the QFT.

This formalism is based on the fact that the Green's functions of the theory can be calculated with path integrals through the ratio [60]

$$\langle \Omega | T \{ \phi_i(x_1) \dots \phi_j(x_n) \} | \Omega \rangle = \frac{\int \mathcal{D}[\phi] \phi_i(x_1) \dots \phi_j(x_n) e^{iS[\phi]}}{\int \mathcal{D}[\phi] e^{iS[\phi]}}, \quad (2.1)$$

where Ω is the interacting vacuum, T is the time ordering operator, ϕ_i is a scalar field with the index i denoting its type or degree of freedom, and $S = \int d^4x \mathcal{L}$ is the action of the theory. The symbol ϕ represents the collective of fields ϕ_i , so that the integral measure is

$$\mathcal{D}[\phi] \equiv \prod_i \mathcal{D}[\phi_i]. \quad (2.2)$$

An efficient way to calculate these path integrals is through the *generating*

functional

$$Z[J] = \int \mathcal{D}[\phi] \exp \left\{ iS[\phi] + i \int d^4x J_i(x) \phi_i(x) \right\}, \quad (2.3)$$

where $J_i(x)$ is the external source associated with the scalar field $\phi_i(x)$, and J represents the collective of sources $J_i(x)$.

Note that the Green's functions appearing on the left-hand side (LHS) of Eq. (2.1) can be obtained from $Z[J]$ by taking functional derivatives of Eq. (2.3) with respects to the source, *i.e.*,

$$\langle \Omega | T \{ \phi_i(x_1) \dots \phi_j(x_n) \} | \Omega \rangle = (-i)^n \frac{1}{Z[0]} \frac{\partial^n Z}{\partial J_i(x_1) \dots \partial J_j(x_n)} \Bigg|_{J=0}. \quad (2.4)$$

From Eq. (2.4) one can see that the propagator of the scalar field ϕ_i is given by

$$\langle \Omega | T \{ \phi_i(x_1) \phi_i(x_2) \} | \Omega \rangle = - \frac{1}{Z[0]} \frac{\partial^2 Z}{\partial J_i(x_1) \partial J_i(x_2)} \Bigg|_{J=0}. \quad (2.5)$$

The complete n-point function given by Eq. (2.4) contains disconnected and connected contributions. Diagrammatic examples of these two types of contributions are illustrated in Fig. 2.1. We have two classes of connected contributions: (i) the *improper* and (ii) the *proper* ones. The improper diagrams can be split into two independent diagrams by removing a unique line. On the other hand, the improper or *one-particle irreducible* (1PI) cannot be separated by removing one line.

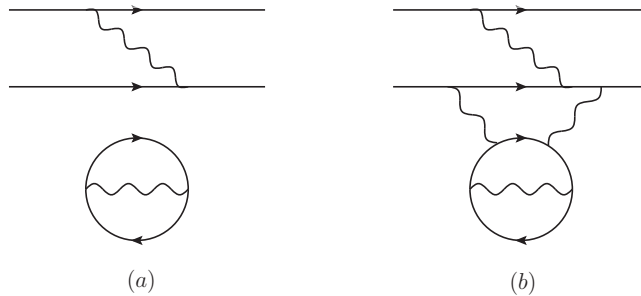


Figure 2.1: The diagram (a) is an example of a disconnected diagram while (b) is a connected one.

Disconnected diagrams do not contribute to the final observable and introduce infinities to the formalism. Then, to eliminate their contribution we use the generating functional

$$W[J] = -i \ln Z[J]. \quad (2.6)$$

Combining Eqs. (2.4) and (2.6) one can express the n-point Green's function in terms of only 1PI diagrams in the following way

$$\langle \Omega | T \{ \phi_i(x_1) \dots \phi_j(x_n) \} | \Omega \rangle = \frac{1}{i^{n-1}} \frac{\partial^n W[J]}{\partial J_i(x_1) \dots \partial J_j(x_n)} \Big|_{J=0}. \quad (2.7)$$

To obtain the three-point or higher n-point Green's functions, it is necessary to do a *Legendre transformation* of $W[J]$, given by

$$\Gamma[\bar{\phi}] = W[J] - \int d^4x J_i(x) \bar{\phi}_i(x), \quad (2.8)$$

where $\Gamma[\bar{\phi}]$ is the vertices generator, the so-called *effective action*, and $\bar{\phi}_i(x)$ is the vacuum expectation value (VEV) of the field $\phi_i(x)$ in the presence of the source $J_i(x)$. By taking derivatives of Eq. (2.8), one can obtain the following relations

$$\bar{\phi}_i = \frac{\delta W[J]}{\delta J_i(x)} = \frac{-i}{Z[J]} \frac{\delta Z[J]}{\delta J_i(x)}, \quad \frac{\delta \Gamma[\bar{\phi}]}{\delta \bar{\phi}_i(x)} = -J_i(x). \quad (2.9)$$

In the above expression, the external current, $J(x_i)$, acts only in the differentiation and then is set to zero. When this is done, usually the VEVs of the fields go to zero as well. The only exception will be in the case of spontaneously broken symmetry theories.

We close this Section showing two significant results. The first one relates the two-point connected Green's function to the 1PI. This relation can be derived rewriting the Dirac delta function with the help of Eq. (2.9). More specifically, we have that

$$\begin{aligned} \frac{\delta \bar{\phi}_i(x)}{\delta \bar{\phi}_j(z)} &= \delta_{ij} \delta(x-z) = \int d^4y \frac{\delta \bar{\phi}_i(x)}{\delta J_k(y)} \frac{\delta J_k(y)}{\delta \bar{\phi}_j(z)} \\ &= - \int d^4y \left(\frac{\delta^2 W[J]}{\delta J_k(y) \delta J_i(x)} \right) \left(\frac{\delta^2 \Gamma[\bar{\phi}]}{\delta \bar{\phi}_j(z) \delta \bar{\phi}_k(y)} \right), \end{aligned} \quad (2.10)$$

and thus we arrive at

$$\frac{\delta^2 \Gamma[\bar{\phi}]}{\delta \bar{\phi}_i(x) \delta \bar{\phi}_i(z)} = - \left(\frac{\delta^2 W[J]}{\delta J_i(x) \delta J_i(z)} \right)^{-1}. \quad (2.11)$$

The second result is the derivative of inverse propagators, and its derivation

explores the identity relation of an operator, *i.e.*,

$$\frac{\delta(O^{-1}[\phi]O[\phi])}{\delta\phi} = 0. \quad (2.12)$$

Applying the above relation for the two-point connected Green's function, one finds

$$\begin{aligned} \frac{\delta}{\delta\bar{\phi}_i(x)} \left(\frac{\delta^2\Gamma[\bar{\phi}]}{\delta\bar{\phi}_j(y)\bar{\phi}_k(z)} \right)^{-1} &= - \int d^4u d^4v \left(\frac{\delta^2\Gamma[\bar{\phi}]}{\delta\bar{\phi}_j(y)\bar{\phi}_m(u)} \right)^{-1} \times \\ &\times \frac{\delta^3\Gamma[\bar{\phi}]}{\delta\bar{\phi}_m(u)\delta\bar{\phi}_i(x)\bar{\phi}_n(v)} \left(\frac{\delta^2\Gamma[\bar{\phi}]}{\delta\bar{\phi}_n(v)\bar{\phi}_k(z)} \right)^{-1}. \end{aligned} \quad (2.13)$$

2.2 Background Field Method

The basic idea of the BFM is to split the gauge field, A_μ^a , into a *classical background field*, B_μ^a , and a fluctuating quantum field, Q_μ^a , [61, 62] *i.e.*,

$$A_\mu^a \rightarrow B_\mu^a + Q_\mu^a. \quad (2.14)$$

First, we will be interested in the effect of this shift at the level of the generating functional of the quenched QCD (*i.e.*, without quark fields).

After applying the Faddeev-Popov procedure to quantize the quenched QCD Lagrangian [57], one obtains that its generating functional will be given by

$$Z[J_\mu] = \int \mathcal{D}[A] \det[M] \exp \left\{ i \int d^4x [\mathcal{L}_{\text{YM}} + \mathcal{L}_{\text{GF}} + J_\mu^a(x) A_\mu^a(x)] \right\}, \quad (2.15)$$

where \mathcal{L}_{YM} is given in Eq. (1.3), and M is the *Faddeev-Popov operator*, defined as

$$M = \frac{\delta F^a[A(x)]}{\delta\omega^b(y)}, \quad (2.16)$$

with $F^a[A(x)]$ the gauge fixing condition, and ω^b the gauge transformation parameter related with the gauge field by

$$\delta A_\mu^a = \frac{1}{g} \partial_\mu \omega^a - f^{abc} \omega^b A_\mu^c. \quad (2.17)$$

First, let us analyze Eq. (2.15) in the Lorentz gauge, *i.e.*, $F^a[A(x)] = \partial^\mu A_\mu(x)$. In this case \mathcal{L}_{GF} is given by Eq. (1.4) and the Faddeev-Popov operator reduces to M_{xy}^{ab}

given by

$$M_{xy}^{ab} = \partial_x^\mu D_{\mu,x}^{ab} \delta(x-y). \quad (2.18)$$

The term $\det[M]$ in Eq. (2.15) may be conveniently expressed as a path integral over the ghost and antighosts fields. Thus, Eq. (2.15) becomes

$$Z[J_\mu^a, j_c, j_{\bar{c}}] = \int \mathcal{D}[A] \mathcal{D}[\bar{c}] \mathcal{D}[c] \exp \left\{ i \int d^4x [\mathcal{L}_{\text{YM}} + \mathcal{L}_{\text{GF}} + \mathcal{L}_{\text{Ghost}} + \mathcal{J}] \right\}, \quad (2.19)$$

with

$$\mathcal{J} = J_\mu^a(x) A_\mu^a(x) + \bar{c}^a(x) j_c^a(x) + \bar{j}_c^a(x) c^a(x), \quad (2.20)$$

and

$$\mathcal{L}_{\text{Ghost}} = - \int_y \bar{c}^a(x) M_{xy}^{ab} c^b(y) = \bar{c}^a(x) (-\partial^\mu D_\mu^{ab}) c^b(y), \quad (2.21)$$

where $\bar{j}_c^a(x)$ and $j_c^a(x)$ are the external currents associated with the ghost and antighost fields, respectively.

Now that we have the expression for the generating functional written in terms of the ghost fields, we want to see how it will be affected by the shift from Eq. (2.14). From now on we will employ a general gauge fixing condition given by

$$\mathcal{L}_{\text{GF}} = - \frac{(F^a[A])^2}{2\xi}. \quad (2.22)$$

When performing the shift, we treat the classical field, B_μ^a , as a fixed field configuration [54], and the fluctuating part, Q_μ^a , as the integration variable of the functional integral. Under these considerations we arrive that

$$Z[J] \rightarrow \tilde{Z}[J, B], \quad F^a[A] \rightarrow \tilde{F}^a[Q, B], \quad \mathcal{L}_{\text{YM}} \rightarrow \mathcal{L}'_{\text{YM}}. \quad (2.23)$$

Then, applying this change of variables into the generating functional of Eq. (2.19),

we obtain

$$\tilde{Z}[J, B] = \int \mathcal{D}[Q] \det[\tilde{M}] \exp \left\{ i \int d^4x [\mathcal{L}'_{\text{YM}} + \mathcal{L}'_{\text{GF}} + J_\mu^a(x) Q_\mu^a(x)] \right\}, \quad (2.24)$$

with the Faddeev-Popov operator being

$$\tilde{M}_{xy}^{ab} = \frac{\delta \tilde{F}^a[Q(x), B(x)]}{\delta \omega^b(y)}, \quad (2.25)$$

and $\omega^b(y)$ the parameter appearing in the gauge transformation of the field Q_μ^a ,

$$\delta Q_\mu^a = D_\mu^{ab}[Q + B] \omega^b \equiv [\delta^{ab} \partial_\mu + g f^{acb} (Q + B)_\mu^c] \omega^b. \quad (2.26)$$

Similarly, one can define the generating functional for connected functions, $\tilde{W}[J, B]$, as

$$\tilde{W}[J, B] = i \ln \tilde{Z}[J, B], \quad (2.27)$$

and for the 1PI, $\tilde{\Gamma}[Q, B]$, as

$$\tilde{\Gamma}[Q, B] = \tilde{W}[J, B] - \int d^4x J_\mu^a(x) Q_\mu^a(x), \quad (2.28)$$

with $Q_\mu^a(x)$ being the VEV¹ of the quantum field, that is,

$$Q_\mu^a = \frac{\delta \tilde{W}}{\delta J_\mu^a}. \quad (2.29)$$

It is possible to show performing the shift $Q_\mu^a \rightarrow A_\mu^a - B_\mu^a$ in Eq. (2.24) that $\tilde{Z}[J, B]$ is connected to $Z[J]$ by the relation

$$\tilde{Z}[J, B] = Z[J] \exp \left[-i \int d^4x J_\mu^a(x) B_\mu^a(x) \right], \quad (2.30)$$

where $Z[J]$ is computed in a gauge fixing condition $F^a[Q] = \tilde{F}^a[A - B, B]$.

¹Notice that we dropped the VEV notation as a bar over the field, which was introduced in the previous Section, to avoid misunderstanding with the antighost field.

Taking the logarithm of Eq. (2.30) we arrive that

$$\widetilde{W}[J, B] = i \ln Z[J] - \int d^4x J_\mu^a(x) B_\mu^a(x) = W[J] - \int d^4x J_\mu^a(x) B_\mu^a(x). \quad (2.31)$$

Using Eq. (2.28) into Eq. (2.31) we get that

$$\widetilde{\Gamma}[Q, B] = W[J] - \int d^4x J_\mu^a(x) A_\mu^a(x) = \Gamma[A] = \Gamma[Q + B]. \quad (2.32)$$

From the above result, particularly from $\widetilde{\Gamma}[0, B] = \Gamma[B]$, one can see that the BFM effective action corresponds to the usual effective action when the VEV of the quantum field is set to zero. Therefore, since the same effective action describes the BFM, one can conclude that the BFM is physically equivalent to the conventional formalism of the theory [63].

Moreover, a specific choice of gauge,

$$\widetilde{F}^a[Q, B] = \partial_\mu Q_\mu^a + g f^{abc} B_\mu^b Q_\mu^c, \quad (2.33)$$

the so-called *BFM gauge*, it will make both $\widetilde{Z}[J, B]$ and $\widetilde{W}[J, B]$ invariants under the transformations [55]

$$\delta B_\mu^a = -f^{abc} \omega^b B_\mu^c + \frac{1}{g} \partial_\mu \omega^a, \quad (2.34)$$

$$\delta J_\mu^a = -f^{abc} \omega^b J_\mu^c, \quad (2.35)$$

and $\widetilde{\Gamma}[Q, B]$ invariant under the transformation given in Eq. (2.34), and

$$\delta Q_\mu^a = -f^{abc} \omega^b Q_\mu^c. \quad (2.36)$$

With Eq. (2.34) we see that B_μ^a carries the local gauge transformation, and with Eq. (2.36) we see that Q_μ^a transforms as a matter field in the adjoint representation. When the VEV of Q_μ^a is zero, then $\delta Q_\mu^a = 0$, and $\widetilde{\Gamma}[0, B]$ is an explicitly gauge invariant functional of B_μ^a .

This is a very crucial result, since will imply that the 1PI Green's functions generated by the derivation of $\widetilde{\Gamma}[0, B]$ will respect WTIs, instead of complicated STIs satisfied by the conventional functions.

Since the focus of this work is to analyze the nonperturbative behaviour of a vertex that contains a ghost and an antighost leg, let us check what is the effect of the BFM change at the level of the ghost Lagrangian. The Faddeev-Popov operator, given by Eq. (2.25), combined with the BFM gauge of Eq. (2.33), becomes

$$\widetilde{M}_{xy}^{ab} = D_\mu[B(x)]^{ac} D_\mu[Q(x) + B(x)]^{cb}. \quad (2.37)$$

Then, with Eq. (2.37) at hand, one can see that the ghost Lagrangian of Eq. (1.5) becomes

$$\begin{aligned} \mathcal{L}_{\text{Ghost}} &= - \int d^4y \bar{c}^a(x) \widetilde{M}_{xy}^{ab} c^b(y) \\ &= c^a \partial^2 \bar{c}^a + g f^{abd} B_\mu^d \bar{c}^a \partial_\mu c^b + g f^{abe} (\partial_\mu \bar{c}^a) (Q + B)_\mu^e c^b - g^2 f^{adc} f^{ceb} B_\mu^d (Q + B)_\mu^e \bar{c}^a c^b. \end{aligned} \quad (2.38)$$

The above Lagrangian generates more Green's functions than the one given by Eq. (1.5). Particularly, the last term in Eq. (2.38) generates the four-point vertices, in particular the BB $\bar{c}c$ vertex, which is the main focus of this work. In the next Section, we detail some of the Green's functions emerging in the BFM.

2.3 BFM Green's functions

The aim of this Section is to introduce the new BFM Green's functions and establish their conventions and notations. Within the BFM, we have three gluon propagators: (i) the conventional one, $\Delta_{\mu\nu}(q)$, composed by two quantum gluons external legs (namely QQ), (ii) the mixed propagator, $\widetilde{\Delta}_{\mu\nu}(q)$, composed by one quantum gluon and one background gluon external leg (QB), and finally (iii) the background propagator, $\widehat{\Delta}_{\mu\nu}(q)$, composed by two background gluons external legs (BB). Note that the propagator with one background gluon external leg is represented by a “tilde”, while the one with two background gluons is represented by a “hat”. The diagrammatic representations of these three gluon propagators are shown in Fig. 2.2.

The Feynman rules for these vertices at tree-level are listed in Fig. 2.4.

	$\tilde{\Gamma}_{\alpha\mu\nu}^{(0)abc}(q, r, p) = g f^{abc} \tilde{\Gamma}_{\alpha\mu\nu}^{(0)}$ <p style="text-align: center;">(BQQ)</p>	$\begin{aligned} \tilde{\Gamma}_{\alpha\mu\nu}^{(0)}(q, r, p) &= g_{\mu\nu}(r-p)_\alpha \\ &+ g_{\alpha\nu}(p-q + \xi^{-1}r)_\mu \\ &+ g_{\alpha\mu}(q-r - \xi^{-1}p)_\nu \end{aligned}$
	$\tilde{\Gamma}_\mu^{(0)mna}(r, p, q) = -g f^{mna} \tilde{\Gamma}_\mu^{(0)}$ <p style="text-align: center;">(Bcc)</p>	$\tilde{\Gamma}_\mu^{(0)}(r, p, q) = (r-p)_\mu$
	$\tilde{\Gamma}_{\alpha\beta\mu\nu}^{(0)abcd}(q, r, p, t) = -ig^2 \tilde{\Gamma}_{\alpha\beta\mu\nu}^{(0)abcd}$ <p style="text-align: center;">(BQQQ)</p>	$\begin{aligned} \tilde{\Gamma}_{\alpha\beta\mu\nu}^{(0)abcd} &= f^{adx} f^{xcb} (g_{\alpha\mu} g_{\beta\nu} - g_{\alpha\beta} g_{\mu\nu}) \\ &+ f^{abx} f^{xdc} (g_{\alpha\nu} g_{\beta\mu} - g_{\alpha\mu} g_{\beta\nu}) \\ &+ f^{acx} f^{xdb} (g_{\alpha\nu} g_{\beta\mu} - g_{\alpha\beta} g_{\mu\nu}) \end{aligned}$
	$\hat{\Gamma}_{\alpha\beta\mu\nu}^{(0)abcd}(q, r, p, t) = -ig^2 \hat{\Gamma}_{\alpha\beta\mu\nu}^{(0)abcd}$ <p style="text-align: center;">(BBQQ)</p>	$\begin{aligned} \hat{\Gamma}_{\alpha\beta\mu\nu}^{(0)abcd} &= f^{abx} f^{xdc} (g_{\alpha\nu} g_{\beta\mu} - g_{\alpha\mu} g_{\beta\nu}) \\ &+ f^{adx} f^{xbc} (g_{\alpha\beta} g_{\mu\nu} - g_{\alpha\mu} g_{\beta\nu} + \xi^{-1} g_{\alpha\nu} g_{\beta\mu}) \\ &+ f^{acx} f^{xdb} (g_{\alpha\nu} g_{\beta\mu} - g_{\alpha\beta} g_{\mu\nu} - \xi^{-1} g_{\alpha\mu} g_{\beta\nu}) \end{aligned}$
	$\tilde{\Gamma}_{\mu\nu}^{(0)abmn}(q, r, p, t) = -ig^2 \tilde{\Gamma}_{\mu\nu}^{(0)abmn}$ <p style="text-align: center;">(BQcc)</p>	$\tilde{\Gamma}_{\mu\nu}^{(0)abmn} = f^{max} f^{xbn} g_{\mu\nu}$
	$\hat{\Gamma}_{\mu\nu}^{(0)abmn}(q, r, p, t) = -ig^2 \hat{\Gamma}_{\mu\nu}^{(0)abmn}$ <p style="text-align: center;">(BBcc)</p>	$\hat{\Gamma}_{\mu\nu}^{(0)abmn} = g_{\mu\nu} (f^{max} f^{xbn} + f^{mbx} f^{xan})$

Figure 2.4: The diagrammatic representations of the BFM new vertices and their respective Feynman rules at tree-level [12].

2.4 SDE for the gluon propagator

Truncating SDEs of a non-Abelian theory leaving the symmetries unharmed is highly nontrivial. In this Section we exemplify this issue for the conventional gluon propagator in order to motivate the need of a formalism that makes this truncation possible.

The SDE for the conventional gluon propagator is diagrammatically represented in Fig. 2.5 and written as²

$$[\Delta_{\mu\nu}(q)]^{-1} = [\Delta_{\mu\nu}^{(0)}(q)]^{-1} + \Pi_{\mu\nu}(q), \quad (2.42)$$

where $\Delta_{\mu\nu}(q)$ is the full propagator, and $\Pi_{\mu\nu}(q)$ is the gluon *self-energy*. In the general covariant gauge, the full propagator is given by

$$\Delta_{\mu\nu}(q) = P_{\mu\nu}(q)\Delta(q) + \xi \frac{q_\mu q_\nu}{q^4}, \quad (2.43)$$

where $P_{\mu\nu}(q)$ is the *transverse projector* given by

$$P_{\mu\nu}(q) = g_{\mu\nu} - \frac{q_\mu q_\nu}{q^2}, \quad (2.44)$$

and $\Delta(q)$ is the gluon scalar function which receives the all-order corrections.

For quenched QCD, $\Pi_{\mu\nu}(q)$ is given by the sum of the five diagrams, $(a_i)_{\mu\nu}$, shown in Fig. 2.5, *i.e.*,

$$\Pi_{\mu\nu}(q) = \sum_{i=1}^5 (a_i)_{\mu\nu}. \quad (2.45)$$

Notice that the longitudinal part of the gluon propagator does not acquire radiative contributions. This is a direct consequence of the STI satisfied by the gluon propagator, given by

$$q^\mu q^\nu \Delta_{\mu\nu}(q) = \xi. \quad (2.46)$$

Thus, combining Eqs. (2.42) and (2.46), one concludes that the gluon self-energy is trans-

²Here we omit the color structure of the gluon propagator, given by $\Delta_{\mu\nu}^{ab}(q) = -i\delta^{ab}\Delta_{\mu\nu}(q)$.

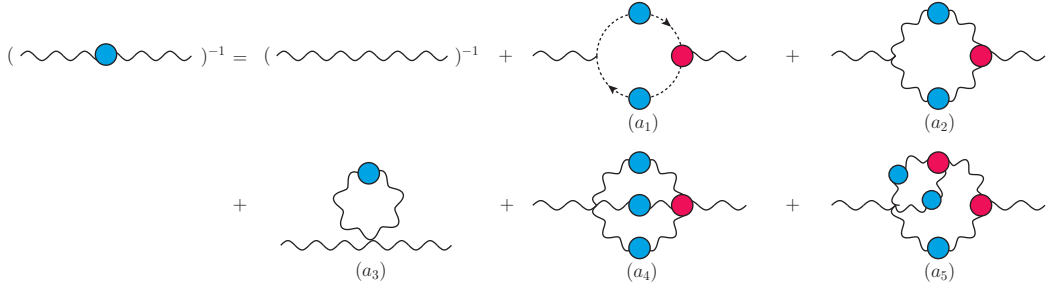


Figure 2.5: Diagrammatic representation for the gluon propagator SDE in Eq. (2.42) in quenched QCD. The sum of diagrams (a_i) furnishes the full gluon self-energy, $\Pi_{\mu\nu}(q)$. The blue circles represent the fully dressed propagators, and the pink circles correspond to the fully dressed vertices.

verse, *i.e.*,

$$q^\mu \Pi_{\mu\nu}(q) = 0, \quad (2.47)$$

with $\Pi_{\mu\nu}(q) = P_{\mu\nu}(q)\Pi(q)$. In particular, in the *Landau gauge*, where $\xi = 0$, the gluon propagator is purely transverse, a fact we will use throughout this work.

As we will see in Chapter 3, the SDEs form an infinite set of coupled integral equations, one for each n-point Green's functions. Evidently, this system cannot be solved exactly, and requires the implementation of a truncation scheme that preserves the fundamental QCD symmetries. However, enforce a scheme that fulfils such criteria is highly nontrivial. In the particular case of the SDE for the gluon propagator, it transpires that the process of truncation violates the gauge invariance of the theory, *i.e.*, Eq. (2.47) will not be satisfied.

One can see that by performing the one-loop perturbative calculations for the diagrams (a_1) , (a_2) and (a_3) in Eq. (2.45). The contribution of the ghost loop (in Minkowski space) is

$$\Pi_{\mu\nu}^{(1)}(q)|_{(a_1)} = -\frac{\lambda}{36}(3g_{\mu\nu}q^2 + 6q_\mu q_\nu)\ln\left(\frac{-q^2}{\mu^2}\right), \quad (2.48)$$

with

$$\lambda = \frac{iC_A g^2}{16\pi^2}. \quad (2.49)$$

The above expression was renormalized using the momentum subtraction scheme (MOM), such that $\Pi_{\mu\nu}(q)$ recovers its tree-level value at the momentum $q^2 = -\mu^2$. We can see

that Eq. (2.48) is not transverse, since it is not proportional to the transverse projector given in Eq. (2.44).

We obtain for the UV logarithms of diagrams (a_2) and (a_3)

$$\Pi_{\mu\nu}^{(1)}(q)|_{(a_2)} + \Pi_{\mu\nu}^{(1)}(q)|_{(a_3)} = -\frac{\lambda}{36}(75g_{\mu\nu}q^2 - 84q_\mu q_\nu)\ln\left(\frac{-q^2}{\mu^2}\right), \quad (2.50)$$

which is also not transverse. However, when we add the contributions from Eqs. (2.48) and (2.50), we obtain

$$\Pi_{\mu\nu}^{(1)}(q)|_{(a_1)} + \Pi_{\mu\nu}^{(1)}(q)|_{(a_2)} + \Pi_{\mu\nu}^{(1)}(q)|_{(a_3)} = -\frac{13\lambda}{6}(g_{\mu\nu}q^2 - q_\mu q_\nu)\ln\left(\frac{-q^2}{\mu^2}\right), \quad (2.51)$$

which is clearly transverse.

Therefore, we see that the ghost sector cannot be separated from the gluon sector, since diagram (a_1) has to be computed together with (a_2) and (a_3) to guarantee the transversality at one-loop level. Furthermore, already at two-loops, retaining only the first three diagrams would not be sufficient. We will see in the next Sections that it is possible to perform the separation of the self-energies of $\widehat{\Delta}_{\mu\nu}(q)$ and $\widetilde{\Delta}_{\mu\nu}(q)$ in blocks which are independently transverse [11, 12, 46]. The complete proof of this statement is presented to the mixed gluon propagator in Section 2.6.

2.5 Ward-Takahashi identities

Before embarking on the analysis of the transversality of the mixed gluon self-energy, one needs some of the WTIs that the new BFM Green's functions obey.

In this Section, we collect the WTIs which will be crucial to prove the blockwise transversality of the mixed gluon self-energy in Section 2.6, and to establish the all-soft limit of the $BB\bar{c}c$ vertex in Chapter 4.

Here we present the WTIs for the BQQ , $B\bar{c}c$, $BQQQ$, $BQ\bar{c}c$, and $BB\bar{c}c$ vertices summarized in Fig. 2.6. These identities are valid to all orders in perturbation theory. In particular, they can be verified at tree-level, applying the Feynman rules shown in Figs. 1.1, 1.2 and 2.4.

BQQ WTI	$q^\alpha \tilde{\Gamma}_{\alpha\mu\nu}(q, r, p) = \Delta_{\mu\nu}^{-1}(p) - \Delta_{\mu\nu}^{-1}(r)$
B $\bar{c}c$ WTI	$q^\mu \tilde{\Gamma}_\mu(r, p, q) = D^{-1}(p) - D^{-1}(r)$
BQQQ WTI	$q^\mu \tilde{\Gamma}_{\alpha\beta\mu\nu}^{abmn}(q, r, p, t) = f^{adb} f^{dmn} \Gamma_{\beta\mu\nu}(q + r, p, t)$ $+ f^{adm} f^{dbn} \Gamma_{\mu\beta\nu}(q + p, r, t)$ $+ f^{adn} f^{dbm} \Gamma_{\nu\beta\mu}(q + t, r, p)$
BQ $\bar{c}c$ WTI	$q^\mu \tilde{\Gamma}_{\mu\nu}^{abmn}(q, r, p, t) = f^{nax} f^{bmx} \Gamma_\nu(p, q + t, r)$ $+ f^{nbx} f^{max} \Gamma_\nu(q + p, t, r)$ $+ f^{nmx} f^{abx} \Gamma_\nu(p, t, q + r)$
BB $\bar{c}c$ WTI	$q^\mu \hat{\Gamma}_{\mu\nu}^{abmn}(q, r, p, t) = f^{max} f^{bnx} \tilde{\Gamma}_\nu(t, q + r, p)$ $+ f^{mbx} f^{nax} \tilde{\Gamma}_\nu(t + q, r, p)$ $+ f^{mnx} f^{abx} \tilde{\Gamma}_\nu(t, r, q + p)$

Figure 2.6: The WTIs satisfied by the BQQ, B $\bar{c}c$, BQQQ, BQ $\bar{c}c$, and BB $\bar{c}c$ vertices.

2.6 Background gluon propagator

In this Section, we follow the discussion of [39, 46] to show that the mixed gluon self-energy, $\tilde{\Pi}_{\mu\nu}(q)$, can be split into independent transverse groups, allowing for a truncation scheme that maintains the gauge symmetry.

The SDE for the mixed gluon propagator (QB), $\tilde{\Delta}_{\mu\nu}(q)$, is diagrammatically represented in Fig. 2.7. The diagrams contributing to its self-energy, $\tilde{\Pi}_{\mu\nu}(q)$, are the (a_i) , with $i = 1, 2, \dots, 6$.

In order to prove the transversality of $\tilde{\Pi}_{\mu\nu}(q)$, expressed by the condition given by Eq. (2.47), we will contract each one of the (a_i) diagrams with the background gluon momentum, q_ν , to trigger one of the corresponding WTIs listed in Fig. 2.4, and thus we check what are the combinations of diagrams which will be jointly transverse.

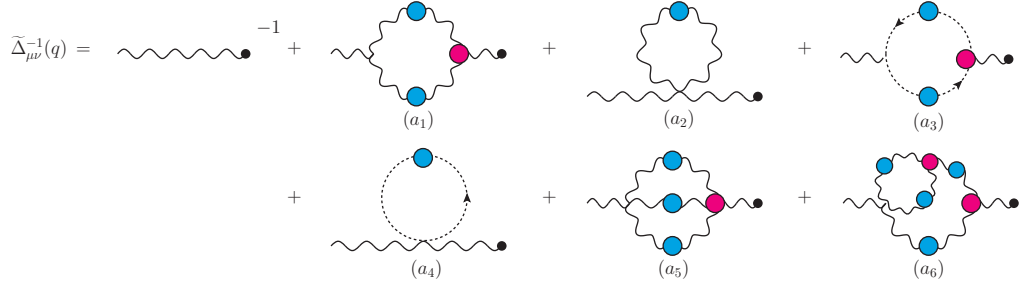


Figure 2.7: Diagrammatic representation of the SDE for the mixed gluon propagator (QB), $\tilde{\Delta}_{\mu\nu}(q)$. The sum of the contributions given by the diagrams (a_i) gives the full gluon self-energy, $\tilde{\Pi}_{\mu\nu}(q)$.

In what follows, we refer as “one-loop dressed” diagrams those contributions containing a unique dressed loop, *i.e.*, diagrams (a_1) , (a_2) , (a_3) , and (a_4) ; whereas those with two loops, *i.e.*, (a_5) and (a_6) , we call “two-loop dressed” contributions. Moreover, we introduce the shorthand notation

$$\int_k := \frac{1}{(2\pi)^4} \int d^4k . \quad (2.52)$$

At one-loop dressed level, the diagrams (a_1) and (a_2) furnish the gluonic contribution. Their respective analytical expressions are given by

$$\tilde{\Pi}_{\mu\nu}^{ab}(q)|_{(a_1)} = \frac{1}{2} \int_k \tilde{\Gamma}_{\nu\rho\beta}^{bd'c'}(-q, k+q, k) \Delta_{\alpha\beta}^{c'c}(k) \Delta_{\sigma\rho}^{dd'}(k+q) \Gamma_{\mu\alpha\sigma}^{(0)acd}(q, k, -q-k), \quad (2.53)$$

$$\tilde{\Pi}_{\mu\nu}^{ab}(q)|_{(a_2)} = \frac{1}{2} \int_k \Delta_{\alpha\beta}^{c'c}(k) \tilde{\Gamma}_{\nu\mu\beta\alpha}^{(0)bacc'}(-q, q, k, -k). \quad (2.54)$$

First, we contract the above equations with the momentum q_ν . Then, after the contraction, we replace into Eq. (2.54) the tree-level expression for the BQQQ vertex, $\tilde{\Gamma}_{\nu\mu\beta\alpha}^{(0)bacc'}(-q, q, k, -k)$, quoted in Fig. 2.4. On the other hand, for Eq. (2.53), the q_ν hits the fully dressed three gluon vertex, with one gluon in the background, and triggers the BQQ WTI, given in Fig. 2.6. Substituting the tree-level expression for the conventional three gluon vertex, $\Gamma_{\mu\alpha\sigma}^{(0)acd}(q, k, -q-k)$, given in Fig. 1.2, we find after performing a shift $k \rightarrow k - q$, that

$$q^\nu \tilde{\Pi}_{\mu\nu}^{ab}(q)|_{(a_1)} = -g^2 C_A \delta^{ab} \int_k [\Delta_{\mu\sigma}(k) q_\sigma - \Delta_{\alpha\alpha}(k) q_\mu], \quad (2.55)$$

$$q^\nu \tilde{\Pi}_{\mu\nu}^{ab}(q)|_{(a_2)} = g^2 C_A \delta^{ab} \int_k [\Delta_{\mu\sigma}(k) q_\sigma - \Delta_{\alpha\alpha}(k) q_\mu]. \quad (2.56)$$

Clearly, the sum of Eqs. (2.55) and (2.55) combines to produce

$$q^\nu \left[\tilde{\Pi}_{\mu\nu}(q)|_{(a_1)} + \tilde{\Pi}_{\mu\nu}(q)|_{(a_2)} \right] = 0. \quad (2.57)$$

At one-loop dressed level, the ghost sector is described by the diagrams (a_3) and (a_4) , whose closed expressions are given by

$$\tilde{\Pi}_{\mu\nu}^{ab}(q)|_{(a_3)} = - \int_k \tilde{\Gamma}_\nu^{d'c'b}(k+q, -k, -q) D^{cc'}(k) D^{dd'}(k+q) \Gamma_\mu^{(0)cda}(k, -k-q, q), \quad (2.58)$$

$$\tilde{\Pi}_{\mu\nu}^{ab}(q)|_{(a_4)} = - \int_k D^{cc'}(k) \tilde{\Gamma}_{\nu\mu}^{(0)bcc'}(-q, q, k, -k). \quad (2.59)$$

Now we repeat the same procedure, *i.e.*, contract the above expressions with the external background momentum, q^ν . In Eq. (2.59), we substitute the tree-level expression for the BQ $\bar{c}c$ vertex, given in Fig. 2.4. As long as for the diagram (a_3) , when the q_ν hits the fully dressed B $\bar{c}c$ vertex, it triggers the B $\bar{c}c$ WTI, given in Fig. 2.6, and subsequently, substituting the tree-level expression for the conventional ghost-gluon vertex given in Fig. 1.2, and performing the shift $k \rightarrow k - q$ one finds that,

$$q^\nu \tilde{\Pi}_{\mu\nu}^{ab}(q)|_{(a_3)} = -g^2 C_A \delta^{ab} q_\mu \int_k D(k), \quad (2.60)$$

$$q^\nu \tilde{\Pi}_{\mu\nu}^{ab}(q)|_{(a_4)} = g^2 C_A \delta^{ab} q_\mu \int_k D(k). \quad (2.61)$$

Once again, it is clear that the sum of both diagrams produces an independent transverse result, *i.e.*,

$$q^\nu \left[\tilde{\Pi}_{\mu\nu}(q)|_{(a_3)} + \tilde{\Pi}_{\mu\nu}(q)|_{(a_4)} \right] = 0. \quad (2.62)$$

Now, let us focus on the gluonic two-loops dressed contributions given by (a_5) and (a_6) . Their respective analytical expressions are given by

$$\tilde{\Pi}_{\mu\nu}^{ab}(q)|_{(a_5)} = \frac{1}{6} \int_k \int_\ell \Delta_{\alpha\beta}^{cc'}(k) \Delta_{\sigma\rho}^{dd'}(q+k+\ell) \Delta_{\lambda\gamma}^{ee'}(\ell) \tilde{\Gamma}_{\nu\gamma\rho\beta}^{be'd'c'}(-q, -\ell, q+k+\ell, -k) \times \Gamma_{\mu\alpha\sigma\lambda}^{(0)acde}(q, k, -q-k-\ell, \ell), \quad (2.63)$$

$$\tilde{\Pi}_{\mu\nu}^{ab}(q)|_{(a_6)} = \frac{1}{2} \int_k \int_\ell \Delta_{\alpha\beta}^{cc'}(k) \Delta_{\sigma\rho}^{dd'}(q+k+\ell) \Delta_{\lambda\gamma}^{ee'}(\ell) \Delta_{\chi\omega}^{gg'}(q+\ell) \tilde{\Gamma}_{\nu\gamma\omega}^{be'g'}(-q, -\ell, q+\ell) \times \Gamma_{\mu\alpha\sigma\lambda}^{(0)acde}(q, k, -q-k-\ell, \ell) \Gamma_{\beta\lambda\rho}^{c'gd'}(-k, -q-\ell, k+q+\ell). \quad (2.64)$$

Then, contracting with the external background momentum q_ν , and using in Eqs. (2.63) and (2.64) the BQQQ and the BQQ WTIs shown in Fig. 2.6, we arrive at

$$q^\nu \tilde{\Pi}_{\mu\nu}^{ab}(q)|_{(a_5)} = \frac{g}{6} \int_k \int_\ell \Delta_{\alpha\beta}(k) \Delta_{\sigma\rho}(q+k+\ell) \Delta_{\lambda\epsilon}(\ell) \Gamma_{\mu\alpha\sigma\lambda}^{(0)acde}(q, k, -q-k-\ell, \ell) \times \quad (2.65)$$

$$[f^{bxe} \Gamma_{\epsilon\rho\beta}^{xdc}(-q-\ell, q+k+\ell, -k) + f^{bad} \Gamma_{\rho\epsilon\beta}^{xec}(k+\ell, -\ell, -k) + f^{bxc} \Gamma_{\epsilon\rho\beta}^{xed}(-q-k, -\ell, q+k+\ell)],$$

$$q^\nu \tilde{\Pi}_{\mu\nu}^{ab}(q)|_{(a_6)} = \frac{g}{2} f^{beg} \int_k \int_l \Delta_{\alpha\beta}(k) \Delta_{\sigma\rho}(q+k+\ell) [\Delta_{\lambda\epsilon}(\ell) - \Delta_{\lambda\epsilon}(q+\ell)] \times \quad (2.66)$$

$$\Gamma_{\mu\alpha\sigma\lambda}^{(0)acde}(q, k, -q-k-\ell, \ell) \Gamma_{\beta\epsilon\rho}^{cgd}(-k, -q-\ell, k+q+\ell).$$

Now, notice that terms in square brackets, appearing in the second line of Eq. (2.65), after applying shifts in both momenta k and ℓ , and relabelling some dummy Lorentz and color indices can be converted to

$$-3f^{beg} \Gamma_{\beta\epsilon\rho}^{cgd}(-k, -q-\ell, k+q+\ell). \quad (2.67)$$

Conversely, the term proportional to the propagator $\Delta_{\lambda\epsilon}(q+\ell)$ in Eq. (2.64) vanishes. To see that, we shift $\ell \rightarrow \ell - q$, turning this term in an expression independent of q , and therefore making the free index of Lorentz, μ , impossible to saturate. Then, one finds that the sum of the above contributions give

$$q^\nu [\Pi_{\mu\nu}(q)|_{(a_5)} + \Pi_{\mu\nu}(q)|_{(a_6)}] = 0. \quad (2.68)$$

Combining the results of Eqs. (2.57), (2.62) and (2.68) we prove that the mixed gluon self-energy, $\hat{\Pi}_{\mu\nu}(q)$, has a blockwise transversality. In addition, the transversality of the gluonic and the ghost sector emerge independently. As a result, one can truncate the SDE for the QB propagator without violating the transversality of the gluon self-energy, as long as we consider all diagrams within the chosen blocks.

We finish this Chapter by making two observations. Firstly, the proof of blockwise transversality for the background gluon self-energy, $\hat{\Pi}_{\mu\nu}(q)$, can be carried out in the same lines as above. Second, when we mention that the full self-energy can be truncated without compromising the transversality, this does not mean that the neglected part is subleading.

Schwinger-Dyson Equations

In this thesis, we employ the SDE formalism to study the QCD nonperturbative properties. The SDEs were first derived in QED by Dyson [66] and Schwinger [67], and they can be understood as the equations of motion of the theory which governs the dynamics of the Green's functions. They form an infinite system of nonlinear integral equations that couples all Green's functions, *i.e.*, the propagators, vertices, and higher n-point functions.

In the previous Chapter, we have seen that the BFM Green's functions satisfy Abelian-like WTIs, and this property is a powerful feature that should be explored to build a self-consistent SDE truncation.

In this Chapter, we will focus on the formal derivation of the SDEs from the generating functional, with a particular interest in the new BFM ghost sector.

We begin this Chapter with the derivation of the master SDE in Section 3.1, which is the starting point to derive every SDE. Then, we proceed, and, in Section 3.2, we specify our formalism to the BFM QCD, and derive the ghost propagator SDE. In Section 3.3, we present the main result of this Chapter: the derivation of the $BB\bar{c}c$ vertex SDE. This derivation is a novel result, and as far as we know, this is the first time that the SDE for this vertex is derived in the literature.

3.1 The Schwinger-Dyson master equation

In this Section, we derive the SD master equation following the steps of [40, 68]. To derive the SD master equation, first, we perform a change of variables on the

VEVs of the fields inside the generating functional $Z[J]$ given by

$$\bar{\phi}_i(x) \rightarrow \bar{\phi}'_i(x) + \epsilon f_i(x), \quad (3.1)$$

where ϵ is an infinitesimal parameter, and $f_i(x)$ is an arbitrary function of x , independent of the fields. Then, the generating functional reads

$$Z[J] = \int \mathcal{D}[\bar{\phi}] \exp \left\{ iS[\bar{\phi}] + i\epsilon \int d^4x \frac{\delta S[\bar{\phi}]}{\delta \bar{\phi}_i(x)} f_i(x) + i \int d^4x J_i(x) [\bar{\phi}'_i(x) + \epsilon f_i(x)] \right\}. \quad (3.2)$$

Note that we have used that the Jacobian of the transformation is unit, since $f_i(x)$ is independent of the field, *i.e.*, $\mathcal{D}[\bar{\phi}] = \mathcal{D}[\bar{\phi}']$.

Then, the next step is to notice that an expansion around the parameter ϵ generates, at zeroth order, the original $Z[J]$ before the change of variables in the field, whereas at first order in ϵ , we have that

$$0 = \int \mathcal{D}[\bar{\phi}] \exp \left[iS[\bar{\phi}] + i \int d^4x J_i(x) \bar{\phi}_i(x) \right] \times \left[i\epsilon \int d^4x' \left(\frac{\delta S[\bar{\phi}]}{\delta \bar{\phi}_i(x')} + J_i(x') \right) f_i(x') \right]. \quad (3.3)$$

Since $f_i(x')$ is arbitrary, the integrand in x must be zero and then one finds

$$\left(\frac{\delta S[\bar{\phi}]}{\delta \bar{\phi}_i(x')} + J_i(x') \right) Z[J] = 0. \quad (3.4)$$

Eq. (3.4) is the SD master equation. Its functional differentiation generates the SDEs for the disconnected Green's functions. To obtain the SDEs for the 1PI functions, one only needs to substitute in Eq. (3.4) the $Z[J]$ in terms of the connected generating functional $W[J]$, *i.e.*, $Z[J] = e^{-iW[J]}$ [see Eq. (2.6)]. Then, the functional differentiation of Eq. (3.4) creates an infinite tower of nonlinear coupled integral equations relating all the n-point Green's functions of a given theory [37, 40, 68].

Note that the derivation of the SD master equation proceeds analogously to the one for the Euler-Lagrange equation, where we perform an infinitesimal change in the classical field and obtain that the variation of the action is null. Therefore, the SDEs are considered a generalization of the Euler-Lagrange equations for the Green's functions of a quantum theory governing their dynamical evolution.

3.2 The SDE for the ghost propagator

In this Section, we derive the SDE for the ghost propagator. We can proceed in two equivalent ways to derive this equation. The first one is to use the conventional Lagrangian, \mathcal{L}_{QCD} , given by Eq. (1.1), and thus define the action, S_{QCD} ; or equivalently, one can use the BFM ghost Lagrangian, \mathcal{L}_{ghost} , given by Eq. (2.38), then, define the corresponding action, \tilde{S} .

We want to highlight that both ways are possible, leading to precisely the same result because there are no background ghosts. Here we will follow the second route because it will be more convenient for the derivation of the SDE for the $BB\bar{c}c$ vertex, which is the central result of this Chapter, to be presented in the next Section.

Then, the relevant part of the BFM action, where the (anti)ghost fields appear, is given by

$$\begin{aligned} \tilde{S}[Q, \bar{c}, c] = \int d^4x [c^d \partial^2 \bar{c}^d - g f^{edg} B_\alpha^d \bar{c}^e \partial_\alpha c^g + g f^{deg} (\partial_\alpha \bar{c}^d) (Q + B)_\alpha^e c^g \\ - g^2 f^{gdx} f^{xeh} B_\alpha^d (Q + B)_\alpha^e \bar{c}^g c^h]. \end{aligned} \quad (3.5)$$

Thus, the BFM generating functional reads

$$\tilde{Z}[J_\alpha, j_c, \bar{j}_c] = \int \mathcal{D}[A] \mathcal{D}[\bar{c}] \mathcal{D}[c] \exp \left\{ i \tilde{S}[Q, \bar{c}, c] + \int d^4x (J_\alpha^a Q_\alpha^a + \bar{c}^a j_c^a + \bar{j}_c^a c^a) \right\}. \quad (3.6)$$

Looking on the perspective of $\widetilde{W}[A, \bar{c}, c]$, and its Legendre transformation,

$$\widetilde{\Gamma}[Q, \bar{c}, c] = \widetilde{W}[J_\alpha, j_c, \bar{j}_c] - \int d^4x (J_\alpha^a Q_\alpha^a + \bar{c}^a j_c^a + \bar{j}_c^a c^a), \quad (3.7)$$

we obtain the following relations

$$\begin{aligned} \frac{\delta \widetilde{W}}{\delta J_\alpha^a} = Q_\alpha^a, & \quad \frac{\delta \widetilde{W}}{\delta \bar{j}_c^a} = -c^a, & \quad \frac{\delta \widetilde{W}}{\delta j_c^a} = \bar{c}^a, \\ \frac{\delta \widetilde{\Gamma}}{\delta Q_\alpha^a} = -J_\alpha^a, & \quad \frac{\delta \widetilde{\Gamma}}{\delta c^a} = \bar{j}_c^a, & \quad \frac{\delta \widetilde{\Gamma}}{\delta \bar{c}^a} = -j_c^a. \end{aligned} \quad (3.8)$$

Applying the SD master equation, given in Eq. (3.4), for the ghost field, c^n ,

with $\tilde{Z}[J] = e^{-i\tilde{W}[J]}$, we find that

$$e^{-i\tilde{W}[J_\alpha, j_c, \bar{j}_c]} \left(\frac{\delta \tilde{S}}{\delta c^n} \left[-i \frac{\delta}{\delta J_\alpha}, -i \frac{\delta}{\delta j_c}, i \frac{\delta}{\delta \bar{j}_c} \right] + \bar{j}_c^n \right) e^{i\tilde{W}[J_\alpha, j_c, \bar{j}_c]} = 0. \quad (3.9)$$

Next, computing the functional derivative of $\tilde{S}[Q, \bar{c}, c]$, given in Eq. (3.5), with respect to the ghost, $c^n(z)$, we obtain

$$\begin{aligned} \frac{\delta \tilde{S}[Q, \bar{c}, c]}{\delta c^n(z)} &= \partial_z^2 \bar{c}^n(z) - g f^{adn} B_\alpha^d(z) \partial_\alpha \bar{c}^a(z) - g f^{ane} [\partial_z^\alpha \bar{c}^a(z)] [Q(z) + B(z)]_\alpha^e \\ &\quad + g^2 f^{adc} f^{cen} B_\alpha^d(z) [Q(z) + B(z)]_\alpha^e \bar{c}^a(z). \end{aligned} \quad (3.10)$$

Then, using Eq. (3.10) into Eq. (3.9), we arrive at

$$\begin{aligned} \partial_z^2 \frac{\delta \tilde{W}}{\delta j_c^n(z)} &+ g f^{adn} B_\alpha^d(z) \partial_z^\alpha \frac{\delta \tilde{W}}{\delta j_c^a(z)} - g f^{ane} \partial_z^\alpha \left[\frac{\delta \tilde{W}}{\delta J_\alpha^e(z)} \frac{\delta \tilde{W}}{\delta j_c^a(z)} \right] + i g f^{ane} \partial_z^\alpha \left[\frac{\delta^2 \tilde{W}}{\delta j_c^a(z) \delta J_\alpha^e(z)} \right] + \\ &- g f^{ane} \partial_z^\alpha B_\alpha^e(z) \frac{\delta \tilde{W}}{\delta j_c^a(z)} + g^2 f^{adc} f^{cen} B_\alpha^d(z) \frac{\delta \tilde{W}}{\delta J_\alpha^e(z)} \frac{\delta \tilde{W}}{\delta j_c^a(z)} - i g^2 f^{adc} f^{cen} B_\alpha^d(z) \frac{\delta^2 \tilde{W}}{\delta J_\alpha^e(z) \delta j_c^a(z)} \\ &+ g^2 f^{adc} f^{cen} B_\alpha^d(z) B_\alpha^e(z) \frac{\delta \tilde{W}}{\delta j_c^a(z)} + \bar{j}_c^n(z) = 0. \end{aligned} \quad (3.11)$$

To proceed, we rewrite Eq. (3.11) as a function of the functional derivative of the effective action, $\tilde{\Gamma}$, with respect to the fields, instead of \tilde{W} . To do that, we use Eqs. (2.11) and (3.8), then Eq. (3.11) becomes

$$\begin{aligned} \partial_z^2 \bar{c}^n(z) &+ g f^{adn} B_\alpha^d(z) \partial_z^\alpha \bar{c}^a(z) - g f^{ane} \partial_z^\alpha Q_\alpha^e(z) \bar{c}^a(z) - i g f^{ane} \partial_z^\alpha \left(\frac{\delta^2 \tilde{\Gamma}}{\delta Q_\alpha^e(z) \delta \bar{c}^a(z)} \right)^{-1} + \\ &- g f^{ane} \partial_z^\alpha B_\alpha^e(z) \bar{c}^a(z) + g^2 f^{adc} f^{cen} B_\alpha^d(z) Q_\alpha^e(z) \bar{c}^a(z) + i g^2 f^{adc} f^{cen} B_\alpha^d(z) \left(\frac{\delta^2 \tilde{\Gamma}}{\delta Q_\alpha^e(z) \delta \bar{c}^a(z)} \right)^{-1} + \\ &+ g^2 f^{adc} f^{cen} B_\alpha^d(z) B_\alpha^e(z) \bar{c}^a(z) - \frac{\delta \tilde{\Gamma}}{\delta c^n(z)} = 0. \end{aligned} \quad (3.12)$$

Now, taking the functional derivative of the above expression with respect to the antighost field, $\bar{c}^m(y)$, and setting the VEVs to zero, we find that

$$\frac{\delta^2 \tilde{\Gamma}}{\delta \bar{c}^m(y) \delta c^n(z)} - \delta^{nm} \partial_z^2 \delta(y-z) + i g f^{ane} \partial_z^\alpha \frac{\delta}{\delta \bar{c}^m(y)} \left(\frac{\delta^2 \tilde{\Gamma}}{\delta Q_\alpha^e(z) \delta \bar{c}^a(z)} \right)^{-1} = 0. \quad (3.13)$$

Employing the relation given by Eq. (2.13), the above equation can be rewritten as

$$\begin{aligned} & \frac{\delta^2 \tilde{\Gamma}}{\delta \bar{c}^m(y) \delta c^n(z)} - \delta^{nm} \partial_z^2 \delta(y-z) \\ & - ig f^{ane} \partial_z^\alpha \int d^4 u d^4 v \left(\frac{\delta^2 \tilde{\Gamma}}{\delta Q_\alpha^e(z) \delta Q_\beta^i(u)} \right)^{-1} \frac{\delta^3 \tilde{\Gamma}}{\delta Q_\beta^i(u) \delta \bar{c}^m(y) \delta c^j(v)} \left(\frac{\delta^2 \tilde{\Gamma}}{\delta c^j(v) \delta \bar{c}^a(z)} \right)^{-1} = 0. \end{aligned} \quad (3.14)$$

As a final step, one needs to identify the quantities appearing in Eq. (3.14). The fully dressed ghost propagator is defined in terms of the effective action as,

$$D^{nm}(z-y) = i \left(\frac{\delta^2 \tilde{\Gamma}}{\delta \bar{c}^m(y) \delta c^n(z)} \right)^{-1}. \quad (3.15)$$

Similarly, the full gluon propagator is given by

$$\Delta_{\alpha\beta}^{ei}(z-u) = i \left(\frac{\delta^2 \tilde{\Gamma}}{\delta Q_\alpha^e(z) \delta Q_\beta^i(u)} \right)^{-1}, \quad (3.16)$$

whereas the conventional ghost-gluon vertex is defined as

$$\Gamma_\beta^{mji}(y, v, u) = \frac{\delta^3 \tilde{\Gamma}}{\delta \bar{c}^m(y) \delta c^j(v) \delta Q_\beta^i(u)}. \quad (3.17)$$

Notice that the first term, $\delta^{nm} \partial_z^2 \delta(y-z)$, is nothing else than the ghost propagator, at tree-level, in coordinate space.

Applying the above definitions into Eq. (3.14), the SDE for the ghost propagator in coordinate space reads

$$[D^{nm}(z-y)]^{-1} = [D_{(0)}^{nm}(z-y)]^{-1} - ig f^{ane} \partial_z^\alpha \int d^4 u d^4 v \Delta_{\alpha\beta}^{ei}(z-u) D^{aj}(z-v) \Gamma_\beta^{mji}(y, v, u). \quad (3.18)$$

Now, applying the Fourier transformation to convert the above equation in momenta space, we obtain

$$[D^{nm}(q)]^{-1} = [D_{(0)}^{nm}(q)]^{-1} - \int_k \Delta_{\alpha\beta}^{ei}(k) D^{aj}(k+q) \Gamma_\alpha^{(0)ane}(-k-q, q, k) \Gamma_\beta^{mji}(-q, k+q, -k). \quad (3.19)$$

Eq. (3.19) is the SDE for ghost propagator, whose diagrammatic representation is shown in the upper panel of Fig. 3.1.

It is also important to point out that one could use the SD master equation

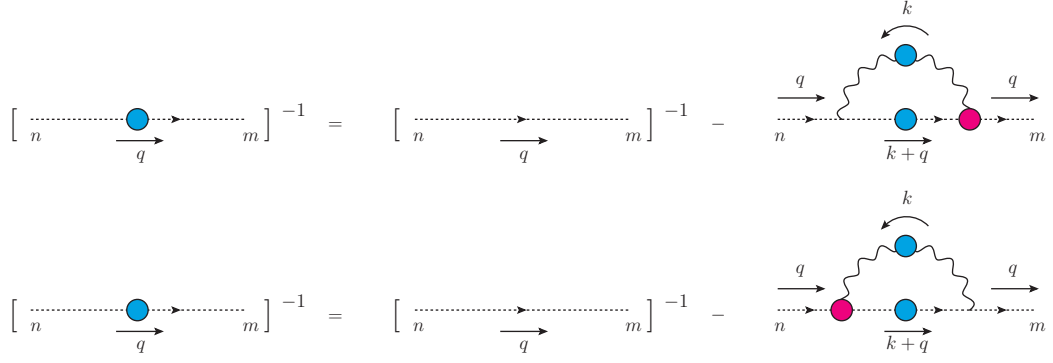


Figure 3.1: The diagrammatic representations of the ghost SDE, derived from two different perspectives. In the upper panel, we show the derivation from the perspective of the ghost leg, while in the lower panel, we have the view from antighost leg.

for the antighost field as a starting point, instead of the one for the ghost, as we did here [see Eq. (3.9)]. In that case, the difference would be that the bare vertex, appearing in the resulting ghost propagator SDE, would appear attached to the antighost external leg, instead of the ghost leg. In the lower panel of Fig. 3.1, we show the ghost SDE from this new perspective.

3.3 The SDE for the $BB\bar{c}c$ vertex

Now, we are in the position to derive the main result of this Chapter, namely the SDE for the $BB\bar{c}c$ vertex.

To do that, we can take advantage of the previous derivation and use Eq. (3.12) as a starting point. Thus, the SDE for the $BB\bar{c}c$ can be obtained by simply taking the functional derivative of the Eq. (3.12) with respect to the background gluon fields, $B_\nu^b(x)$, and $B_\mu^a(w)$, respectively. After doing that, we set the VEVs to zero, and we arrive at

$$\begin{aligned}
& - \frac{\delta^4 \tilde{\Gamma}}{\delta B_\mu^a(w) \delta B_\nu^b(x) \delta \bar{c}^m(y) \delta c^n(z)} + i \widehat{\Pi}_{\mu\nu}^{(0)abmn}(w, x, y, z) - ig f^{xne} \partial_z^\alpha \mathcal{Q}_{\mu\nu\alpha}^{abmex}(w, x, y, z, z) \\
& + ig^2 f^{xbc} f^{cen} \delta(z-x) \mathcal{K}_{\mu\nu}^{amex}(w, y, z, z) + ig^2 f^{xac} f^{cen} \delta(z-w) \mathcal{K}_{\nu\mu}^{bmex}(x, y, z, z) = 0, \quad (3.20)
\end{aligned}$$

where we define the one-particle reducible (1PR) five-point function, $\mathcal{Q}_{\mu\nu\alpha}^{abmex}(w, x, y, z, z)$, as

$$\mathcal{Q}_{\mu\nu\alpha}^{abmex}(w, x, y, z, z) = \frac{\delta}{\delta B_\mu^a(w)} \frac{\delta}{\delta B_\nu^b(x)} \frac{\delta}{\delta \bar{c}^m(y)} \left(\frac{\delta^2 \tilde{\Gamma}}{\delta Q_\alpha^e(z) \delta \bar{c}^x(z)} \right)^{-1}, \quad (3.21)$$

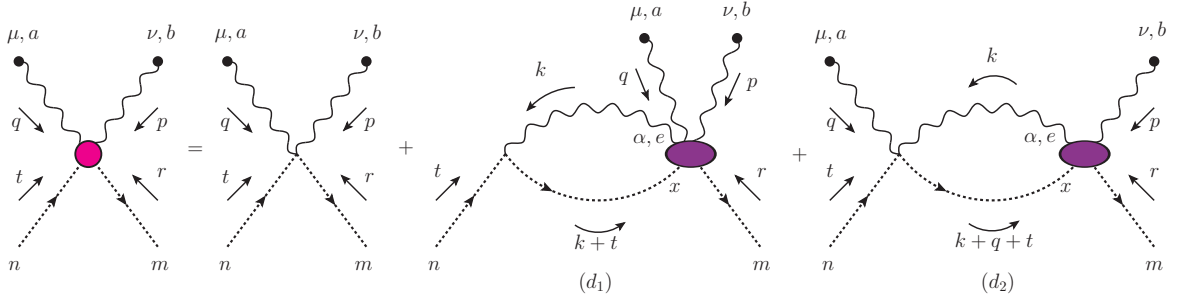


Figure 3.2: The diagrammatic representation of the $BB\bar{c}$ SDE. The purple ellipses represent the 1PR four- and five-points kernels. We have omitted the contribution of the counterpart of the diagram (d_2) , where the two background gluon legs are crossed.

and the 1PR four-point function, $\mathcal{K}_{\nu\mu}^{bme x}(x, y, z, z)$, given by

$$\mathcal{K}_{\nu\mu}^{bme x}(x, y, z, z) = \frac{\delta}{\delta B_\nu^b(x)} \frac{\delta}{\delta \bar{c}^m(y)} \left(\frac{\delta^2 \tilde{\Gamma}}{\delta Q_\mu^e(z) \delta \bar{c}^x(z)} \right)^{-1}. \quad (3.22)$$

Already, at the level of Eq. (3.20), one can identify the first term as the complete vertex $\hat{\Pi}_{\mu\nu}^{abmn}(w, x, y, z)$ (our $BB\bar{c}$ vertex), which in terms of the effective action is given by

$$i\hat{\Pi}_{\mu\nu}^{abmn}(w, x, y, z) = i \frac{\delta^4 \tilde{\Gamma}}{\delta B_\mu^a(w) \delta B_\nu^b(x) \delta \bar{c}^m(y) \delta c^n(z)}. \quad (3.23)$$

In addition, the second term appearing in Eq. (3.20), we have identified it as the tree-level counterpart of the $BB\bar{c}$ (in the coordinates space), *i.e.*,

$$i\hat{\Pi}_{\mu\nu}^{(0)abmn}(w, x, y, z) = g^2 (f^{mbc} f^{can} + f^{mac} f^{cbn}) g_{\mu\nu} \delta(z-x) \delta(z-w) \delta(z-y), \quad (3.24)$$

whose Feynman rule in the momentum space was already mentioned in Fig. 2.4.

Now, notice that the last two terms of Eq. (3.20) are equal under the simultaneous exchange of the Lorentz indices, $\mu \leftrightarrow \nu$, color indices, $a \leftrightarrow b$, and coordinates, $w \leftrightarrow x$. Their appearance is a direct consequence of the Bose symmetry that the $BB\bar{c}$ SDE obeys with respect to the exchange of the two background gluon legs.

The five- and four-point functions of Eqs. (3.21) and (3.22) are the 1PR kernels, whose decomposition into 1PI vertices may be obtained using the relation Eq. (2.13). The diagrammatic representation of the SDE for the $BB\bar{c}$, in terms of 1PR kernels, is shown

in Fig. 3.2. For the sake of simplicity, in this Figure, we omit the counterpart of the diagram (d_2), where the two background gluon legs are crossed.

Now, using Eq. (2.13) to decompose the connected function in Eq. (3.22) we get that

$$\begin{aligned} \mathcal{K}_{\nu\mu}^{bmex}(x, y, z, z) = & -i \int_{[u]} \Delta_{\mu\alpha}^{ei}(z - u_1) \tilde{\Pi}_{\nu\alpha}^{bimj}(x, u_1, y, u_2) D^{xj}(z - u_2) \\ & + i \int_{[u,v]} \Delta_{\mu\beta}^{eg}(z - v_1) \tilde{\Gamma}_{\nu\beta\rho}^{bgh}(x, v_1, v_2) \Delta_{\rho\alpha}^{hi}(v_2 - u_1) \Gamma_{\alpha}^{mji}(y, u_2, u_1) D^{xj}(z - u_2) \\ & + i \int_{[u,v]} \Delta_{\mu\alpha}^{ei}(z - u_1) \Gamma_{\alpha}^{mji}(y, u_2, u_1) D^{hj}(v_1 - u_2) \tilde{\Gamma}_{\nu}^{hgb}(v_1, v_2, x) D^{xg}(z - v_2), \end{aligned} \quad (3.25)$$

where we have introduced the definitions for the dressed BQQ vertex, $\tilde{\Gamma}_{\nu\beta\rho}^{bgh}(x, v_1, v_2)$, as

$$\tilde{\Gamma}_{\nu\beta\rho}^{bgh}(x, v_1, v_2) = \frac{\delta^3 \tilde{\Gamma}}{\delta B_{\nu}^b(x) \delta Q_{\beta}^g(v_1) \delta Q_{\rho}^h(v_2)}, \quad (3.26)$$

for the $B\bar{c}c$ vertex, $\tilde{\Gamma}_{\nu}^{hgb}(v_1, v_2, x)$, as

$$\tilde{\Gamma}_{\nu}^{hgb}(v_1, v_2, x) = \frac{\delta^3 \tilde{\Gamma}}{\delta \bar{c}^h(v_1) \delta c^g(v_2) \delta B_{\nu}^b(x)}, \quad (3.27)$$

and for the BQ $\bar{c}c$ vertex, $\tilde{\Pi}_{\nu\alpha}^{bimj}(x, u_1, y, u_2)$, as

$$\tilde{\Pi}_{\nu\alpha}^{bimj}(x, u_1, y, u_2) = i \frac{\delta^4 \tilde{\Gamma}}{\delta B_{\nu}^b(x) \delta Q_{\beta}^i(u_1) \delta \bar{c}^m(y) \delta c^j(u_2)}. \quad (3.28)$$

We also used a shorthand notation for the integrals, given by

$$\int_{[u]} = \int d^4 u_1 d^4 u_2, \quad \int_{[u,v]} = \int d^4 u_1 d^4 u_2 d^4 v_1 d^4 v_2. \quad (3.29)$$

Now, using Eq. (2.13) repeatedly to decompose the 1PR kernel of Eq. (3.21),

we arrive at

$$\begin{aligned}
\mathcal{Q}_{\mu\nu\alpha}^{abmex}(w, x, y, z, z) = & \tag{3.30} \\
& - \int_{[u,v,t]} \Delta_{\alpha\lambda}^{ek}(z-t_1) \tilde{\Gamma}_{\mu\gamma\lambda}^{alk}(w, t_2, t_1) \Delta_{\gamma\rho}^{lg}(t_2-v_1) \tilde{\Gamma}_{\nu\sigma\rho}^{bhg}(x, v_2, v_1) \Delta_{\sigma\beta}^{hi}(v_2-u_1) \Gamma_{\beta}^{jmi}(u_2, y, u_1) D^{jx}(u_2-z) \\
& + \int_{[u,v]} \Delta_{\alpha\rho}^{eg}(z-v_1) \hat{\Pi}_{\mu\nu\sigma\rho}^{abhg}(w, x, v_2, v_1) \Delta_{\sigma\beta}^{hi}(v_2-u_1) \Gamma_{\beta}^{jmi}(u_2, y, u_1) D^{jx}(u_2-z) \\
& - \int_{[u,v,t]} \Delta_{\alpha\rho}^{eg}(z-v_1) \tilde{\Gamma}_{\nu\sigma\rho}^{bhg}(x, v_2, v_1) \Delta_{\sigma\lambda}^{hk}(v_2-t_1) \tilde{\Gamma}_{\mu\gamma\lambda}^{alk}(w, t_2, t_1) \Delta_{\gamma\beta}^{li}(t_2-u_1) \Gamma_{\beta}^{jmi}(u_2, y, u_1) D^{jx}(u_2-z) \\
& + \int_{[u,v]} \Delta_{\alpha\rho}^{eg}(z-v_1) \tilde{\Gamma}_{\nu\sigma\rho}^{bhg}(x, v_2, v_1) \Delta_{\sigma\beta}^{hi}(v_2-u_1) \tilde{\Pi}_{\mu\beta}^{ajmi}(w, u_2, y, u_1) D^{jx}(u_2-z) \\
& - \int_{[u,v,t]} \Delta_{\alpha\rho}^{eg}(z-v_1) \tilde{\Gamma}_{\nu\sigma\rho}^{bhg}(x, v_2, v_1) \Delta_{\sigma\beta}^{hi}(v_2-u_1) \Gamma_{\beta}^{jmi}(u_2, y, u_1) D^{jk}(u_2-t_1) \tilde{\Gamma}_{\mu}^{hgb}(t_2, t_1, w) D^{lx}(t_2-z) \\
& - \int_{[u,v,t]} \Delta_{\alpha\rho}^{eg}(z-t_1) \tilde{\Gamma}_{\mu\sigma\rho}^{ahg}(w, t_2, t_1) \Delta_{\sigma\beta}^{hi}(t_2-u_1) \Gamma_{\beta}^{jmi}(u_2, y, u_1) D^{jg}(u_2-v_1) \tilde{\Gamma}_{\nu}^{hgb}(v_2, v_1, x) D^{hx}(v_2-z) \\
& + \int_{[u,v]} \Delta_{\alpha\beta}^{ei}(z-u_1) \tilde{\Pi}_{\mu\beta}^{aijm}(w, u_1, u_2, y) D^{jg}(u_2-v_1) \tilde{\Gamma}_{\nu}^{hgb}(v_2, v_1, x) D^{hx}(v_2-z) \\
& - \int_{[u,v,t]} \Delta_{\alpha\beta}^{ei}(z-u_1) \Gamma_{\beta}^{jmi}(u_2, y, u_1) D^{jk}(u_2-t_1) \tilde{\Gamma}_{\mu}^{lka}(t_2, t_1, w) D^{lg}(t_2-v_1) \tilde{\Gamma}_{\nu}^{hgb}(v_2, v_1, x) D^{hx}(v_2-z) \\
& + \int_{[u,v]} \Delta_{\alpha\beta}^{ei}(z-u_1) \Gamma_{\beta}^{jmi}(u_2, y, u_1) D^{jg}(u_2-v_1) \hat{\Gamma}_{\mu\nu}^{abhg}(w, x, v_2, v_1) D^{hx}(v_2-z) \\
& - \int_{[u,v,t]} \Delta_{\alpha\beta}^{ei}(z-u_1) \Gamma_{\beta}^{jmi}(u_2, y, u_1) D^{jg}(u_2-v_1) \tilde{\Gamma}_{\nu}^{hgb}(v_2, v_1, x) D^{hk}(v_2-t_1) \tilde{\Gamma}_{\mu}^{lka}(t_2, t_1, w) D^{lx}(t_2-z) \\
& + \int_{[u,v]} \Delta_{\alpha\rho}^{eg}(z-v_1) \tilde{\Gamma}_{\mu\sigma\rho}^{ahg}(w, v_2, v_1) \Delta_{\sigma\beta}^{hi}(v_2-u_1) \tilde{\Pi}_{\nu\beta}^{bijm}(x, u_1, u_2, z) D^{jx}(u_2-z) \\
& + \int_{[u]} \Delta_{\alpha\beta}^{ei}(z-u_1) \hat{\Pi}_{\mu\nu\beta}^{abijm}(w, x, u_1, u_2, z) D^{jx}(u_2-z) \\
& + \int_{[u,v]} \Delta_{\alpha\beta}^{ei}(z-u_1) \tilde{\Pi}_{\nu\beta}^{bijm}(x, u_1, u_2, z) D^{jg}(u_2-v_1) \tilde{\Gamma}_{\mu}^{kga}(v_2, v_1, w) D^{kx}(v_2-z).
\end{aligned}$$

Once more, we introduced new definitions: the vertex BBQQ, $\hat{\Pi}_{\mu\nu\sigma\rho}^{abhg}(w, x, v_2, v_1)$, as

$$\hat{\Pi}_{\mu\nu\sigma\rho}^{abhg}(w, x, v_2, v_1) = i \frac{\delta^4 \tilde{\Gamma}}{\delta B_{\mu}^a(w) \delta B_{\nu}^b(x) \delta Q_{\sigma}^h(v_2) \delta Q_{\rho}^g(v_1)}, \tag{3.31}$$

the 5-point function $\hat{\Gamma}_{\mu\nu\beta}^{abijd}(w, x, u_1, u_2, z)$ as

$$\hat{\Gamma}_{\mu\nu\beta}^{abijd}(w, x, u_1, u_2, z) = \frac{\delta^5 \tilde{\Gamma}}{\delta B_{\mu}^a(w) \delta B_{\nu}^b(x) \delta Q_{\beta}^i(u_1) \delta \bar{c}^j(u_2) \delta c^d(z)}, \tag{3.32}$$

and the integral measure,

$$\int_{[u,v,t]} = \int d^4u_1 d^4u_2 d^4v_1 d^4v_2 d^4t_1 d^4t_2. \quad (3.33)$$

In the case where we expand the connected functions in terms of the 1PI vertices, like we did in Eqs. (3.25) and (3.30), one gets the representation given in Fig. 3.3. Once again, we omit the diagrams with crossed legs for the sake of simplicity.

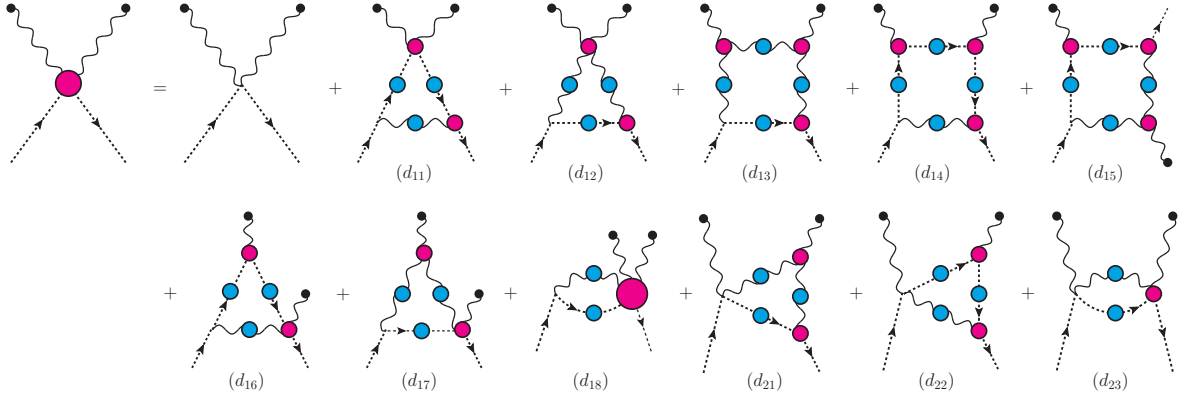


Figure 3.3: The diagrammatic representation of the $BB\bar{c}$ SDE expanded in terms of 1PI vertices. The diagrams with crossed legs are omitted for the sake of simplicity. Note that, in our notation, the diagrams (d_{1i}) with $i = 1, 2, \dots, 8$ are the ones coming from the expansion of the connected function in diagram (d_1) in Fig. 3.2, while (d_{2i}) with $i = 1, 2, 3$ are the ones coming from (d_2) .

All-soft limit for the $BB\bar{c}c$ vertex

In Chapter 2, we introduced the functional formalism, and in this scenario, in the last Chapter we derived the SDE for the $BB\bar{c}c$ vertex in two formats. The first one is a compact form, expressed in terms of “one-particle reducible” four- and five-point kernels. Then, in the second format, we performed the skeleton expansion of the reducible kernels in terms of 1PI contributions. In this Chapter, we will contextualize them as we present the main objective of this work: the study of the $BB\bar{c}c$ vertex in the so-called all-soft configuration, wherein the momenta of the four legs are set to zero.

We will show that, in this limit, the tensorial structure of this vertex simplifies enormously, reducing from 35 independent tensors (Lorentz + color indices) to only two contributions, the metric $g_{\mu\nu}$ times two different color factors.

In order to implement the all-soft limit on the SDE for the $BB\bar{c}c$ vertex, we will have to apply the WTIs that the BFM vertices satisfy judiciously. In addition, as typical from the BFM calculation, we will see that it will be crucial to fix the Landau gauge at the very end of the calculation procedure to not distort the final result.

The Chapter is organized as follows. In Section 4.1, we shall elaborate on a few features of the $BB\bar{c}c$ vertex, starting with its most general tensorial structure in general kinematics. At this point, it will become manifest the inherent complexity in the treatment of this vertex. Then, we will start arguing in the direction of the all-soft configuration of this vertex. In order to derive this limit, in Section 4.2, we set important definitions and notations for the fully dressed vertices. In particular, we recall known results for the fully dressed BFM ghost-gluon vertex ($B\bar{c}c$). Finally, in Section 4.3, we will look into the individual contributions of the 1PI version of $BB\bar{c}c$ SDE, and then we perform the all-soft limit for each of these diagrams, deriving an exact result for this vertex in the all-soft kinematic limit. We show, using the WTI that the $BQ\bar{c}c$ vertex satisfies, that the above relation can be written in a rather compact form, expressed

only in terms of the ghost dressing function, $F(q)$. Then, Section 4.4 shows an alternative way, based entirely on the WTIs, to derive the same relation. Finally, we will close the Chapter with our numerical analysis. In particular, we envisage a possible application for the all-soft exact relation established here. This relation can be used as a benchmark to establish the best truncation scheme to be adopted in a future study of the BB \bar{c} c SDE in general kinematics. In particular, in Section 4.5, we propose three truncation schemes for the BB \bar{c} c SDE and check which one is in better agreement with the exact relation.

4.1 The general tensorial structure

In this Section, we will elaborate on a few features of the BB \bar{c} c vertex, which will be of interest in what follows. We will start by addressing the most general tensorial structure of the BB \bar{c} c vertex. To do that, we present the elements of the Lorentz and the color basis. We also discuss the restrictions that the Bose symmetry, which the background gluon legs should respect, imposes on the form factors. After this Section, the intrinsic complexity of treating this vertex in general kinematics will become clear.

The BB \bar{c} c vertex, $\widehat{\Pi}_{\mu\nu}^{abmn}(q, r, p, t) = -ig^2\widehat{\Gamma}_{\mu\nu}^{abmn}(q, r, p, t)$, is a complete four-point Green's function composed by two background gluons, an antighost, and a ghost field, which is diagrammatically represented in the Fig. 4.1.

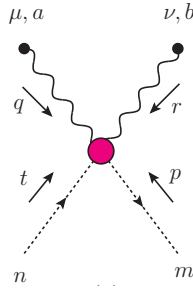


Figure 4.1: The diagrammatic representation of the BB \bar{c} c vertex, $\widehat{\Pi}_{\mu\nu}^{abmn}(q, r, p, t)$, and its respective adopted momenta convention.

This object has two Lorentz indices (2-rank) and effectively three momenta scales, such that there are 10 independent tensorial structures available for the decomposition, obtained from the combination of these momenta and metric tensors. On the other hand, its color structure is also cumbersome, the vertex has four color indices (4-rank) and therefore, there are 8 independent tensors which are formed as combination of the Kronecker delta, δ^{ab} , and the totally antisymmetric, f^{abc} , and symmetric, d^{abc} , structure constants.

In order to carry out this decomposition, we will employ a naive basis, where the vertex can be written as

$$\widehat{\Gamma}_{\mu\nu}^{abmn}(q, r, p, t) = \sum_{i=1}^{10} \sum_{j=1}^8 \mathcal{C}_{ij}(q, r, p, t) \ell_{\mu\nu}^i c_j^{abmn}, \quad (4.1)$$

where $\ell_{\mu\nu}^i$ are the Lorentz elements of the naive basis¹ given by

$$\begin{aligned} \ell_{\mu\nu}^1 &= g_{\mu\nu}, & \ell_{\mu\nu}^2 &= q_\mu r_\nu, & \ell_{\mu\nu}^3 &= q_\mu p_\nu, & \ell_{\mu\nu}^4 &= q_\nu r_\mu, & \ell_{\mu\nu}^5 &= q_\nu p_\mu, \\ \ell_{\mu\nu}^6 &= r_\mu p_\nu, & \ell_{\mu\nu}^7 &= p_\mu r_\nu, & \ell_{\mu\nu}^8 &= q_\mu q_\nu, & \ell_{\mu\nu}^9 &= r_\mu r_\nu, & \ell_{\mu\nu}^{10} &= p_\mu p_\nu, \end{aligned} \quad (4.2)$$

c_j^{abmn} are the color basis elements expressed as [69, 70]

$$\begin{aligned} c_1^{abmn} &= f^{anx} f^{mbx}, & c_2^{abmn} &= f^{max} f^{bnx}, & c_3^{abmn} &= \delta^{ab} \delta^{mn}, & c_4^{abmn} &= \delta^{am} \delta^{nb}, \\ c_5^{abmn} &= \delta^{an} \delta^{bm}, & c_6^{abmn} &= d^{abr} f^{mnr}, & c_7^{abmn} &= d^{amr} f^{bnr}, & c_8^{abmn} &= d^{anr} f^{bmr}, \end{aligned} \quad (4.3)$$

and $\mathcal{C}_{ij}(q, r, p, t)$ are the form factors. Notice that at tree-level, only the tensorial component proportional to the metric, *i.e.*, $\ell_{\mu\nu}^1$, survives, then the only nonvanishing form factors are

$$\mathcal{C}_{11}^{(0)}(q, r, p, t) = \mathcal{C}_{12}^{(0)}(q, r, p, t) = 1. \quad (4.4)$$

Therefore, the most general decomposition of the BB \bar{c} vertex, given in Eq. (4.1), depends on 80 tensors. Each one of them will be accompanied by its corresponding form factor. The form factors are multidimensional functions depending on six variables, *i.e.*, the three independent momenta and the three angles between them.

Bose symmetry with respect to the two background legs requires that $\widehat{\Gamma}_{\mu\nu}^{abmn}(q, r, p, t)$ is invariant under the simultaneous interchange of the corresponding Lorentz index, $\mu \leftrightarrow \nu$, color index, $a \leftrightarrow b$, and momenta $q \leftrightarrow r$; this, in turn, furnishes a series of relations between different form factors, which reduce the number of independent form factors from the original 80 to only 35.

In Appendix B, we expand our discussion about the construction of the Lorentz and color basis, given by Eqs. (4.2) and (4.3), respectively. In addition, we explain, in more detail, how the Bose symmetry constrains the various form factors, reducing them down to 35 independent ones.

Although there is a substantial reduction in the number of the form factors due to

¹In Appendix B we explain, in detail, the construction of the elements of the naive basis.

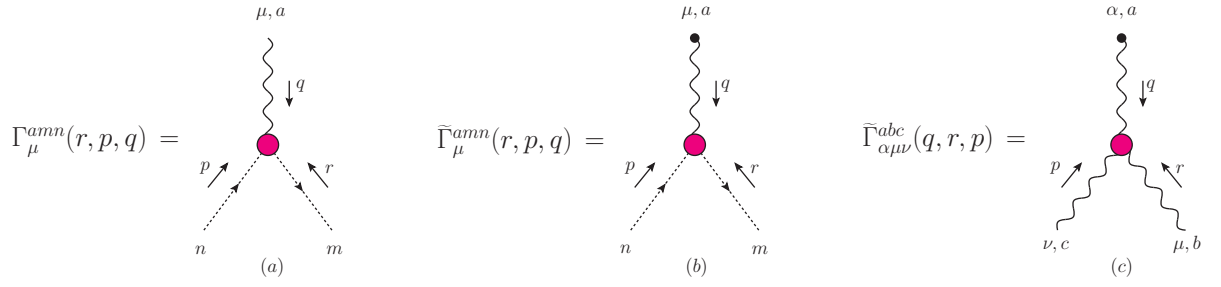


Figure 4.2: Diagrammatic representations of the fully dressed three-point vertices. In particular, we show in the panels (a) the conventional ghost-gluon vertex (Q $\bar{c}c$), (b) the background ghost-gluon vertex (B $\bar{c}c$), and (c) the three-background-quantum-quantum vertex (BQQ) with their respective momenta conventions.

the Bose symmetry, one may still appreciate the high degree of non-triviality that a complete analysis of the structure of the BB $\bar{c}c$ encompasses. However, as we will show in the following, this does not remain true as one goes from general kinematics to specific momenta configurations - in this case, the all-soft configuration. More specifically, in the all-soft limit, the momenta of all leg of $\widehat{\Gamma}_{\mu\nu}^{abmn}(q, r, p, t)$ are set to zero, that is, $q \rightarrow 0$, $r \rightarrow 0$, $p \rightarrow 0$, and $t \rightarrow 0$.

Already at the level of the tensorial basis, given in Eq. (4.2), it is straightforward to see that the unique tensor that will survive in this limit will be $\ell_{\mu\nu}^1$. Using the fact that the answer, in this limit, should be Bose symmetric, the color tensors which will be available are the combinations of (i) c_1^{abmn} and c_2^{abmn} , (ii) c_4^{abmn} and c_5^{abmn} , and (iii) c_3^{abmn} . However, options (ii) and (iii) violate the ghost-antighost symmetry between the ghost legs. Therefore, it is natural to expect that in the all-soft limit the BB $\bar{c}c$ vertex may be written as

$$\widehat{\Gamma}_{\mu\nu}^{abmn}(0, 0, 0, 0) = g_{\mu\nu}(f^{max} f^{xbn} + f^{mbx} f^{xan}) \mathcal{C}_{11}(0, 0, 0, 0), \quad (4.5)$$

where we have used Eq. (B.10) to fix $\mathcal{C}_{11}(q, r, p, t) = \mathcal{C}_{12}(r, q, p, t)$.

4.2 Definitions of the full Green's functions

Before embarking on the main purpose of this work, *i.e.*, the calculation of the BB $\bar{c}c$ SDE in the all-soft limit, let us first present some basic definitions and conventions necessary to evaluate the $\widehat{\Gamma}_{\mu\nu}^{abmn}$ in the kinematic configuration of interest.

4.2.1 Three-point sector

Let us start with quantities appearing in the three-point sector, shown in Fig. 4.2. In panel (a), we display the fully dressed conventional ghost-gluon vertex, $\Gamma_{\mu}^{amn}(r, p, q) = -g f^{amn} \Gamma_{\mu}(r, p, q)$,

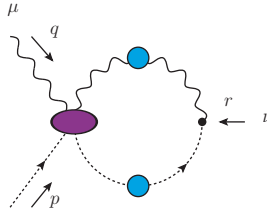
$$H_{\mu\nu}(r, p, q) = g_{\mu\nu} +$$


Figure 4.3: The diagrammatic representation of the ghost-gluon scattering kernel and the momenta convention adopted.

whose most general tensorial decomposition is given by

$$\Gamma_{\mu}(r, p, q) = B_1(r, p, q)r_{\mu} + B_2(r, p, q)q_{\mu}, \quad (4.6)$$

where $B_1(r, p, q)$ and $B_2(r, p, q)$ are the form factors. At tree-level $B_1^{(0)} = 1$, and $B_2^{(0)} = 0$, and we recover the Feynman rule quoted in Fig. 1.2.

The ghost-gluon vertex respects the following STI

$$\Gamma_{\mu}(r, p, q) = r^{\nu} H_{\mu\nu}(r, p, q), \quad (4.7)$$

where $H_{\mu\nu}(r, p, q)$ is the *ghost-gluon scattering kernel*, depicted in Fig. 4.3.

A well-known result for the ghost-gluon vertex is a direct consequence of the so-called Taylor theorem [71], which states that the ghost-gluon vertex reduces to its tree-level value in the $p \rightarrow 0$ limit. This configuration in the literature is referred to soft-ghost or Taylor kinematics [10, 72, 73].

For later convenience, it is also crucial to check the soft antighost limit, *i.e.*, when one sets r to 0, which will be extensively employed to evaluate the BB̄c vertex. From Eq. (4.7), one can see that, when $r \rightarrow 0$, the ghost-gluon vertex vanishes. Furthermore, using the decomposition in Eq. (4.6), it is possible to see that the form factor B_2 also vanishes in this kinematic limit.

The vertex appearing in the panel (b) of Fig. 4.2 is the complete background ghost-gluon vertex (B̄c̄c), $\tilde{\Gamma}_{\mu}^{amn}(r, p, q) = -gf^{amn}\tilde{\Gamma}_{\mu}(r, p, q)$. As it was mentioned in the Chapter 2 [see Fig. 2.6], this vertex satisfies an Abelian-like WTI, which we repeat here for convenience

$$q^{\mu} \tilde{\Gamma}_{\mu}(r, p, q) = D^{-1}(p) - D^{-1}(r). \quad (4.8)$$

Then, employing the gauge technique procedure [74]², one can construct an Ansatz

²The gauge technique amounts to solving the WTI (or STI in the non-Abelian case) in favor of the vertex involved. One of its limitations is the inaccessibility of the transverse part of the vertex.

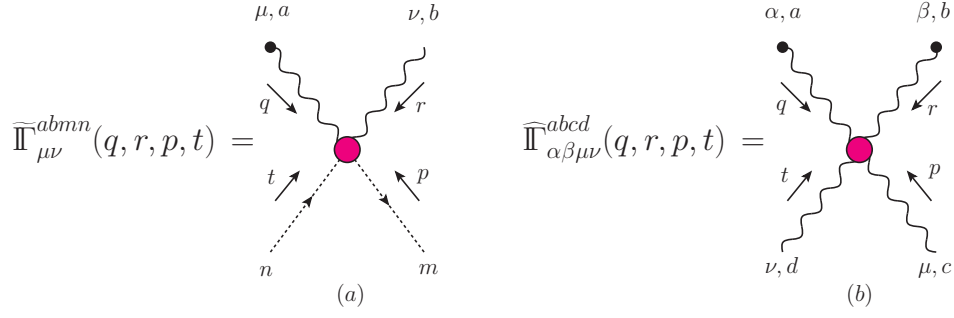


Figure 4.4: Diagrammatic representations of the fully dressed four-point vertices. In particular, we show in the panels (a) the BQ $\bar{c}c$ and (b) BBQQ vertices with their respective momenta conventions.

for this vertex which is given by

$$\tilde{\Gamma}_{\mu}(r, p, q) = \left[\frac{D^{-1}(p) - D^{-1}(r)}{p^2 - r^2} \right] (2r + q)_{\mu}. \quad (4.9)$$

The full background vertex $\tilde{\Gamma}_{\alpha\mu\nu}^{abc}(q, r, p) = g f^{abc} \tilde{\Gamma}_{\alpha\mu\nu}^{abc}(q, r, p)$, appearing in the panel (c) of Fig. 4.2, is the BQQ vertex. This vertex displays a ξ -dependence already at tree-level [see its Feynman rule in Fig. 2.4], and this feature will persist to all-orders. Thus, one may write that

$$\tilde{\Gamma}_{\alpha\mu\nu}(q, r, p) = \tilde{\Gamma}'_{\alpha\mu\nu}(q, r, p) + \frac{1}{\xi} [g_{\alpha\nu} r_{\mu} - g_{\alpha\mu} p_{\nu}]. \quad (4.10)$$

4.2.2 Four-point sector

As for the four-point sector, besides the full BB $\bar{c}c$ vertex already defined in Eq. (4.1), in Fig. 4.4, we show in panel (a) the full BQ $\bar{c}c$ vertex defined as

$$\tilde{\Pi}_{\mu\nu}^{abmn}(q, r, p, t) = -i g^2 \tilde{\Gamma}_{\mu\nu}^{abmn}(q, r, p, t). \quad (4.11)$$

Finally, in panel (b) of the same Figure, we show the complete BBQQ vertex, which also depends on the gauge parameter. This vertex can be written as

$$\widehat{\Pi}_{\alpha\beta\mu\nu}^{abcd}(q, r, p, t) = \widehat{\Gamma}_{\alpha\beta\mu\nu}^{abcd}(q, r, p, t) + \frac{1}{\xi} f^{acx} f^{xbd} g_{\alpha\mu} g_{\beta\nu} - \frac{1}{\xi} f^{adx} f^{xbc} g_{\alpha\nu} g_{\beta\mu}. \quad (4.12)$$

It is important to stress here that the contributions involving the BQQ and BBQQ vertices have to be computed in a general covariant gauge ξ , only taking the gauge parameter to zero (to set the Landau gauge), at the very end of the calculation, when all terms containing

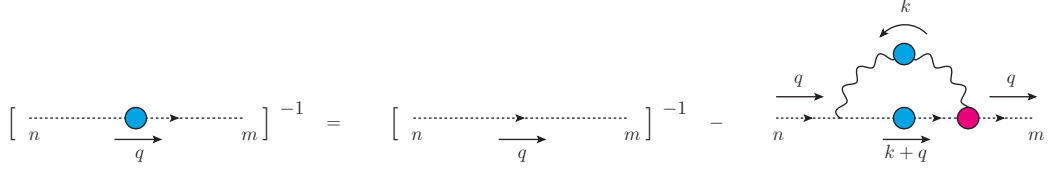


Figure 4.5: The diagrammatic representation of the ghost SDE.

$1/\xi$ terms were canceled entirely.

4.2.3 Two-point sector

Now we turn our attention to the two main functions of the two-point sector: the full gluon propagator, $\Delta_{\mu\nu}^{ab}(q) = -i\delta^{ab}\Delta_{\mu\nu}(q)$, and the complete ghost propagator, $D^{ab}(q) = i\delta^{ab}D(q)$. For the gluon propagator, in general covariant gauges, one has

$$\Delta_{\mu\nu}(q) = P_{\mu\nu}(q)\Delta(q) + \xi \frac{q_\mu q_\nu}{q^4}, \quad P_{\mu\nu}(q) = g_{\mu\nu} - \frac{q_\mu q_\nu}{q^2}. \quad (4.13)$$

As has been firmly established by a variety of large-volume simulations and continuous studies, $\Delta(q)$ saturates at a finite nonvanishing value, a feature which is widely attributed to the emergence of a gluonic mass scale [7, 11].

The ghost propagator, $D(q)$, is expressed in terms of its dressing function, $F(q)$, as

$$D(q) = \frac{F(q)}{q^2}, \quad (4.14)$$

and it is known that, in the Landau gauge, $F(q)$ saturates at a finite value in the deep infrared [11, 28, 75, 76].

The nonperturbative dynamics of $F(q)$ is governed by the ghost SDE, given by Eq. (3.19) and represented in Fig. 4.5. Factoring out the color terms and writing the LHS in terms of the ghost dressing function, $F(q) = q^2 D(q)$, Eq. (3.19) becomes

$$F^{-1}(q) = 1 - \frac{ig^2 C_A}{q^2} \int_k D(k+q) q_\nu \Delta^{\mu\nu}(k) \Gamma_\mu(-q, k+q, -k). \quad (4.15)$$

Next, we replace the conventional full ghost-gluon vertex, $\Gamma_\mu(-q, k+q, -k)$, by its most general tensorial decomposition given by Eq. (4.6) and obtain that

$$F^{-1}(q) = 1 + \Sigma(q), \quad (4.16)$$

with $\Sigma(q)$ given by

$$\Sigma(q) = ig^2 C_A \int_k D(k+q) \Delta(k) \left[1 - \frac{(k \cdot q)^2}{q^2 k^2} \right] B_1(-q, k+q, -k). \quad (4.17)$$

For later convenience, let us write the above expression in Euclidean space. Applying the rules to convert from Minkowski to Euclidean space presented in the Appendix C, we arrive at

$$F^{-1}(q) = 1 + \Sigma(q), \quad (4.18)$$

where $\Sigma(q)$ is the ghost self-energy given (in Euclidean space) by

$$\Sigma(q) = -\frac{g^2 C_A}{(2\pi)^3} \int_0^\infty dk^2 k^2 \Delta(k) \int_0^\pi d\varphi_1 \sin^4 \varphi_1 D(p) B_1(q^2, p^2, \varphi_1), \quad (4.19)$$

with $p = k + q$, and φ_1 the angle between $-q$ and p .

For later convenience, now we compute the limit of the ghost self-energy when $q \rightarrow 0$. In this limit, the angular integration can be performed trivially, and thus one obtains that (in Euclidean space)

$$\Sigma(0) = -\frac{3g^2 C_A}{(8\pi)^2} \int_0^\infty dk^2 F(k) \Delta(k) B_1(k^2), \quad (4.20)$$

where $B_1(k^2)$ is a shorthand notation to the form factor B_1 in the soft antighost limit, *i.e.*, $B_1(0, k, -k)$, that will only depend on the momentum k since the angle dependence is washed out completely.

Applying again the transformations rules, presented in the Appendix C, one can rewrite this equation back in the Minkowski space. In doing that we find that (in Minkowski space) the self-energy at the origin is given by

$$\Sigma(0) = \frac{3}{4} ig^2 C_A \int_k \Delta(k) D(k) B_1(0, k, -k). \quad (4.21)$$

4.2.4 Renormalization

In the next section, it will be necessary to address the renormalization of the SDE and, subsequently, define a particular scheme for fixing the renormalization constants. Let us then define Z_g , Z_A , and Z_c , the renormalization constants for the coupling, the gluon, and the

ghost fields, respectively,

$$g := Z_g g^{\text{R}}, \quad \Delta(q) := Z_A \Delta^{\text{R}}(q), \quad F(q) := Z_c F^{\text{R}}(q), \quad (4.22)$$

where the superscript “R” denotes the renormalized quantity. As for those related to the conventional ghost-gluon (Q $\bar{c}c$), Z_1 , background ghost-gluon (B $\bar{c}c$), \tilde{Z}_1 , and the background four-point functions BQ $\bar{c}c$, \tilde{Z}_4 , and BB $\bar{c}c$, \hat{Z}_4 , vertices, they are defined by

$$\begin{aligned} \Gamma_\mu(r, p, q) &:= Z_1^{-1} \Gamma_\mu^{\text{R}}(r, p, q), & \tilde{\Pi}_{\mu\nu}(q, r, p, t) &:= \tilde{Z}_4^{-1} \tilde{\Pi}_{\mu\nu}^{\text{R}}(q, r, p, t), \\ \tilde{\Gamma}_\mu(r, p, q) &:= \tilde{Z}_1^{-1} \tilde{\Gamma}_\mu^{\text{R}}(r, p, q), & \hat{\Pi}_{\mu\nu}(q, r, p, t) &:= \hat{Z}_4^{-1} \hat{\Pi}_{\mu\nu}^{\text{R}}(q, r, p, t), \end{aligned} \quad (4.23)$$

where we have omitted the color structures for simplicity.

However, not all of these renormalization constants are independent. Indeed, one can use the WTIs, given in Fig. 2.6, to relate them. One can see that the BB $\bar{c}c$, B $\bar{c}c$, and BQ $\bar{c}c$ WTIs impose the following relations between the renormalization constants, respectively

$$\hat{Z}_4 = \tilde{Z}_1, \quad \tilde{Z}_1 = Z_c, \quad \tilde{Z}_4 = Z_1. \quad (4.24)$$

In addition, the renormalization constants of the coupling, Z_g , should satisfy the relation

$$Z_g^{-1} = Z_1^{-1} Z_A^{1/2} Z_c. \quad (4.25)$$

The renormalization of the SDE for the ghost propagator, given by Eq. (4.16), proceeds through the replacement of the bare quantities by the renormalized ones listed in Eqs. (4.22) and (4.23). Then, the ghost SDE becomes

$$F_{\text{R}}^{-1}(q) = Z_c + Z_1 \Sigma(q). \quad (4.26)$$

In what follows, the renormalization is implemented within the well-known variant of the momentum subtraction (MOM) scheme known as “Taylor scheme” [77, 78]³, which fixes the (finite) vertex renormalization constant at the special value $Z_1 = 1$.

The actual closed expression of Z_c is obtained from Eq. (4.26) itself, by imposing the MOM renormalization condition, $F_{\text{R}}^{-1}(\mu) = 1$, where μ is the renormalization scale. Imple-

³In the literature this scheme is also known as minimal momentum subtraction (MiniMOM) scheme [79], and has been employed for a recent determination of α_{MS} from unquenched lattice simulations [80], consistent with the experimental *world average*.

menting this condition at the level of Eq. (4.26) yields

$$Z_c = 1 - \Sigma(\mu), \quad (4.27)$$

and Eq. (4.26) may be cast in the form

$$F_R^{-1}(q) = 1 + \Sigma(q) - \Sigma(\mu). \quad (4.28)$$

4.3 Evaluation of the all-soft limit

In Chapter 3, we have derived the SDE for the $BB\bar{c}c$ vertex in the compact form, as illustrated in Fig. 3.2. In addition, we have performed the skeleton expansion of the 1PR kernels, in terms of the 1PI vertices. Thus, in Fig. 3.3, we show the final diagrammatic representation for the $BB\bar{c}c$ SDE. As one can see, the SDE contains $3 + (8 \times 2)$ contributions, where the number 2 contemplates the possibility of a given diagram display the same topology but with external background gluon legs crossed. These diagrams with crossed legs were omitted in Figs. 3.2 and 3.3 for simplicity.

We are now ready to take the all-soft limit in the SDE of Fig. 3.3. We conduct this analysis by evaluating the contribution of the 11 diagrams represented in Fig. 3.3 individually. The other counterpart contributions (with crossed legs which were omitted in the Figure) can be evaluated using the same line of reasoning which will be presented below.

First, notice that the diagrams in Fig. 3.3 may vanish for two reasons: either (i) they have a gluon propagator that carries a transverse projector, for example, $P_{\mu\nu}(k)$, which contracts with the antighost momentum coming from the bare ghost-gluon vertex, k^μ , or (ii) there is a ghost-gluon vertex in the soft antighost limit, which is zero.

Case (i) happens with diagrams (d_{11}) , (d_{14}) , (d_{16}) , and (d_{18}) . Case (ii) happens with the diagrams (d_{11}) , (d_{14}) , and (d_{22}) .

However, one has to be careful with the calculations of diagrams (d_{12}) , (d_{13}) , (d_{15}) , (d_{17}) , and (d_{21}) , since they involve the full BQQ and BBQQ vertices, which explicitly depend on the inverse of gauge fixing parameter $1/\xi$ [see Eqs. (4.10) and (4.12)]. Therefore, as we will see soon, one must compute these contributions in a general ξ gauge, and after canceling the $1/\xi$ terms, we take the Landau limit, $\xi \rightarrow 0$. Note in passing that the 5-point 1PI function in (d_{18}) is assumed to have no explicit dependence on the gauge parameter.

As we will see, out of these five diagrams shown in Fig. 4.6, four vanish in the all-soft limit. We may now proceed with the explicit calculation of these contributions in this kinematic

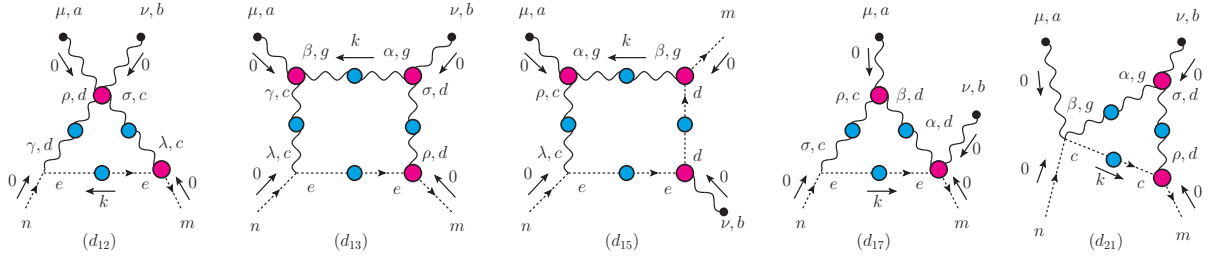


Figure 4.6: Diagrams of the SDE for the $BB\bar{c}$ containing either the BQQ or the BBQQ vertices. Out of these five diagrams, only (d_{17}) furnishes a nonvanishing answer in the all-soft limit.

configuration. Let us start with the diagram (d_{12}) , whose expression, when we set all external momenta to zero, *i.e.*, $q = r = p = t = 0$, is written as

$$(d_{12})_{\mu\nu}^{abmn} = g^4 c_1^{cndm} \int_k \left(\frac{k^\rho}{k^2} \right) \xi \left[\widehat{\Gamma}_{\mu\nu\sigma\rho}^{abcd}(0, 0, -k, k) + \frac{1}{\xi} c_1^{adbc} g_{\mu\sigma} g_{\nu\rho} - \frac{1}{\xi} c_1^{acbd} g_{\mu\rho} g_{\nu\sigma} \right] \times D(k) \Delta^{\sigma\lambda}(k) \Gamma_\lambda(0, -k, k), \quad (4.29)$$

where c_1^{cndm} is defined in Eq. (4.3).

As mentioned previously, first, one has to perform the calculations in general covariant gauges, using for the $\Delta^{\gamma\rho}(k)$ the expression given in Eq. (4.13). In doing that, one can see that the terms containing $1/\xi$ will explicitly cancel against the ξ -dependent part of the gluon propagator. Thus, only after this procedure one can safely set the gauge parameter to the Landau gauge, *i.e.*, $\xi \rightarrow 0$. For the particular case of the above equation, after doing the above steps, one arrives at

$$(d_{12})_{\mu\nu}^{abmn} = g^4 c_1^{cndm} \int_k D(k) \Delta^{\sigma\lambda}(k) \Gamma_\lambda(0, -k, k) \left(\frac{k^\rho}{k^2} \right) \left[c_1^{adbc} g_{\mu\sigma} g_{\nu\rho} - c_1^{acbd} g_{\mu\rho} g_{\nu\sigma} \right]. \quad (4.30)$$

Once $\Gamma_\lambda(0, -k, k) = 0$, we find that the contribution of $(d_{12})_{\mu\nu}^{abmn}$ is null.

The next diagram to be evaluated is (d_{13}) , which can be written in the all-soft limit as

$$(d_{13})_{\mu\nu}^{abmn} = g^4 c_1^{cdba} c_1^{dcnm} \int_k D(k) \Gamma_\rho(0, k, -k) \left(\frac{k^\gamma}{k^2} \right) \xi \left[\widetilde{\Gamma}'_{\mu\beta\gamma}(0, k, -k) + \frac{1}{\xi} (g_{\mu\gamma} k_\beta + g_{\mu\beta} k_\gamma) \right] \times \left(\Delta^{\rho\sigma}(k) \Delta^{\alpha\beta}(k) \widetilde{\Gamma}'_{\nu\sigma\alpha}(0, k, -k) + \Delta_\nu^\rho(k) \frac{k^\beta}{k^2} + \Delta_\nu^\beta(k) \frac{k^\rho}{k^2} \right). \quad (4.31)$$

Repeating the same procedure applied in the previous diagram, *i.e.*, first, performing the cancellations of all $1/\xi$ terms, and only after that, fixing our calculation in the Landau gauge, we

find that

$$(d_{13})_{\mu\nu}^{abmn} = g^4 c_1^{cdba} c_1^{dcnm} \int_k D(k) \Gamma_\rho(0, k, -k) \left(\frac{k^\gamma}{k^2} \right) [g_{\mu\gamma} k_\beta + g_{\mu\beta} k_\gamma] \times \quad (4.32)$$

$$\left(\Delta^{\rho\sigma}(k) \Delta^{\alpha\beta}(k) \tilde{\Gamma}'_{\nu\sigma\alpha}(0, k, -k) + \Delta_\nu^\rho(k) \frac{k^\beta}{k^2} + \Delta_\nu^\beta(k) \frac{k^\rho}{k^2} \right),$$

which again vanishes, due to the presence of the ghost-gluon vertex in the soft antighost limit, *i.e.*, $\Gamma_\rho(0, k, -k) = 0$. Therefore, we obtain that $(d_{13})_{\mu\nu}^{abmn} = 0$.

Now, we proceed with the analysis of the contribution of (d_{15}) . In the all-soft limit (d_{15}) reduces to

$$(d_{15})_{\mu\nu}^{abmn} = g^4 c_1^{cdma} c_1^{ndbc} \int_k \Delta_{\alpha\beta}(k) D^2(k) \tilde{\Gamma}'_\nu(-k, k, 0) \Gamma_\beta(0, k, -k) \times \quad (4.33)$$

$$\left(\frac{k_\rho}{k^2} \right) \xi [\tilde{\Gamma}'_{\mu\alpha\rho}(0, k, -k) + \frac{1}{\xi} (g_{\mu\rho} k_\alpha + g_{\mu\alpha} k_\rho)].$$

From the above equation, one can see that the $1/\xi$ factor cancels against the left-over of ξ -dependent part of the gluon propagator. Then, performing these cancellations and setting the Landau gauge, one finds that

$$(d_{15})_{\mu\nu}^{abmn} = g^4 c_1^{cdma} c_1^{ndbc} \int_k \Delta_{\alpha\beta}(k) D^2(k) \tilde{\Gamma}'_\nu(-k, k, 0) \Gamma_\beta(0, k, -k) (g_{\mu\rho} k_\alpha + g_{\mu\alpha} k_\rho) \frac{k_\rho}{k^2}, \quad (4.34)$$

once again, leading to a vanishing contribution due to the ghost-gluon vertex in the soft antighost limit, *i.e.*, $\Gamma_\beta(0, k, -k)$. Thus, we find that $(d_{15})_{\mu\nu}^{abmn} = 0$.

Let us now check what the diagram (d_{17}) produces in the all-soft limit. In this configuration, (d_{17}) is given by

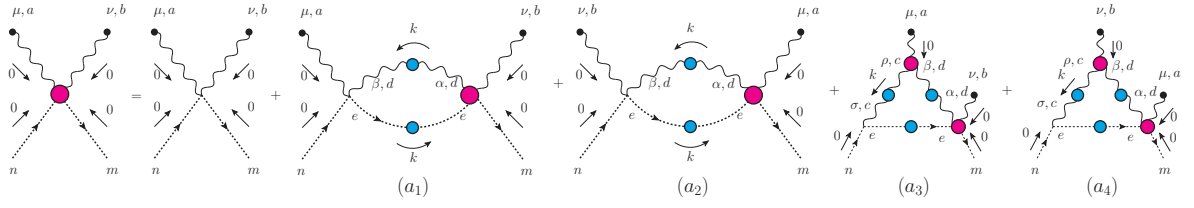
$$(d_{17})_{\mu\nu}^{abmn} = g^4 c_1^{aend} \int_k \Delta_{\alpha\beta}(k) D(k) \tilde{\Gamma}'_{\nu\alpha}{}^{bdme}(0, -k, 0, k) \times \quad (4.35)$$

$$\left(\frac{k_\rho}{k^2} \right) \xi \left[\tilde{\Gamma}'_{\mu\beta\rho}(0, k, -k) + 2k_\mu g_{\beta\rho} + g_{\mu\beta} \left(\frac{k_\rho}{\xi} - k_\rho \right) + g_{\mu\rho} \left(\frac{k_\beta}{\xi} - k_\beta \right) \right].$$

Then, one can see that the $1/\xi$ factors cancels also against the left-over of ξ -dependent part of the gluon propagator. Then, performing these cancellations and setting the Landau gauge, one finds that

$$(d_{17})_{\mu\nu}^{abmn} = g^4 c_1^{aend} \int_k \Delta_{\mu\alpha}(k) D(k) \tilde{\Gamma}'_{\nu\alpha}{}^{bdme}(0, -k, 0, k), \quad (4.36)$$

which is a nonvanishing contribution. Then, the diagram $(d_{17})_{\mu\nu}^{abmn}$ and its crossed legs counterpart, $(d_{17})_{\nu\mu}^{bamn}$, contribute to the SDE in the all-soft limit.

Figure 4.7: The diagrammatic representation of the SDE for the $BB\bar{c}$ in the all-soft limit.

We may now proceed with the analysis of diagram (d_{21}) , whose expression in the all-soft limit is given by

$$(d_{21})_{\mu\nu}^{abmn} = g^4 c_1^{gcm b} c_1^{cnga} g_{\mu\beta} \int_k D(k) \Gamma_\rho(0, k, -k) \left(\Delta(k) P^{\rho\sigma}(k) + \xi \frac{k^\rho k^\sigma}{k^4} \right) \times \quad (4.37)$$

$$\left(\Delta(k) P^{\alpha\beta}(k) + \xi \frac{k^\alpha k^\beta}{k^4} \right) \left[\tilde{\Gamma}'_{\nu\sigma\alpha}(0, k, -k) + \frac{1}{\xi} (g_{\nu\sigma} k_\alpha + g_{\nu\alpha} k_\sigma) \right].$$

Repeating the same steps applied in the previous calculations, we find that in the Landau gauge the above equation reduces to

$$(d_{21})_{\mu\nu}^{abmn} = g^4 c_1^{gcm b} c_1^{cnga} g_{\mu\beta} \int_k D(k) \Gamma_\rho(0, k, -k) \left(\Delta_\nu^\rho(k) \frac{k^\beta}{k^2} + \Delta_\nu^\beta(k) \frac{k^\rho}{k^2} \right), \quad (4.38)$$

which again will be zero due to the presence of the ghost-gluon vertex in the soft antighost limit, *i.e.*, $\Gamma_\rho(0, k, -k)$, so we find that $(d_{21})_{\mu\nu}^{abmn} = 0$.

After scrutinizing the contributions of the five diagrams appearing in Fig. 4.6, it is missing to evaluate one last diagram, which does not fit in any of the cases mentioned previously. The diagram in question is (d_{23}) of Fig. 3.3. Its expression, in the all-soft limit and Landau gauge is given by

$$(d_{23})_{\mu\nu}^{abmn} = g^4 c_1^{edna} \int_k \Delta_{\mu\alpha}(k) D(k) \tilde{\Gamma}_{\nu\alpha}^{bdme}(0, -k, 0, k), \quad (4.39)$$

which is non-null. This diagram also has a crossed legs counterpart, $(d_{23})_{\nu\mu}^{bamn}$, which should also be taken into account.

In this way, summing the nonvanishing contributions given by Eqs. (4.36) and (4.39) and their respective crossed legs counterparts, one arrives that the SDE of the $BB\bar{c}$ vertex, in the all-soft limit, is diagrammatically represented in Fig. 4.7, and it may be written as

$$\hat{\Gamma}_{\mu\nu}^{abmn}(0, 0, 0, 0) = (f^{max} f^{xbn} + f^{mbx} f^{xan}) g_{\mu\nu} - i g^2 \sum_{i=1}^4 (a_i)_{\mu\nu}^{abmn}, \quad (4.40)$$

where the diagrams $(a_i)_{\mu\nu}^{abmn}$ are given by

$$\begin{aligned}
(a_1)_{\mu\nu}^{abmn} &= f^{eax} f^{dnx} \int_k \Delta_{\mu\alpha}(k) D(k) \tilde{\Gamma}_{\nu\alpha}^{bdme}(0, -k, 0, k), \\
(a_2)_{\mu\nu}^{abmn} &= f^{ebx} f^{dnx} \int_k \Delta_{\nu\alpha}(k) D(k) \tilde{\Gamma}_{\mu\alpha}^{adme}(0, -k, 0, k), \\
(a_3)_{\mu\nu}^{abmn} &= f^{enx} f^{adx} \int_k \Delta_{\mu\alpha}(k) D(k) \tilde{\Gamma}_{\nu\alpha}^{bdme}(0, -k, 0, k), \\
(a_4)_{\mu\nu}^{abmn} &= f^{enx} f^{bdx} \int_k \Delta_{\nu\alpha}(k) D(k) \tilde{\Gamma}_{\mu\alpha}^{adme}(0, -k, 0, k).
\end{aligned} \tag{4.41}$$

The (multiplicative) renormalization of Eq. (4.40) proceeds in the standard way. Specifically, one must introduce the propagators and vertices renormalization relations given in Eqs. (4.22) and (4.23). Then, it is possible to show that the renormalized version of Eq. 4.40 reads

$$\hat{\Gamma}_{\mu\nu}^{abmn}(0, 0, 0, 0) = Z_c (f^{max} f^{xbn} + f^{mbx} f^{xan}) g_{\mu\nu} - ig^2 Z_1 \sum_{i=1}^4 (a_i)_{\mu\nu}^{abmn}. \tag{4.42}$$

In what follows, we will invoke Taylor's theorem [see discussion next Eq. (4.26)], in order to finally set $Z_1 = 1$ to all orders. Then, the renormalized version of SDE becomes

$$\hat{\Gamma}_{\mu\nu}^{abmn}(0, 0, 0, 0) = Z_c (f^{max} f^{xbn} + f^{mbx} f^{xan}) g_{\mu\nu} - ig^2 \sum_{i=1}^4 (a_i)_{\mu\nu}^{abmn}, \tag{4.43}$$

where the renormalized constant Z_c was already fixed from the ghost SDE, given by Eq. (4.27).

As we have seen above, the expression of the SDE for the $\text{BB}\bar{c}c$ vertex in the all-soft limit depends crucially on the $\text{BQ}\bar{c}c$ vertex on a particular kinematic limit, more specifically, on $\tilde{\Gamma}_{\mu\nu}^{abmn}(0, -k, 0, k)$. It turns out that, for this specific limit, one can determine, without resort to any approximation, what is the exact answer for the $\text{BQ}\bar{c}c$ with the help of the WTI that it satisfies.

To be clear about the procedure, let us rewrite here the WTI that the $\text{BQ}\bar{c}c$ vertex satisfies, which was already presented in Fig. 2.6,

$$\begin{aligned}
q^\mu \tilde{\Gamma}_{\mu\nu}^{abmn}(q, r, p, t) &= f^{nax} f^{bm x} \Gamma_\nu(p, q+t, r) + f^{nbx} f^{max} \Gamma_\nu(q+p, t, r) \\
&\quad + f^{nm x} f^{abx} \Gamma_\nu(p, t, q+r).
\end{aligned} \tag{4.44}$$

Then, one can compute $\tilde{\Gamma}_{\mu\nu}^{abmn}(0, -k, 0, k)$ by taking the background gluon, q , and the antighost, p , momenta to zero. Setting $r = -t$, and by means of a Taylor expansion around $q = 0$, we find

that

$$q^\mu \tilde{\Gamma}_{\mu\nu}^{abmn}(0, -t, 0, t) = -f^{nax} f^{bmx} q^\mu \frac{\partial}{\partial q^\mu} \left[B_1(-q, q+t, -t) q_\nu + B_2(-q, q+t, -t) t_\nu \right] \Big|_{q=0} \quad (4.45)$$

$$- f^{nmx} f^{abx} q^\mu \frac{\partial}{\partial q^\mu} \left[B_1(-q, t, q-t) q_\nu + B_2(-q, t, q-t) (q-t)_\nu \right] \Big|_{q=0},$$

where the terms of order zero in q on the right-hand side (RHS) of the equation vanish, since they are proportional to the Jacobi identity (see Eq. (A.5) in Appendix A). Then, using the fact that the ghost-gluon form factor B_2 is zero in the soft antighost limit, and knowing that the momentum t is independent of q , we arrive at

$$\tilde{\Gamma}_{\mu\nu}^{abmn}(0, -t, 0, t) = -g_{\mu\nu} (f^{nax} f^{bmx} + f^{nmx} f^{abx}) B_1(0, t, -t). \quad (4.46)$$

Armed with the above result, we can rewrite Eq. (4.43) in the following compact form

$$\hat{\Gamma}_{\mu\nu}^{abmn}(0, 0, 0, 0) = g_{\mu\nu} (f^{max} f^{xbn} + f^{mbx} f^{xan}) [Z_c + \Sigma(0)], \quad (4.47)$$

where Z_c is given in Eq. (4.27), and we have identified the ghost self-energy at the origin, $\Sigma(0)$, given in Eq. (4.21). Replacing the renormalization constant Z_c by Eq. (4.27), and keeping only the terms of $\mathcal{O}(\alpha_s)$, we find that

$$\hat{\Gamma}_{\mu\nu}^{abmn}(0, 0, 0, 0) = g_{\mu\nu} (f^{max} f^{xbn} + f^{mbx} f^{xan}) [1 + \Sigma_R(0)], \quad (4.48)$$

where

$$\Sigma_R(0) = \Sigma(0) - \Sigma(\mu). \quad (4.49)$$

Identifying the term in squared brackets in the above expression using Eq. (4.28), we find that

$$\hat{\Gamma}_{\mu\nu}^{abmn}(0, 0, 0, 0) = g_{\mu\nu} (f^{max} f^{xbn} + f^{mbx} f^{xan}) F_R^{-1}(0). \quad (4.50)$$

Some remarks here are in order: First, notice that the above relation was derived without employing any approximation. Therefore, we have established an exact relation, valid to all-orders in the all-soft limit. As already mentioned in Eq. (4.5), the BB̄c vertex, in the all-soft limit, suffers a drastic simplification in its tensorial structure, depending just on the metric, with the corresponding form factor identified as being $\mathcal{C}_{11}(0, 0, 0, 0) = \mathcal{C}_{12}(0, 0, 0, 0) = F_R^{-1}(0)$.

From Eq. (4.48), one can see that the quantity $\Sigma_R(0)$ quantifies the nonperturbative correction that the form factor $\mathcal{C}_{11}(0, 0, 0, 0)$ acquires beyond the tree-level.

It is important to mention that the derivation of this exact relation constitutes the main novelty of the present work.

Finally, let us point out that in the context of the SDE framework, obtaining such exact relations is unusual, even if we restrict our analysis to a particular kinematic configuration, as it was done here. For this reason, one may take advantage of this relation to check the validity or the accuracy of a particular truncation scheme proposed for this vertex in general kinematics.

4.4 All-soft limit from the WTI of the BB̄c vertex

In this Section, after establishing an exact constraint on the form factor comprising the BB̄c vertex in the all-soft limit (all external legs have zero momenta) directly from the SDE satisfied by $\widehat{\Gamma}_{\mu\nu}^{abmn}$, we derive the same relation using only the WTI that this vertex satisfies.

Let us start by considering the WTI that relates the BB̄c with the background ghost-gluon vertices, which reads,

$$q^\mu \widehat{\Gamma}_{\mu\nu}^{abmn}(q, r, p, t) = f^{max} f^{bnx} \widetilde{\Gamma}_\nu(t, q+r, p) + f^{mbx} f^{nax} \widetilde{\Gamma}_\nu(t+q, r, p) + f^{mnx} f^{abx} \widetilde{\Gamma}_\nu(t, r, q+p). \quad (4.51)$$

Now, we replace the background ghost-gluon vertices by Eq. (4.9), and take the limit of $r \rightarrow 0$ and $t \rightarrow 0$, and arrive at

$$q^\mu \widehat{\Gamma}_{\mu\nu}^{abmn}(q, 0, -q, 0) = q_\nu (f^{max} f^{xbn} + f^{mbx} f^{xan}) \frac{D^{-1}(q)}{q^2}. \quad (4.52)$$

Expanding both sides of the above expression around $q \rightarrow 0$, and writing the ghost propagator as a function of its dressing, $F(q)$, using Eq. (4.14), we find that

$$q^\mu \widehat{\Gamma}_{\mu\nu}^{abmn}(q, 0, -q, 0) \Big|_{q=0} = q^\mu g_{\mu\nu} (f^{max} f^{xbn} + f^{mbx} f^{xan}) F^{-1}(q) \Big|_{q=0}, \quad (4.53)$$

which, cancelling the terms q^μ , leads immediately to the same exact relation, given in Eq. (4.50), but now derived entirely from the point of view of the WTI that the BB̄c vertex satisfies.

4.5 Numerical Analysis: Beyond the all-soft configuration

In Section 4.3, we have established an exact result for the $BB\bar{c}c$ vertex in the all-soft configuration, where all four momenta of this vertex vanish. In this Section, we want to explore the possibility of using this exact result as a guideline in a future study of this vertex beyond the all-soft kinematic limit.

To do that, we will propose three truncated versions of the $BB\bar{c}c$ SDE in the all-soft limit. Then, to quantify what would be the best truncation scheme that could be applied in future analysis which goes beyond the all-soft configuration, we will compare the numerical results obtained with each one of the truncated versions of the $BB\bar{c}c$ SDE with the exact answer derived in Section 4.3.

More specifically, we will concentrate on the differences that each new truncation scheme will generate at the level of $\Sigma_R(0)$, given in Eq. (4.49), since it is precisely this quantity that carries the information of the nonperturbative corrections of the $BB\bar{c}c$ vertex. In order to quantify that, let us define the percentage error as being

$$\%_{error} = \frac{|\Sigma_R(0) - \bar{\Sigma}_R^i(0)|}{\Sigma_R(0)} \times 100\%, \quad \text{with } i = 1, 2, 3, \quad (4.54)$$

where $\bar{\Sigma}_R^i(0)$ is the ghost self-energy computed in the truncated scheme called scenario “i”.

Before embarking on the numerical analysis of the three truncated versions, first, we will briefly introduce the necessary nonperturbative ingredients to perform the above comparison. Besides the gluon propagator and the ghost-gluon form factor, we also need the ghost dressing function, $F(q)$. In particular, for $F(q)$, we solve the ghost SDE using two approximations for the form factor B_1 that enters on it. The different solutions obtained for $F(q)$ will feed our analysis of different truncation schemes for the $BB\bar{c}c$ vertex.

4.5.1 Nonperturbative inputs

First, let us summarize the necessary external inputs for solving the renormalized ghost SDE, given in Eq. (4.28) with $\Sigma(q)$ in Euclidean space given by Eq. (4.19). To evaluate numerically Eq. (4.28), one needs two external inputs: (i) the full gluon propagator, $\Delta(q)$, and (ii) the form factor B_1 .

Let us start with the gluon propagator, $\Delta(q)$, for which we employ a fit for a combined set of lattice data shown in Fig. 4.8. This data set corresponds to the reanalysis of the results obtained in the simulations performed by [81] after the continuum extrapolation, combined with the data from [82] after the scale resetting procedure. The details of the procedure

adopted in this analysis are described in [73]. This data set can be accurately fitted by following functional form

$$\Delta^{-1}(q) = q^2 \left[1 + \left(\kappa_1 - \frac{\kappa_2}{1 + (q^2/\kappa_4^2)^2} \right) \ln \left(\frac{q^2}{\mu^2} \right) \right] + R(q^2) - R(\mu^2), \quad (4.55)$$

with

$$R(q^2) = \frac{\sigma_0 + \sigma_1 q^2}{1 + (q^2/\sigma_2^2) + (q^2/\sigma_4^2)^2}, \quad (4.56)$$

where the fitting parameters are $\kappa_1 = 0.11$, $\kappa_2 = 0.03$, $\kappa_4^2 = 4.93 \text{ GeV}^2$, $\sigma_0 = -0.41 \text{ GeV}^2$, $\sigma_1 = -0.52$, $\sigma_2^2 = 10.27 \text{ GeV}^2$, and, $\sigma_4^2 = 4.63 \text{ GeV}^2$.

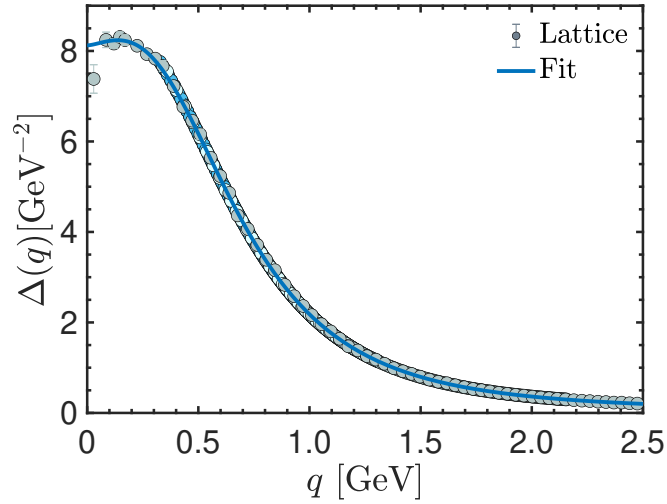


Figure 4.8: Lattice data for the gluon propagator, $\Delta(q)$, after performing the continuum extrapolation of [81] to the data set of [82], together with the corresponding fit given by Eq. (4.55). The gluon propagator is renormalized at $\mu = 4.3 \text{ GeV}$.

The adjusted curve is represented by the continuous line on Fig. 4.8, together with the lattice data. Notice that the IR saturation of $\Delta(q)$ to a finite nonvanishing value can be understood in terms of a dynamically generated gluon mass [7, 11].

Regarding the form factor B_1 entering into the ghost SDE in Eq. (4.28), we will solve the SDE considering two approximations for this quantity. In the first one, B_1 will be employed in general kinematics, whereas in the second one, we consider its tree-level value, *i.e.*, $B_1^{(0)} = 1$.

The data we shall use as an input for $B_1(q^2, p^2, \varphi_1)$, in general kinematics, was obtained in [73]. There, in the SDE for $B_1(q^2, p^2, \varphi_1)$, an approximate form of the three-gluon vertex is employed where only the tree-level tensorial structures are retained, and the associated form factors are taken from the STI-based derivation of [83].

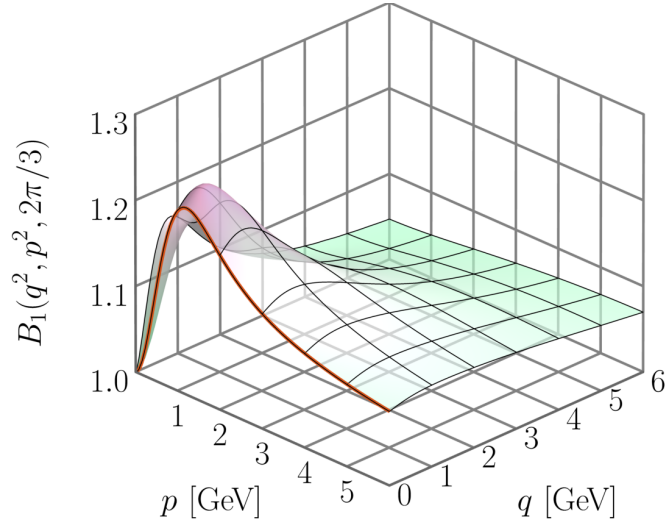


Figure 4.9: Form factor $B_1(q^2, p^2, 2\pi/3)$ in general kinematics as a function of the antighost momentum, q , and ghost momentum, p , for a fixed value of angle $\varphi_1 = 2\pi/3$. The red curve is the soft antighost limit of B_1 , where $q = 0$. This particular kinematic configuration, $B_1(k^2)$, contributes to $\Sigma(0)$.

A representative result for $B_1(q^2, p^2, \varphi_1)$ in general kinematic is depicted in Fig. 4.9, where we plot B_1 as a function of the antighost momentum, q , and ghost momentum, p , with a fixed value for the angle $\varphi_1 = 2\pi/3$. For latter convenience, in the same plot, we highlight by the continuous red line, located on the plane where $q = 0$, the soft antighost limit, $B_1(k^2)$.

With the inputs introduced above, the SDE for $F_R(q)$, given in Eq. (D.6), is solved numerically determining the coefficients of the Chebyshev expansion through the Newton's method. The external momenta, q^2 , is distributed on a logarithmic grid, with 50 points in the interval $[5.7 \times 10^{-4}, 1.8 \times 10^3]$ GeV². The interpolations in three variables, needed for evaluating the B_1 , is performed with B-splines [84], and the double integrals (radial and angular) are computed with a Gauss-Legendre method [85] [see Appendix D].

In Fig. 4.10, we show the numerical results for $F(q)$ obtained with both B_1 . The continuous blue curve represents the case where B_1 is in general kinematics, whereas in the pink curve, the form factor is at tree-level, *i.e.*, $B_1^{(0)} = 1$. We emphasize that the renormalization point is fixed at $\mu = 4.3$ GeV, which coincides with the highest value of the momentum accessible by the lattice simulation of [82]. In particular, one can observe that when the constant coupling assumes the value $\alpha_s(\mu) = 0.244$, the solution obtained with B_1 in general kinematics yields a $F(q)$ that is in outstanding agreement with the $F(q)$ of [81], which were properly extrapolated to the physical continuum limit.

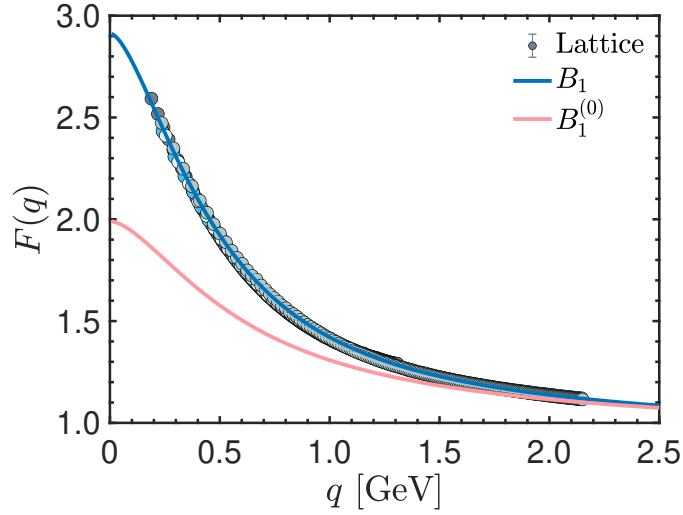


Figure 4.10: The numerical solution for the ghost dressing function with the ghost-gluon vertex dressed (blue continuous line) compared with the lattice data of [81], and the numerical solution for the ghost dressing function with the ghost-gluon vertex at tree-level (pink continuous curve).

4.5.2 Exploring truncations schemes for the $BB\bar{c}c$ SDE

Back at Section 4.3, we have derived the exact relation which states that the form factor \mathcal{C}_{11} in the all-soft limit is given by [see Eq. (4.50)]

$$\mathcal{C}_{11}(0, 0, 0, 0) = 1 + \Sigma_R(0), \quad (4.57)$$

where $\Sigma_R(0) = \Sigma(0) - \Sigma(\mu)$ was already defined in Eq. (4.49), and the corresponding self-energies (in Minkowski space) are given by Eqs. (4.21) and (4.17) setting $q \rightarrow \mu$ in the latter one. It is important to highlight here that the numerical determination of $\Sigma_R(0)$ requires B_1 not only in the soft antighost limit [see Eq. (4.21)] but also in general kinematics [see Eq. (4.17)]. In Fig. 4.9, we have already shown a representative case of B_1 for both configurations.

Now, we will propose a new truncation scheme for the $BB\bar{c}c$ SDE, where we approximate all dressed vertices by their respective tree-level counterparts. In this case, the $BB\bar{c}c$ SDE in the all-soft limit is diagrammatically represented in Fig. 4.11, and the approximated version of the form factor \mathcal{C}_{11} , to be denoted by $\bar{\mathcal{C}}_{11}$, may be expressed as

$$\bar{\mathcal{C}}_{11}(0, 0, 0, 0) = 1 + \bar{\Sigma}_R(0) \quad (4.58)$$

where $\bar{\Sigma}_R(0) = \bar{\Sigma}(0) - \bar{\Sigma}(\mu)$ is the renormalized ghost self-energy in this new approximation,

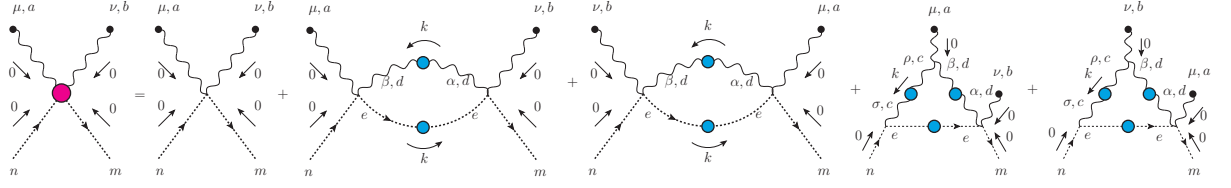


Figure 4.11: Diagrammatic representation of the SDE for the $BB\bar{c}$ vertex in the all-soft limit. In this equation, we approximate all dressed vertices by their tree-level counterparts.

and the corresponding self-energies (in Minkowski space) are given by ⁴

$$\bar{\Sigma}(0) = \frac{3}{4}ig^2C_A \int_k \Delta(k)D(k), \quad \bar{\Sigma}(\mu) = ig^2C_A \int_k D(k+\mu)\Delta(k) \left[1 - \frac{(k \cdot \mu)^2}{\mu^2 k^2} \right]. \quad (4.59)$$

We may now proceed with the determination of the percentage error, defined in Eq. (4.54), considering the following scenarios:

- **Scenario $i = 1$ - Propagators and coupling constant fixed:** To compute the $\%_{error}$ in this scenario, we employ the fit for $\Delta(k)$ given by Eq. (4.55). For $D(k)$, we use the solution of the SDE, which perfectly recovers the lattice data (blue curve in Fig. 4.10). In addition, we fix the value of $\alpha_s(\mu) = 0.244$. Within this scenario we will be able to determine $\bar{\Sigma}_R^1(0)$.
- **Scenario $i = 2$ - Gluon propagator and coupling constant fixed:** In this scenario, we employ the fit for $\Delta(k)$ given by Eq. (4.55). In addition, we set $\alpha_s(\mu) = 0.244$. As in this truncation scheme for the $BB\bar{c}$ vertex we are considering all vertices at tree-level, when we couple the ghost SDE to this system, the ghost-gluon vertex contributing to this equation should also be considered at tree-level. In doing that, we obtain for $F(q)$ the continuous pink curve shown in Fig. 4.10. It is precisely this data that will be used as input to compute $\bar{\Sigma}_R^2(0)$.
- **Scenario $i = 3$ - Adjusting the value of coupling constant:** In this scenario, the only difference between $\Sigma_R(0)$ and $\bar{\Sigma}_R^3(0)$ appearing in the numerator of Eq. (4.54) are the values of the coupling constant employed in the calculation of both quantities. As we have already mentioned, in the case of $\Sigma_R(0)$, we fix $\alpha_s(\mu) = 0.244$. On the other hand, for computing $\bar{\Sigma}_R^3(0)$, the value of $\alpha_s(\mu)$ is adjusted until the solution for $F(q)$ reproduces the lattice data shown in Fig. 4.10. To do that, we have to increase the coupling value to $\alpha_s(\mu) = 0.283$.

⁴To obtain $\bar{\Sigma}(0)$ go to Eq. (D.5), set $B1(q^2, k^2, \varphi_1) = 1$ and $q \rightarrow 0$. In this case the angular integration can be done easily, since $\int_0^\pi d\varphi_1 \sin^4 \varphi_1 = 3\pi/8$. After that, one only needs to use the rules in Appendix C to get back to Minkowski space.

With the help of Eqs. (4.21), (4.17) and (4.59), we are ready to compute $\Sigma_{\text{R}}(0)$ and $\bar{\Sigma}_{\text{R}}^i(0)$, for the three scenarios described above. After that, we determine the percentage error, $\%_{\text{error}}$, using the definition of Eq. (4.54). Table 4.1 compares the $\%_{\text{error}}$ for three truncation schemes applied for the SDE of the $\text{BB}\bar{\text{c}}\text{c}$ vertex in the all-soft configuration. The scenarios that display the smaller value for the $\%_{\text{error}}$ better agree with the exact relation given by Eq. (4.48).

Scenario	$i = 1$	$i = 2$	$i = 3$
$\%_{\text{error}}$	12.59%	23.98%	15.98%

Table 4.1: The corresponding percentage error, $\%_{\text{error}}$, defined by Eq. (4.54), and computed for the three truncation scenarios for the $\text{BB}\bar{\text{c}}\text{c}$ vertex.

From this analysis, we clearly see that scenario 2 is the most unfavorable case. One can understand this result easily if we recall that to solve the ghost SDE, we have approximated the full ghost-gluon vertex to its tree-level value. As a result, we obtain a $F(q)$ (pink curve in Fig. 4.10), which is already 40% more suppressed at the origin compared to lattice data. Thus, when we employ this solution for $F(q)$ in the calculation of $\Sigma_{\text{R}}^2(0)$, the error mentioned above combines with the intrinsic error of the truncated version of the SDE for the $\text{BB}\bar{\text{c}}\text{c}$ vertex itself, producing a final error of 23.98%.

Concerning scenarios 1 and 3, we can note that both display percentage errors in the same ballpark, with slightly better results achieved by scenario 1. The reason for this small difference in the values of $\%_{\text{error}}$ can be easily understood. First, we recall that $\Sigma(0)$ depends on $B_1(k^2)$ in the soft antighost limit. This kinematic limit corresponds to one of the configurations which maximizes the deviation of B_1 from the tree-level value⁵. Thus, moving away from this region, the nonperturbative corrections that B_1 acquires becomes smaller. Therefore, when we approximate the entire momentum dependence of ghost-gluon vertex just by its tree-level value (instead of integrating over the soft antighost configuration in the case of $\Sigma(0)$, and over all configurations for $\Sigma(\mu)$), we underestimate the contribution of the ghost-gluon vertex to the ghost SDE roughly by a value that should be smaller than 21%. Indeed, this is precisely what happens in scenario 3, where we observe that with an adjustment of approximately 16% to the value of $\alpha_s(\mu)$, one can compensate, at least effectively, the role played by the dressed ghost-gluon vertex in the ghost SDE.

At the level of the ghost SDE equation, the fact that B_1 provides considerable

⁵In particular, observe in Fig. 4.9, at $p = 1.12$ GeV, one has $B_1 = 1.21$, which means an enhancement of 21% from the tree-level value, $B_1^{(0)} = 1$.

support to the integral kernel of the ghost SDE was already well-known in the literature [86, 87]. It is known that without its dressed contribution, the unique way of reproducing the lattice results for $F(q)$ rather accurately is to increase the value of the running coupling, $\alpha_s(\mu)$, artificially. Therefore, from the analysis presented here, one can conclude that the same pattern emerges from the $BB\bar{c}c$ vertex.

Conclusions

In the thesis, we have presented a preliminary study about the nonperturbative structure of the $BB\bar{c}c$ vertex through its SDE. We have seen that this vertex emerges naturally from the BFM framework, and in addition, it is endowed with desirable properties for serving as a perfect starting point for a nonperturbative study of four-point Green's functions. Among these properties, we should highlight that the $BB\bar{c}c$ vertex has one of the simplest tensorial structures between the four-point Green's functions containing gauge fields and four color indices. Furthermore, the two background gluon legs respect Bose symmetry, which imposes additional constraints on the $BB\bar{c}c$ structure. Finally, the $BB\bar{c}c$ satisfies simple Abelian-like WTIs, instead of the complicated STIs satisfied by the conventional vertices [12, 55].

Although simpler, the most general tensorial decomposition of the $BB\bar{c}c$ vertex contains 80 independent tensors (combination of Lorentz and color basis). Each of these tensors will be accompanied by the corresponding form factor depending on six variables: the three independent momenta and the angles between them. However, the Bose symmetry of the background gluon legs imposes constraints on these form factors, reducing the number of independent form factors down to 35¹.

We have shown that a considerable simplification occurs if one imposes the all-soft limit, where we set all four external momenta to zero. Out of the 35 form factors, only one survives in this special kinematic limit, namely $\mathcal{C}_{11}(0, 0, 0, 0)$.

In Chapter 3, we have presented the derivation of the SDE that controls the dynamics of the $BB\bar{c}c$ using the functional formalism. It is the first time that this derivation has appeared in the literature, as far as we know. The pictorial representation of this SDE is composed of eleven Feynman diagrams and is shown in Fig. 3.3.

¹The ghost and antighost symmetry will reduce even more this number of independent form factors, but we have not explored this fact in this work.

Part of Chapter 4 was dedicated to implementing the all-soft limit at the BB̄c SDE level. After a thorough analysis of each one of the eleven Feynman diagrams mentioned above, we have demonstrated that only two of them contribute to this limit.

In order to show which diagrams contributing to the BB̄c SDE vanish in the all-soft limit, we turned our attention to other Green's functions nested in those Feynman diagrams. Particular attention was given to the conventional ghost-gluon vertex since this three-point function plays a key role in the entire analysis. More specifically, we have demonstrated throughout Chapter 4, that the Feynman diagrams appearing in Fig. 3.3 may vanish for two reasons: either (i) they have a gluon propagator that carries a transverse projector, for example, $P_{\mu\nu}(k)$, which contracts with the antighost momentum coming from the bare ghost-gluon vertex, k^μ , or (ii) there is a ghost-gluon vertex in the soft antighost limit, which is zero. Using either one of the above arguments, we have shown that five Feynman diagrams of Fig. 3.3 vanish identically in the all-soft limit.

Then, from the remaining ones, five diagrams depend on the BQQ, and BBQQ vertices. We have shown that their calculations require a careful analysis. More specifically, these vertices depend on the inverse of the gauge parameter, $1/\xi$, [see Eqs. (4.10) and (4.12)]. Therefore, one has to perform the calculations in general covariant gauges and only take the limit to the Landau gauge, *i.e.*, $\xi \rightarrow 0$, at the very end of the calculation, when all terms $1/\xi$ were explicitly canceled. This analysis has shown that only one Feynman diagram is nonvanishing out of five containing the BQQ and BBQQ vertices.

It turns out that the last Feynman diagram does not fit in any of the above cases and furnishes a contribution to the BB̄c SDE in the all-soft limit. Therefore, the final version of the SDE for the BB̄c vertex, in the all-soft limit, is composed of two Feynman diagrams and its counterparts with crossed background gluon legs, as depicted in Fig. 4.7, and its functional form is given by Eq. (4.40).

In the sequence, we have presented the renormalization of the SDE in the all-soft limit. The renormalization of Eq. (4.40) proceeds in the standard way. It turns out that the renormalized version of Eq. (4.40) depends only on the ghost renormalization constant, Z_c , which was fixed imposing the MOM condition. The final result for the renormalized BB̄c SDE in the all-soft limit is given in Eq. (4.43).

Furthermore, we showed that the full nonperturbative content of this SDE, in this particular kinematic limit, depends crucially on the BQ̄c̄ vertex on a particular kinematic limit, where the background gluon and the antighost momenta are zero, *i.e.*, $\tilde{\Gamma}_{\mu\nu}^{abmn}(0, -k, 0, k)$. In this special kinematic configuration, by virtue of the Abelian-like WTI that the BQ̄c̄ vertex satisfies,

one can determine without any approximation the exact value of this vertex which turns out to be proportional to the ghost-gluon vertex form factor in the soft antighost limit, $B_1(0, t, -t)$ [see Eq. (4.46)]. Therefore, we have seen that the form factor B_1 constitutes a central ingredient of the SDE for $\text{BB}\bar{c}c$ vertex when computed in the all-soft limit. Armed with the latter result, we could re-express the $\text{BB}\bar{c}c$ SDE in the all-soft limit in a very compact way, given by Eq. (4.50).

This result given by Eq. (4.50) showed that the structure of the $\text{BB}\bar{c}c$ vertex in the all-soft limit is proportional to the inverse of the ghost dressing function at the origin (or equivalently, it could be expressed in terms of the renormalized ghost self-energy at the origin, $\Sigma_R(0)$ [see Eq. (4.48)]. Moreover, its tensorial structure reduces only to the metric tensor times the combination of two color structures (c_1^{abmn} and c_2^{abmn}), checking the veracity of the statement made in Eq. (4.5), which was based on symmetry grounds. Here, we would like to emphasize that the result established in Eq. (4.50) was derived without employing any approximations, and therefore, it consists of an exact relation, valid to all orders in perturbation theory. In Section 4.4, we have shown that the same relation can also be derived through the WTI that the $\text{BB}\bar{c}c$ satisfies, given in Eq. (4.51).

Therefore, the all-soft configuration of the $\text{BB}\bar{c}c$ vertex revealed itself to be a privileged kinematic configuration since one can take advantage of an elegant interplay that emerges with the ghost-gluon vertex without having to resort to any *Ansätze* or simplifying assumptions for it. As it was stated in this thesis, this observation is the main contribution of our work.

As it was already pointed out in this thesis, obtaining an exact relation within the context of the SDE framework is rare, even if the analysis is restricted to a particular kinematic configuration, as it was done here. For this reason, as the final step of our analysis, we try to take advantage of this relation to plan a future truncation scheme for this vertex, which goes beyond the all-soft limit and thus quantify the accuracy of the new SDE approximated version.

Particularly, we have investigated the effect of setting all dressed vertices contributing to the $\text{BB}\bar{c}c$ SDE to their tree-level value. Under this approximation, the $\text{BB}\bar{c}c$ SDE in the all-soft limit is depicted in Fig. 4.11 and given by Eq. (4.57). Since the $\bar{\Sigma}_R(0)$ in Eq. (4.57) carries the information of the nonperturbative corrections of the vertex, it is precisely this quantity that we employ to compare the truncation schemes.

More specifically, to perform the analysis, we compute the percentage error, $\%_{error}$, between the exact result, $\Sigma_R(0)$, and the approximated one, $\bar{\Sigma}_R^i(0)$, given in Eq. (4.54). We propose using the percentage error as a benchmark for deciding the best truncation among three scenarios that differ from the inputs. In the first scenario, ($i = 1$), the values of $\alpha_s(\mu) = 0.244$, $\Delta(q)$ and $F(q)$ are fixed in order to match with the lattice results. In the case of the second

scenario, ($i = 2$), $\alpha_s(\mu) = 0.244$ and the $\Delta(q)$ is fixed in agreement with the lattice. For $F(q)$, we employ the ghost SDE solution with the bare ghost-gluon vertex. Finally, in scenario 3, we also use for $F(q)$ the solution obtained from ghost SDE with the bare ghost-gluon vertex. However, in this case, we have adjusted the coupling value to $\alpha_s(\mu) = 0.283$, in order to $F(q)$ reproduce the lattice data.

In this way, the last part of Section 4.5 was dedicated to the numerical determination of the percentage error, $\%_{error}$. We have seen that to compute this quantity one needs the following external inputs: the gluon propagator, $\Delta(k)$, the ghost propagator, $D(k)$, and the ghost-gluon form factor, B_1 . For $\Delta(k)$, we used a fit for the combined set of lattice data shown in Fig. 4.8. As for $D(k)$, we solved the ghost SDE using two approximations for the form factor B_1 that enters on it. Either we employed B_1 in general kinematics, $B_1(q^2, p^2, \varphi_1)$, [see a representative case in Fig. 4.9], or we set B_1 at its tree-level value, *i.e.*, $B_1^{(0)} = 1$. In Fig. 4.10, we have shown the corresponding solutions for $F(q)$ in both approximations. Moreover, to compute the exact expression $\Sigma_R(0)$, we also need the form factor B_1 in the soft antighost limit, $B_1(k^2)$, highlighted in red on the 3D surface of Fig. 4.9.

The results we have obtained for the $\%_{error}$ were synthesized on Table 4.1, where we compare the three scenarios. This procedure rendered us a rough estimate of the accuracy for a possible new truncation scheme of the SDE for the $BB\bar{c}c$, where all dressed vertices are approximated at tree-level. Under these assumptions, our preliminary analysis suggests that the best course of action is to employ nonperturbative fits for $\Delta(q)$ and $F(q)$ and keep them fixed instead trying to couple the two-point sector of the theory, as the first attempt of going beyond the all-soft limit of the SDE for the $BB\bar{c}c$.

Bibliography

- ¹W. J. Marciano and H. Pagels, “Quantum Chromodynamics: A Review”, [Phys. Rept. **36**, 137 \(1978\)](#).
- ²C.-N. Yang and R. L. Mills, “Conservation of Isotopic Spin and Isotopic Gauge Invariance”, [Phys. Rev. **96**, 191–195 \(1954\)](#).
- ³D. J. Gross and F. Wilczek, “Ultraviolet Behavior of Nonabelian Gauge Theories”, [Phys. Rev. Lett. **30**, 1343–1346 \(1973\)](#).
- ⁴H. D. Politzer, “Reliable Perturbative Results for Strong Interactions?”, [Phys. Rev. Lett. **30**, 1346–1349 \(1973\)](#).
- ⁵J. Greensite, “The Confinement problem in lattice gauge theory”, [Prog. Part. Nucl. Phys. **51**, 1 \(2003\)](#).
- ⁶J. Greensite, *An introduction to the confinement problem*, Vol. 821 (2011).
- ⁷J. M. Cornwall, “Dynamical Mass Generation in Continuum QCD”, [Phys. Rev. D **26**, 1453 \(1982\)](#).
- ⁸C. D. Roberts and A. G. Williams, “Dyson-Schwinger equations and their application to hadronic physics”, [Prog. Part. Nucl. Phys. **33**, 477–575 \(1994\)](#).
- ⁹R. Alkofer and L. von Smekal, “The Infrared behavior of QCD Green’s functions: Confinement dynamical symmetry breaking, and hadrons as relativistic bound states”, [Phys. Rept. **353**, 281 \(2001\)](#).
- ¹⁰C. S. Fischer, “Infrared properties of QCD from Dyson-Schwinger equations”, [J. Phys. G **32**, R253–R291 \(2006\)](#).

- ¹¹A. C. Aguilar, D. Binosi, and J. Papavassiliou, “Gluon and ghost propagators in the Landau gauge: Deriving lattice results from Schwinger-Dyson equations”, *Phys. Rev.* **D78**, 025010 (2008).
- ¹²D. Binosi and J. Papavassiliou, “Pinch Technique: Theory and Applications”, *Phys. Rept.* **479**, 1–152 (2009).
- ¹³A. C. Aguilar and J. Papavassiliou, “Chiral symmetry breaking with lattice propagators”, *Phys. Rev.* **D83**, 014013 (2011).
- ¹⁴M. Mitter, J. M. Pawłowski, and N. Strodthoff, “Chiral symmetry breaking in continuum QCD”, *Phys. Rev.* **D91**, 054035 (2015).
- ¹⁵A. C. Aguilar, D. Binosi, and J. Papavassiliou, “The Gluon Mass Generation Mechanism: A Concise Primer”, *Front. Phys.(Beijing)* **11**, 111203 (2016).
- ¹⁶P. Maris and C. D. Roberts, “Dyson-Schwinger equations: A Tool for hadron physics”, *Int. J. Mod. Phys.* **E12**, 297–365 (2003).
- ¹⁷I. C. Cloet and C. D. Roberts, “Explanation and Prediction of Observables using Continuum Strong QCD”, *Prog. Part. Nucl. Phys.* **77**, 1–69 (2014).
- ¹⁸C. D. Roberts, “Three Lectures on Hadron Physics”, *J. Phys. Conf. Ser.* **706**, 022003 (2016).
- ¹⁹G. Eichmann, H. Sanchis-Alepuz, R. Williams, R. Alkofer, and C. S. Fischer, “Baryons as relativistic three-quark bound states”, *Prog. Part. Nucl. Phys.* **91**, 1–100 (2016).
- ²⁰K. G. Wilson, “Confinement of quarks”, *Phys. Rev. D* **10**, 2445–2459 (1974).
- ²¹M. Creutz, “Monte Carlo study of quantized SU(2) gauge theory”, *Phys. Rev. D* **21**, 2308–2315 (1980).
- ²²S. Durr et al., “Ab-Initio Determination of Light Hadron Masses”, *Science* **322**, 1224–1227 (2008).
- ²³F. J. Yndurain, *The theory of quark and gluon interactions* (Springer, 2006).
- ²⁴R. Gupta, “Introduction to lattice QCD: Course”, in Les Houches Summer School in Theoretical Physics, Session 68: Probing the Standard Model of Particle Interactions (July 1997).
- ²⁵M. Luscher, “Advanced lattice QCD”, in Les Houches Summer School in Theoretical Physics, Session 68: Probing the Standard Model of Particle Interactions (Feb. 1998).

- ²⁶J. M. Pawłowski, D. F. Litim, S. Nedelko, and L. von Smekal, “Infrared behavior and fixed points in Landau gauge QCD”, *Phys. Rev. Lett.* **93**, 152002 (2004).
- ²⁷J. M. Pawłowski, “Aspects of the functional renormalisation group”, *Annals Phys.* **322**, 2831–2915 (2007).
- ²⁸D. Dudal, J. A. Gracey, S. P. Sorella, N. Vandersickel, and H. Verschelde, “A refinement of the Gribov-Zwanziger approach in the Landau gauge: infrared propagators in harmony with the lattice results”, *Phys. Rev.* **D78**, 065047 (2008).
- ²⁹M. Tissier and N. Wschebor, “Infrared propagators of Yang-Mills theory from perturbation theory”, *Phys. Rev. D* **82**, 101701 (2010).
- ³⁰N. Vandersickel and D. Zwanziger, “The Gribov problem and QCD dynamics”, *Phys. Rept.* **520**, 175–251 (2012).
- ³¹J. Serreau and M. Tissier, “Lifting the Gribov ambiguity in Yang-Mills theories”, *Phys. Lett.* **B712**, 97–103 (2012).
- ³²M. Peláez, M. Tissier, and N. Wschebor, “Three-point correlation functions in Yang-Mills theory”, *Phys. Rev.* **D88**, 125003 (2013).
- ³³L. Corell, A. K. Cyrol, M. Mitter, J. M. Pawłowski, and N. Strodthoff, “Correlation functions of three-dimensional Yang-Mills theory from the FRG”, *SciPost Phys.* **5**, 066 (2018).
- ³⁴A. K. Cyrol, M. Mitter, J. M. Pawłowski, and N. Strodthoff, “Nonperturbative quark, gluon, and meson correlators of unquenched QCD”, *Phys. Rev.* **D97**, 054006 (2018).
- ³⁵B. W. Mintz, L. F. Palhares, S. P. Sorella, and A. D. Pereira, “Ghost-gluon vertex in the presence of the Gribov horizon”, *Phys. Rev.* **D97**, 034020 (2018).
- ³⁶M. Peláez, U. Reinosa, J. Serreau, M. Tissier, and N. Wschebor, “A window on infrared QCD with small expansion parameters”, (2021).
- ³⁷M. R. Pennington, “Swimming with quarks”, *J. Phys. Conf. Ser.* **18**, edited by A. Bashir, J. Erler, R. Hernandez, M. Mondragon, and L. Villasenor, 1–73 (2005).
- ³⁸D. Binosi and J. Papavassiliou, “Gauge-invariant truncation scheme for the Schwinger-Dyson equations of QCD”, *Phys. Rev.* **D77**, 061702 (2008).
- ³⁹D. Binosi and J. Papavassiliou, “New Schwinger-Dyson equations for non-Abelian gauge theories”, *J. High Energy Phys.* **11**, 063 (2008).

- ⁴⁰E. S. Swanson, “A Primer on Functional Methods and the Schwinger-Dyson Equations”, *AIP Conf. Proc.* **1296**, edited by M. Nielsen, F. S. Navarra, and M. E. Bracco, 75–121 (2010).
- ⁴¹J. E. King, “Transverse vertex and gauge technique in quantum electrodynamics”, *Phys. Rev. D* **27**, 1821–1829 (1983).
- ⁴²B. Haeri, “Ultraviolet-improved gauge technique and the effective quark propagator in QCD”, *Phys. Rev. D* **38**, 3799–3810 (1988).
- ⁴³D. C. Curtis and M. R. Pennington, “Truncating the Schwinger-Dyson equations: How multiplicative renormalizability and the Ward identity restrict the three point vertex in QED”, *Phys. Rev. D* **42**, 4165–4169 (1990).
- ⁴⁴C. S. Fischer and R. Alkofer, “Nonperturbative propagators, running coupling and dynamical quark mass of Landau gauge QCD”, *Phys. Rev.* **D67**, 094020 (2003).
- ⁴⁵A. C. Aguilar, J. C. Cardona, M. N. Ferreira, and J. Papavassiliou, “Quark gap equation with non-abelian Ball-Chiu vertex”, *Phys. Rev.* **D98**, 014002 (2018).
- ⁴⁶A. C. Aguilar and J. Papavassiliou, “Gluon mass generation in the PT-BFM scheme”, *J. High Energy Phys.* **12**, 012 (2006).
- ⁴⁷A. Kizilersu and M. Pennington, “Building the Full Fermion-Photon Vertex of QED by Imposing Multiplicative Renormalizability of the Schwinger-Dyson Equations for the Fermion and Photon Propagators”, *Phys. Rev.* **D79**, 125020 (2009).
- ⁴⁸M. Q. Huber, “Nonperturbative properties of Yang-Mills theories”, *Phys. Rept.* **879**, 1–92 (2020).
- ⁴⁹J. M. Cornwall and J. Papavassiliou, “Gauge Invariant Three Gluon Vertex in QCD”, *Phys. Rev. D* **40**, 3474 (1989).
- ⁵⁰D. Binosi and J. Papavassiliou, “Pinch technique to all orders”, *Phys. Rev. D* **66**, 111901 (2002).
- ⁵¹D. Binosi and J. Papavassiliou, “Pinch technique selfenergies and vertices to all orders in perturbation theory”, *J. Phys. G* **G30**, 203 (2004).
- ⁵²J. M. Cornwall, J. Papavassiliou, and D. Binosi, *The Pinch Technique and its Applications to Non-Abelian Gauge Theories*, Vol. 31 (Cambridge University Press, 2010).

- ⁵³B. S. DeWitt, “Quantum Theory of Gravity. II. The Manifestly Covariant Theory”, [Phys. Rev. **162**, 1195–1239 \(1967\)](#).
- ⁵⁴G. 't Hooft, “The Background Field Method in Gauge Field Theories, ” In *Karpacz 1975, Proceedings, Acta Universitatis Wratislaviensis No.368, Vol.1*, Wroclaw 1976, 345-369 (1976).
- ⁵⁵L. Abbott, “The Background Field Method Beyond One Loop”, [Nucl. Phys. B **185**, 189–203 \(1981\)](#).
- ⁵⁶M. E. Peskin and D. V. Schroeder, *An introduction to quantum field theory*, Advanced book program, Autre tirage : 1997 (Westview Press Reading (Mass.), Boulder (CO.), 1995).
- ⁵⁷L. Faddeev and V. Popov, “Feynman diagrams for the Yang-Mills field”, [Physics Letters B **25**, 29–30 \(1967\)](#).
- ⁵⁸C. G. Callan, “Broken scale invariance in scalar field theory”, [Phys. Rev. D **2**, 1541–1547 \(1970\)](#).
- ⁵⁹P. A. Zyla et al. (Particle Data Group), “Review of Particle Physics”, [PTEP **2020**, 083C01 \(2020\)](#).
- ⁶⁰M. D. Schwartz, *Quantum Field Theory and the Standard Model* (Cambridge University Press, Mar. 2014).
- ⁶¹L. F. Abbott, “Introduction to the background field method”, [Acta Phys. Pol. B **13**, 33–50. 30 p \(1981\)](#).
- ⁶²P. Pascual and R. Tarrach, “QCD: Renormalization for the practitioner”, [Lect. Notes Phys. **194**, 1–277 \(1984\)](#).
- ⁶³L. F. Abbott, M. T. Grisaru, and R. K. Schaefer, “The Background Field Method and the S Matrix”, [Nucl. Phys. B **229**, 372–380 \(1983\)](#).
- ⁶⁴P. A. Grassi, T. Hurth, and M. Steinhauser, “Practical algebraic renormalization”, [Annals of Physics **288**, 197–248 \(2001\)](#).
- ⁶⁵D. Binosi and J. Papavassiliou, “Pinch technique and the Batalin-Vilkovisky formalism”, [Phys. Rev. **D66**, 025024 \(2002\)](#).
- ⁶⁶F. J. Dyson, “The S Matrix in Quantum Electrodynamics”, [Phys. Rev. **75**, 1736–1755 \(1949\)](#).

- ⁶⁷J. S. Schwinger, “On the Green’s functions of quantized fields. 1.”, *Proc. Nat. Acad. Sci.* **37**, 452–455 (1951).
- ⁶⁸R. Alkofer, M. Huber, and K. Schwenzer, “Algorithmic derivation of Dyson–Schwinger equations”, *Computer Physics Communications* **180**, 965–976 (2009).
- ⁶⁹P. Pascual and R. Tarrach, “Slavnov-Taylor Identities in Weinberg’s Renormalization Scheme”, *Nucl. Phys. B* **174**, [Erratum: *Nucl.Phys.B* 181, 546 (1981)], 123 (1980).
- ⁷⁰D. Binosi, D. Ibañez, and J. Papavassiliou, “Nonperturbative study of the four gluon vertex”, *J. High Energy Phys.* **09**, 059 (2014).
- ⁷¹J. Taylor, “Ward Identities and Charge Renormalization of the Yang-Mills Field”, *Nucl. Phys. B* **33**, 436–444 (1971).
- ⁷²A. C. Aguilar, D. Binosi, J. Papavassiliou, and J. Rodríguez-Quintero, “Non-perturbative comparison of QCD effective charges”, *Phys. Rev.* **D80**, 085018 (2009).
- ⁷³A. C. Aguilar, C. O. Ambrósio, F. De Soto, M. N. Ferreira, B. M. Oliveira, J. Papavassiliou, and J. Rodríguez-Quintero, “Ghost dynamics in the soft gluon limit”, *Phys. Rev. D* **104**, 054028 (2021).
- ⁷⁴J. S. Ball and T.-W. Chiu, “Analytic Properties of the Vertex Function in Gauge Theories. 2.”, *Phys. Rev. D* **22**, [Erratum: *Phys.Rev.D* 23, 3085 (1981)], 2550 (1980).
- ⁷⁵P. Boucaud, J. Leroy, L. Y. A., J. Micheli, O. Pène, and J. Rodríguez-Quintero, “On the IR behaviour of the Landau-gauge ghost propagator”, *J. High Energy Phys.* **06**, 099 (2008).
- ⁷⁶C. S. Fischer, A. Maas, and J. M. Pawłowski, “On the infrared behavior of Landau gauge Yang-Mills theory”, *Annals Phys.* **324**, 2408–2437 (2009).
- ⁷⁷P. Boucaud, F. De Soto, J. Leroy, A. Le Yaouanc, J. Micheli, et al., “Ghost-gluon running coupling, power corrections and the determination of $\Lambda(\overline{\text{MS}})$ ”, *Phys. Rev.* **D79**, 014508 (2009).
- ⁷⁸P. Boucaud, D. Dudal, J. Leroy, O. Pene, and J. Rodríguez-Quintero, “On the leading OPE corrections to the ghost-gluon vertex and the Taylor theorem”, *J. High Energy Phys.* **12**, 018 (2011).
- ⁷⁹L. von Smekal, K. Maltman, and A. Sternbeck, “The Strong coupling and its running to four loops in a minimal MOM scheme”, *Phys. Lett. B* **681**, 336–342 (2009).

- ⁸⁰S. Zafeiropoulos, P. Boucaud, F. De Soto, J. Rodríguez-Quintero, and J. Segovia, “Strong Running Coupling from the Gauge Sector of Domain Wall Lattice QCD with Physical Quark Masses”, *Phys. Rev. Lett.* **122**, 162002 (2019).
- ⁸¹P. Boucaud, F. De Soto, K. Raya, J. Rodríguez-Quintero, and S. Zafeiropoulos, “Discretization effects on renormalized gauge-field Green’s functions, scale setting, and the gluon mass”, *Phys. Rev.* **D98**, 114515 (2018).
- ⁸²I. Bogolubsky, E. Ilgenfritz, M. Müller-Preussker, and A. Sternbeck, “Lattice gluodynamics computation of Landau gauge Green’s functions in the deep infrared”, *Phys. Lett.* **B676**, 69–73 (2009).
- ⁸³A. C. Aguilar, M. N. Ferreira, C. T. Figueiredo, and J. Papavassiliou, “Nonperturbative Ball-Chiu construction of the three-gluon vertex”, *Phys. Rev.* **D99**, 094010 (2019).
- ⁸⁴C. de Boor, *A practical guide to splines*, Applied Mathematical Sciences (Springer New York, 2001).
- ⁸⁵W. H. Press, S. a. Teukolsky, W. T. Vetterling, and B. P. Flannery, *Numerical Recipes in Fortran 77: the Art of Scientific Computing. Second Edition*, Vol. 1 (1996).
- ⁸⁶A. C. Aguilar, “The impact of the ghost-gluon vertex on the ghost Schwinger-Dyson equations”, *PoS QCD-TNT-III*, 001 (2013).
- ⁸⁷A. C. Aguilar, M. N. Ferreira, C. T. Figueiredo, and J. Papavassiliou, “Nonperturbative structure of the ghost-gluon kernel”, *Phys. Rev.* **D99**, 034026 (2019).
- ⁸⁸M. Q. Huber, “On non-primitively divergent vertices of Yang–Mills theory”, *Eur. Phys. J.* **C77**, 733 (2017).

Appendix A

SU(N) group theoretical identities

QCD is based on the gauge group SU(3), and its representation has eight hermitian and traceless generators that generates the closed algebra

$$\left[\frac{\lambda^a}{2}, \frac{\lambda^b}{2} \right] = i f^{abc} \frac{\lambda^c}{2}, \quad (\text{A.1})$$

with λ being the Gell-Mann matrices, and f^{abc} the totally antisymmetric structure constant. In this Appendix we collect some relations that the structure constant, f^{abc} , satisfy, which will be useful to perform the analytical calculations of the current analysis.

The combinations of different sequences of structure constants satisfy the following relations

$$f^{aex} f^{bex} = C_A \delta^{ab}, \quad (\text{A.2})$$

$$f^{axm} f^{bmn} f^{cnx} = \frac{C_A}{2} f^{abc}, \quad (\text{A.3})$$

$$f^{axm} f^{bmn} f^{cne} f^{dex} - f^{axm} f^{bmn} f^{dne} f^{cex} = -\frac{C_A}{2} f^{abx} f^{cdx}, \quad (\text{A.4})$$

where C_A is the Casimir eigenvalue in the adjoint representation [$C_A = N$ for SU(N)].

In addition, we have the Jacobi identity which reads

$$f^{abx} f^{xcd} + f^{acx} f^{xdb} + f^{adx} f^{xbc} = 0. \quad (\text{A.5})$$

Appendix B

Nonperturbative structure of the $BB\bar{c}c$ vertex

We divide this Appendix into two sections: in the first one we discuss, in detail, the construction of the most general tensorial structure for the $BB\bar{c}c$ vertex. The final result of this discussion is the Lorentz basis, given in Eq. (4.2), and the color basis, in Eq. (4.3). Then, in the other section, we explain how the Bose symmetry of the $BB\bar{c}c$ vertex dramatically reduces the number of independent form factors. More specifically, we start with 80 form factors, and because of the Bose symmetry, we end up with 35 independent form factors.

B.1 Color basis construction

For the construction of the Lorentz and color basis of the $BB\bar{c}c$ vertex, we will follow the lines of [69, 70, 88]. To do that, let us start with the Lorentz part. This vertex has two Lorentz free indices (μ and ν); therefore, the only rank-2 Minkowski tensors allowed in this basis will be: (i) linear terms in the metric or (ii) quadratic terms in the momenta. Schematically, this means that one may write the following structures

$$g, \quad qr, \quad qp, \quad rp, \quad (\text{B.1})$$

where $g_{\mu\nu}$ is the metric, and q , r , and p represent the three independent momenta we have in the $BB\bar{c}c$ vertex.

Permuting the two Lorentz indices (μ and ν) between the three independent momenta of the vertex (q , r , and p), it is possible to see that one obtains the following ten elements, which form the naive Lorentz basis of the $BB\bar{c}c$ vertex

$$\begin{aligned} \ell_{\mu\nu}^1 &= g_{\mu\nu}, & \ell_{\mu\nu}^2 &= q_\mu r_\nu, & \ell_{\mu\nu}^3 &= q_\mu p_\nu, & \ell_{\mu\nu}^4 &= q_\nu r_\mu, & \ell_{\mu\nu}^5 &= q_\nu p_\mu, \\ \ell_{\mu\nu}^6 &= r_\mu p_\nu, & \ell_{\mu\nu}^7 &= p_\mu r_\nu, & \ell_{\mu\nu}^8 &= q_\mu q_\nu, & \ell_{\mu\nu}^9 &= r_\mu r_\nu, & \ell_{\mu\nu}^{10} &= p_\mu p_\nu. \end{aligned} \quad (\text{B.2})$$

Concerning the color basis, the situation is considerably more complex since we have a rank-4 tensor. The possible structures will be quadratic in f , δ and d , with f being the totally antisymmetric structure constant, δ the Kronecker delta, and d the totally symmetric structure constant. In principle, one has 15 allowed structures of the schematic type

$$ff, \quad dd, \quad fd, \quad \delta\delta. \quad (\text{B.3})$$

However, the above tensors are not really independent; they are intertwined by the following set of identities in SU(3) [69]

$$f^{abr} f^{cdr} = \frac{2}{3} [\delta^{ac} \delta^{bd} - \delta^{ad} \delta^{bc}] + d^{acr} d^{dbr} - d^{adr} d^{bcr}, \quad (\text{B.4})$$

$$f^{abr} d^{cdr} + f^{acr} d^{dbr} + f^{adr} d^{bcr} = 0, \quad (\text{B.5})$$

$$\delta^{ab} \delta^{cd} + \delta^{ac} \delta^{bd} + \delta^{ad} \delta^{bc} = 3[d^{abr} d^{cdr} + d^{acr} d^{bdr} + d^{adr} d^{bcr}]. \quad (\text{B.6})$$

Notice that Eqs. (B.4) and (B.5) have two independent permutations for each, generating seven new relations. As a result, out of fifteen (15) starting structures, we end up with only eight (8) independent tensors. Thus, the color basis is given by [69, 70]

$$\begin{aligned} c_1^{abmn} &= f^{anx} f^{mbx}, & c_2^{abmn} &= f^{max} f^{bnx}, & c_3^{abmn} &= \delta^{ab} \delta^{mn}, & c_4^{abmn} &= \delta^{am} \delta^{nb}, \\ c_5^{abmn} &= \delta^{an} \delta^{bm}, & c_6^{abmn} &= d^{abr} f^{mnr}, & c_7^{abmn} &= d^{amr} f^{bnr}, & c_8^{abmn} &= d^{anr} f^{bmr}. \end{aligned} \quad (\text{B.7})$$

B.2 Bose symmetry of the background gluon legs

As discussed in the previous Section, the most general decomposition of the BB \bar{c} c vertex in its Lorentz and color basis is expressed by Eq. (4.1), where the ten tensors defining the Lorentz basis are given in Eq. (4.2); whereas the eight elements of the color basis, appear in Eq. (4.3).

Therefore, the BB \bar{c} c depends on 80 form factors which are functions of six variables, *i.e.*, the three independent momenta: q , r , and, p and the three angles between them.

Nevertheless, to reduce the number of form factors, one can use the Bose symmetry, which the two background gluon legs should satisfy. To do that, we impose the Bose symmetry under the simultaneous exchange $\mu \leftrightarrow \nu$, $a \leftrightarrow b$, and $q \leftrightarrow r$. At the level of the elements forming the Lorentz basis, given by Eq. (4.2), these exchanges lead to

$$\ell_{\mu\nu}^3 \leftrightarrow \ell_{\mu\nu}^7, \quad \ell_{\mu\nu}^5 \leftrightarrow \ell_{\mu\nu}^6, \quad \ell_{\mu\nu}^8 \leftrightarrow \ell_{\mu\nu}^9. \quad (\text{B.8})$$

Meanwhile, the elements of the color basis of Eq. (4.3) under the exchange of $a \leftrightarrow b$ are related

by

$$c_1^{abmn} \leftrightarrow c_2^{abmn}, \quad c_4^{abmn} \leftrightarrow c_5^{abmn}, \quad c_7^{abmn} \leftrightarrow c_8^{abmn}. \quad (\text{B.9})$$

These transformations reduce the i in Eq. (4.1) to 7 and j to 5, totalling 35 independent form factors.

To illustrate how the form factors are related to each other, let us take a closer look at those accompanying the $g_{\mu\nu}$ structure, *i.e.*, $\mathcal{C}_{1j}(q, r, p, t)$, with $j = 1, 2, \dots, 8$. Due to Eq. (B.9), we find the following relations

$$\mathcal{C}_{11}(q, r, p, t) = \mathcal{C}_{12}(r, q, p, t), \quad (\text{B.10})$$

$$\mathcal{C}_{14}(q, r, p, t) = \mathcal{C}_{15}(r, q, p, t),$$

$$\mathcal{C}_{17}(q, r, p, t) = \mathcal{C}_{18}(r, q, p, t).$$

As explained, in the last paragraph of Section 4.1, in the all-soft limit, the decomposition of the structure of the $\text{BB}\bar{c}c$ will depend only on $\ell_{\mu\nu}^1$, c_1^{abmn} , and c_2^{abmn} . Therefore, this configuration is expressed in terms of the form factors $\mathcal{C}_{11}(q, r, p, t)$ and $\mathcal{C}_{12}(q, r, p, t)$. However, as we have just seen, these both are related through Eq. (B.10); thus, the $\text{BB}\bar{c}c$ vertex depends on only one form factor, namely $\mathcal{C}_{11}(q, r, p, t)$, in the all-soft limit.

Transformation rules from Minkowski to Euclidean space

In this Appendix, we summarise the standard conversion rules to pass the expressions from Minkowski to Euclidean space. The first step is to perform a Wick rotation, *i.e.*, convert the time component of any four-momentum, q_μ , in a pure imaginary number,

$$(q_0, q_1, q_2, q_3) \rightarrow (iq_0^E, q_1^E, q_2^E, q_3^E), \quad (\text{C.1})$$

where the q_i^E are real, and the superscript “E” denotes the Euclidean version of a quantity. Simultaneously, the metric is transformed to $g_{\mu\nu} \rightarrow \delta_{\mu\nu}$.

In particular, the scalar products becomes

$$[q^2; p^2; r^2; (q \cdot p); (q \cdot r); (p \cdot r)] \rightarrow [-q_E^2; -p_E^2; -r_E^2; -(q_E \cdot p_E); -(q_E \cdot r_E); -(p_E \cdot r_E)]. \quad (\text{C.2})$$

On the other hand, any dimensionless form factors, such as the ghost-gluon form factor, $B_i(r, p, q)$, appearing in Eq. (4.6), transforms as

$$B_j(r, p, q) \rightarrow B_j(r_E, p_E, q_E). \quad (\text{C.3})$$

As for the dimensionful quantities (with dimensions of $[M]^{-2}$), as the ghost, $D(q)$, and gluon propagators, $\Delta(q)$, they transform from Minkowski to Euclidean as

$$D(q) \rightarrow -D_E(q_E), \quad \Delta(q) \rightarrow -\Delta_E(q_E). \quad (\text{C.4})$$

Additionally, the integral measure becomes

$$\int_k \rightarrow i \int_{k_E}, \quad (\text{C.5})$$

which in 4D spherical coordinates is given by

$$\int_{k_E} = \frac{1}{32\pi^4} \int_0^\infty dk_E^2 k_E^2 \int_0^\pi d\varphi_1 \sin^2 \varphi_1 \int_0^\pi d\varphi_2 \sin \varphi_2 \int_0^{2\pi} d\varphi_3. \quad (\text{C.6})$$

In general, after performing the transformation from Minkowski to Euclidean space, the subscript “E” is omitted for compactness. Thus, when expressions are written in Euclidean space, they will be clear, either by context or by explicit assertion.

A standard choice for the orientation of the Euclidean four-momenta r , p , and the integration momentum k is (from now on we suppress the subscript “E”)

$$r = |r|(1, 0, 0, 0), \quad (\text{C.7})$$

$$p = |p|(\cos \theta, \sin \theta, 0, 0), \quad (\text{C.8})$$

$$k = |k|(\cos \varphi_1, \sin \varphi_1 \cos \varphi_2, \sin \varphi_1 \sin \varphi_2 \cos \varphi_3, \sin \varphi_1 \sin \varphi_2 \sin \varphi_3). \quad (\text{C.9})$$

Evidently, $r^2 = |r|^2$, $p^2 = |p|^2$, and $k^2 = |k|^2$. In addition, the scalar products are given by

$$\begin{aligned} r \cdot p &= |r| |p| \cos \theta, \\ r \cdot k &= |r| |k| \cos \varphi_1, \\ p \cdot k &= |p| |k| (\cos \theta \cos \varphi_1 + \sin \theta \sin \varphi_1 \cos \varphi_2). \end{aligned} \quad (\text{C.10})$$

Therefore, using the parametrization of Eqs. (C.7) and (C.8), we will express the relevant form factors, $B_j(r, p, q)$, in Euclidean space as a function of r^2 , p^2 , and the angle between them θ , namely

$$B_j(r, p, q) \equiv B_j(r^2, p^2, \theta), \quad (\text{C.11})$$

where θ is given by

$$\theta = \arccos \left[\frac{r \cdot p}{|r| |p|} \right]. \quad (\text{C.12})$$

Note that since the quantities entering in the integrals do not depend on the angle φ_3 , the last integral in Eq. (C.5) furnishes simply a factor of 2π .

Appendix D

Numerical method for solving integral equations

The renormalized version of the ghost propagator SDE, given by Eq. (4.28), which we want to solve numerically, was discussed in Chapter 4, and we reproduce it here for convenience

$$F^{-1}(q) = 1 + \Sigma(q) - \Sigma(\mu), \quad (\text{D.1})$$

where the ghost self-energy, $\Sigma(q)$, expressed as

$$\Sigma(q) = ig^2 C_A \int_k D(k+q) \Delta(k) f(k, q) B_1(-q, k+q, -k), \quad (\text{D.2})$$

with

$$f(k, q) := 1 - \frac{(k \cdot q)^2}{q^2 k^2}, \quad (\text{D.3})$$

was already presented by Eq. (4.17).

The first step to solve Eq. (D.1) numerically is to shift the integration momentum, $k \rightarrow k - q$, so that the unknown function, $F(k)$ (or equivalently $D(k)$), appearing on the RHS of Eq. (D.2) will depend only on the momentum k , and the equation for $\Sigma(q)$ may be recast in the form

$$\Sigma(q) = ig^2 C_A \int_k D(k) \Delta(k-q) f(k-q, q) B_1(-q, k, q-k). \quad (\text{D.4})$$

To convert the above expression, which is in Minkowski space, to Euclidean space, we apply the transformation rules of Appendix C. More specifically, employing the rules from

Eqs. (C.2), (C.4), (C.5), (C.6), (C.10), and (C.11), we arrive at

$$\Sigma(q) = -\frac{C_A \alpha_s(\mu)}{2\pi^2} \int_0^\infty dk^2 k^2 F(k) \int_0^\pi d\varphi_1 \sin^4 \varphi_1 \frac{\Delta(k-q)}{(k-q)^2} B_1(q^2, k^2, \varphi_1), \quad (\text{D.5})$$

where φ_1 is the angle between the momenta k and q , $C_A = 3$ for SU(3), and we set the value of the coupling constant renormalized at μ at $\alpha_s(\mu) = g^2/4\pi = 0.244$ [73].

Thus, Eq. (D.1) becomes

$$F^{-1}(x) = 1 - \frac{C_A \alpha_s(\mu)}{2\pi^2} \int_0^\infty dy y F(y) \int_0^\pi d\varphi_1 \sin^4 \varphi_1 \left[\frac{\Delta(z) B_1(x, y, \varphi_1)}{z} - \frac{\Delta(z') B_1(\mu^2, y, \varphi_1)}{z'} \right], \quad (\text{D.6})$$

where we set $x = q^2$, $y = k^2$, $z = (k-q)^2$ and $z' = (k-\mu)^2$. The scale μ is the renormalization point introduced within the MOM scheme, *i.e.*, by requiring that $F^{-1}(\mu) = 1$.

To solve the above integral equation numerically, we will apply for the angular and radial integrations the Gauss-Legendre method. To do that, one needs to map the infinite momentum range of the variable $y \in [0, \infty)$ to the finite range of Gauss-Legendre quadrature, $\bar{y} \in [-1, 1]$, and the finite range of the variable $\varphi_1 \in [0, \pi]$, should be rescaled to $\bar{z} \in [-1, 1]$. Thus, this mapping typically consists in the following change of variables

$$y = \frac{2}{1 - \bar{y}} - 1, \quad \bar{z} = \cos(\varphi_1). \quad (\text{D.7})$$

Then, one can use that

$$\int_{-1}^1 f(\bar{y}) d\bar{y} = \sum_{i=1}^n w_i f(\bar{y}_i), \quad (\text{D.8})$$

with w_i denoting the weight, \bar{y}_i the nodes of the Gauss-Legendre quadrature, and n the number of sample points used.

In addition, we perform the following change of variable for the external momenta x

$$x = \frac{2}{1 - \bar{x}} - 1, \quad (\text{D.9})$$

and we expand the unknown functions, $F(x)$ and $F(y)$, appearing in both sides of the Eq. (D.6), in terms of the Chebyshev polynomials, *i.e.*,

$$F(x) = \sum_{n=0}^N f_n U_n(x), \quad (\text{D.10})$$

where f_n are the coefficients of the expansion that we should determine, and U_n are the Cheby-

shev polynomials of the second kind.

For computing the radial integration with the Gauss-Legendre method, we use a quadrature with $n = 50$ sample points, whereas for the angular part, we employ $n = 30$ points. In the sequence, we apply Newton's method to determine the expansion coefficients f_n . With the coefficients f_n at hand, we replace them in the expansion given by Eq. (D.10) to finally obtain the solution for the unknown ghost dressing function, $F(q)$.